UC Berkeley
UC Berkeley Electronic Theses and Dissertations

Title
Non-Canonical Roles and Variants of Core Translation Initiation Factors

Permalink
https://escholarship.org/uc/item/5db0j3gd

Author
Pulos-Holmes, Mia Christina

Publication Date
2020

Peer reviewed|Thesis/dissertation

Non-Canonical Roles and Variants of Core Translation Initiation Factors

By

Mia Christina Pulos-Holmes

A dissertation submitted in partial satisfaction of the

requirement for the degree of

Doctor of Philosophy

in

Molecular and Cell Biology

in the

Graduate Division

of the

University of California, Berkeley

Committee in charge

Professor Jamie Cate, Co-Chair

Professor Nicholas Ingolia, Co-Chair

Professor Britt Glaunsinger

Professor Christopher Chang

Summer 2020

Abstract

Non-Canonical Roles and Variants of Core Translation Initiation Factors

By

Mia C Pulos-Holmes

University of California, Berkeley

Doctor of Philosophy in Molecular and Cell Biology

Professor Jamie Cate, Co-Chair

Professor Nicholas Ingolia, Co-Chair

Translation initiation has been regarded as a tightly controlled point of commitment for protein synthesis. Dysregulation of the intricate orchestration of the factors responsible for translation initiation has been shown to be a contributing element in cancer progression, neurological disorders, and many more diseases. Throughout this body of work, we aim to better understand specialized translational regulation which can contribute to transcript selection shifts during times of stress and disease. We not only strive to understand novel non-canonical roles of these translation initiation factors, but also appreciate the unique mechanisms of regulation implemented through the diversification of these factors. We highlight an example of these non-canonical roles through the investigation of eukaryotic initiation factor 3 (eIF3) governed repression of *FTL* translation. We further this work by demonstrating how disruption of this repression is the molecular cause of a subset of hyperferritinemia cases. Additionally, we establish a platform to better understand the diversity of cap binding complexes and their control over the translatome. We focus on a poorly understood eIF4E1 family member, eIF4E3, and assess its consequences on cellular transformation. These projects aim to widen our appreciation and understanding of translation initiation, its regulation, and specialization under fluctuating environmental conditions.

Table of Contents

Acknowledgements:

Throughout my Ph.D. career I have had an amazing network of guidance and support, and I cannot fully express how thankful I am to have had the pleasure of working with such an amazing group of people. I would like to thank my Ph.D. advisors, Dr. Cate and Dr. Ingolia, for their guidance, support, patience, belief in me, and for providing me with two incredible lab homes. You both have contributed immensely to my scientific growth and I cannot thank you enough. I would like to thank rest of my thesis committee members Dr. Chris Chang and Dr. Britt Glausinger, for their advice and insight.

Although all present and past members of the Cate and Ingolia labs have contributed to my scientific growth and in some manner, I would like to give an extra thanks to a few individuals. To Dr. Amy Lee, I have been very lucky to have you as a lab mentor and true friend. I thank you so much for all the advice and encouragement you have given me. To Luisa and Zuriah, you both are the core of my support system. From bay mate, to my Comal date, to bridesmaids, thanks for always being there for me. You both helped keep sane and motivated. To Wenfei, Audrey, Annsea, Fred, Rachel, Ryan, Kendra, Sam, Paige, and Lucas: you all have put up with my many questions and helped me through whatever problems I ran into. It has been a pleasure working with you and I am thankful to have you as my friends. To my undergraduate mentees, Daniel Srole and Maria Juarez, I thank you so much for your contributions to this research. It was great seeing you grow as scientists and I can't wait to read all your amazing papers to come. As Danny knows words are hard, so an extra thanks to him for taking the time to review all of my writing! To my collaborators, Chris Nicolai and Natalie Wolf, thank you for your advice and help with all of the mouse work, and to Lucas, Heather, and Paige for their help with ribosome profiling.

Lastly, I would not have been able to do any of this without the support of my family, SCU crew (Christine, Sean, Christina, Sam, and Connor), and meow meow. My grandparents truly instilled in me the importance of education, and I hope I did them proud. To my brother, thanks for always keeping me laughing and for that bio for dummies book. I do not know what I would have done without it. To my parents, I am forever thankful for your unconditional love, support, encouragement, and for always being there for me. To my husband Matt, I know I have put you through a lot during all of this, from quals to brain surgery, but thank you for never wavering and always being by my side. You kept me going when I was down and reminded me to celebrate all the little successes.

Chapter 1: A general review of translation initiation and key initiation factors that allow for specialized translation

Protein synthesis, along with its regulation, is fundamental to all aspects of life. This process of translation completes the conversion of information stored cryptically in the genome into essential protein products. Improper regulation of this process can alter the cell's ability to maintain homeostasis, and if severe enough, can eventually lead to cellular death. Notably, the dysregulation of protein synthesis is the molecular basis of various cancers and neurological disorders (Le Quesne, Spriggs, Bushell, & Willis, 2010). In order to maintain rapid control over gene expression and manage this resource-expensive process, protein synthesis is primarily regulated at the stage of initiation. Translation initiation has been shown to be the rate limiting step of this process, with only 0.5-3.6 initiations occurring per minute compared to elongation which has a rapid rate of 6 amino acid incorporations per second (Choi et al., 2018; Lareau, Hite, Hogan, & Brown, 2014; Voorhees & Ramakrishnan, 2013). This difference in rates provides a key window for the implementation of regulatory control by allowing for the precise ability to modulate the multiple functions and interactions of various translation initiation factors.

Overview of protein synthesis

The process of protein synthesis hinges upon the proper organization, assembly, and function of the ribosome in interaction with a mature mRNA transcript. For this to happen, nuclear pre-mRNA must undergo various post-transcriptional processes to confer stability, proper cytoplasmic localization, and assembly of the ribosome on the mRNA. This includes 5' m^7G capping at the first transcribed nucleotide, 3' cleavage and polyadenylation, splicing, and addition of other post-transcriptional modifications. The addition of the 5' cap occurs through a dimeric capping enzyme associated with RNA polymerase II and links a 7-methylguanylate (m^7G) to the first transcribed nucleotide (Colgan & Manley, 1997). The poly-A tail of mammalian transcripts is a string of 50-250 adenine residues added to the 3' end of the terminal exon (Jalkanen, Coleman, & Wilusz, 2014). In addition to their role in protecting mRNAs from degradation outside of the nucleus, both the 5' cap and poly(A) tail also act as key sites for translation factor interactions (Lodish H, 2000). As a final processing step, these immature capped and tailed RNAs undergo splicing to remove intronic regions and form mature mRNAs that are then exported from the nucleus. Once in the cytosol, mRNAs can undergo translation.

Translation occurs in four main phases: the initiation phase when the ribosome stably associates with the mRNA and fully assembles on the start codon, elongation when the peptidyl transferase reaction occurs, and then termination when the stop codon is recognized and the peptide chain is ejected from the ribosome. The final phase of this stepwise and catalytic process is ribosome recycling. At this point, the ribosome and other factors involved in translation are disassembled for use in future rounds of translation.

Assembly of a functional ribosome from recycled or newly synthesized components occurs via the joining of its two subunits, each composed of a mixture of RNA and proteins. The small subunit, 40S, is made up of numerous small ribosomal proteins (RPS) and the 18S rRNA (Browning & Bailey-Serres, 2015). During translation, the 40S reads the mRNA by stringing the transcript through three sites: the aminoacyl site (A), the peptidyl site (P), and the exit site (E) (Voorhees & Ramakrishnan, 2013). The large subunit, 60S, is composed of large ribosomal proteins (RPLs) and the 5S, 5.8S, and 25-28S rRNAs. This subunit is responsible for the catalysis of peptide bond formation (Doudna & Rath, 2002). The 40S and 60S subunits assemble to form the full 80S ribosome which scans the mRNA in a 5' to 3' manner.

Canonical translation initiation

Canonical translation initiation begins with the formation of the 43S pre-initiation complex (PIC) (Figure 1). After the recycling of intact 80S post-termination or idle 80S ribosomes into the small 40S and large 60S subunits, the 40S ribosomal subunit proceeds to be bound by the multifactor complex (MFC) composed of eIF1, eIF1A, eIF3, and eIF5 (Hinnebusch, 2014; Jackson, Hellen, & Pestova, 2010). Whether or not the factors comprising the MFC can assemble without prior interactions with the 40S remains unclear (Browning & Bailey-Serres, 2015; Hinnebusch, 2014). This interaction facilitates the subsequent binding of the Ternary complex (TC), composed of eIF2, GTP, and Met-tRNA^{imet}, resulting in the formation of the full 43S PIC. These interactions stimulate translation and engage with the ribosomal 40S subunit to prevent premature assembly with the large 60S subunit. This switch from a closed, scanning arrested state of the 40S to an open and competent one can be attributed to the conformational changes induced by the synergistic interactions with eIF1 and eIF1A. eIF1 binds and resides in the P site of the 40S while eIF1A binds the A and P site with its flexible N- and C-termini.

During the assembly of the 43S PIC, exported mRNAs interact with the eIF4F complex and PABP (poly-adenosine-binding protein) in the cytoplasm. eIF4F is formed by the assembly of three core proteins, eIF4E, eIF4A, and eIF4G, which bridge the interaction between the 43S PIC and mRNA. eIF4E recognizes and binds the m^{7}G cap at the 5' end of mRNAs (Sonenberg & Hinnebusch, 2009). eIF4G, a large scaffolding protein, binds eIF4E and organizes other initiation factors such as eIF4A and eIF3 facilitating the docking of the 40S onto the mRNA (Sonenberg & Hinnebusch, 2009). eIF4G and its interaction with PABP bound to the 3' poly-(A) sequence promotes the circularization of the mRNA, termed the close loop formation, and stimulates translation (Browning & Bailey-Serres, 2015). eIF4A, an ATP-dependent DEAD-box RNA helicase, processively unwinds cap-proximal secondary structure found in the 5'-UTR of mRNAs (Sonenberg & Hinnebusch, 2009). This process is stimulated by the binding of RNA-binding proteins eIF4B and eIF4H, as well as eIF4G. Free of hindrance, the mRNA attached 43S PIC scans the mRNA in a unidirectional manner until reaching the initiation codon (AUG) preferentially in an optimal sequence context referred to as the Kozak sequence (GCCACC**AUG**G)(Kozak, 1989). At this point the 43S PIC is now

referred to as the 48S initiation complex (IC) and is switched to a closed confirmation through a cascade of initiation factor releases. Simultaneously to proper start codon recognition, eIF1 is released, GTP is hydrolyzed by eIF2 in an eIF5-stimulated manner, and in an additional GTP dependent reaction eIF5B displaces eIF2-GDP, eIF3, and eIF5 providing an open surface for the 60S to dock (Pisareva & Pisarev, 2014). This prevents further scanning, locks the 48S onto the complementary codon to the anticodon of the Met-tRNA$_i$, and allows for the full formation of the elongation competent 80S. Interestingly, not all translation initiation factors solely aid in during the initiation phase. Recently, eIF3 has been implicated in interacting with the 80S ribosomes during the early elongation process (Bohlen, Fenzl, Kramer, Bukau, & Teleman, 2020; Lin et al., 2020; Wagner et al., 2020; Wolf, Lin, Duan, & Cheng, 2020). This highlights the depth of roles eIF3 and potentially other initiation factors play throughout the process of translation.

Diversification of cap binding proteins

eIF4E1 was first discovered in 1978 through cap crosslinking experiments in rabbit reticulocyte lysate and is now considered the most prominent and highly conserved cap binding protein in eukaryotes (Sonenberg, Morgan, Merrick, & Shatkin, 1978). Through various biochemical and structural follow up studies, the interaction between eIF4E and the methylated guanosine cap has been described in detail (Table 1). The cap is grasped by a "cupped hand" shape conformation of eIF4E with eight β-pleated sheets at the palm and three α-helices supporting the structure at the back (Joshi, Lee, Maeder, & Jagus, 2005). This positions two highly conserved aromatic tryptophan residues, W56 and W102 for *H. sapiens*, in proper proximity and orientation for π-π stacking with the aromatic guanine in the cap (Joshi et al., 2005). A third tryptophan (W166 for *H. sapiens*) interacts with the N^7 methyl moiety of the cap (Altmann, Edery, Sonenberg, & Trachsel, 1985; Joshi et al., 2005; H. Ueda et al., 1991). The binding of eIF4E to the cap is further supported by hydrogen bonding, for example between E-103 and the guanine residue, Van der Waals, and electrostatic interactions (Joshi et al., 2005).

This binding process is tightly regulated by several factors across different pathways. The two foremost mechanisms of regulation are post-translational and are governed by mTORC1/ 4E-BP and ERK/MNK phosphorylation. In mammals there are three eIF4E-binding proteins (4E-BP 1-3) all of which act as competitive inhibitors to the eIF4E:eIF4G interaction and ultimately act as a blockade for eIF4F and 80S assembly (Mamane et al., 2004). In an unphosphorylated, or hypophosphorylated, state 4E-BPs can bind to eIF4E at the same consensus sequence YxxxxLΦ (where Φ is a hydrophobic residue) that eIF4G binds to, ultimately capturing and preventing ribosomal assembly on these transcripts (Joshi et al., 2005; Kamenska, Simpson, & Standart, 2014). The ability of 4E-BPs to interact with eIF4E is disrupted when 4E-BPs become hyperphosphorylated. This phosphorylation is carried out in an environmentally responsive manner by the shared downstream target of AKT and phosphoinositide-3 (PI3) kinase, mTOR, which phosphorylates 4E-BP and ultimately promotes translation (Mamane et al., 2004) . eIF4E can also be regulated through a direct phosphorylation

event. Here MNK, via the mitogen-activated protein kinase (MAPK) pathway, phosphorylates eIF4E at the conserved S209 residue near its C terminus (Wendel et al., 2007). The effects of this sole eIF4E phosphorylation are not fully resolved but have been implicated in modulating the strength of the eIFE4:m^{7}G cap interaction (Bramham, Jensen, & Proud, 2016; Wendel et al., 2007). It may also serve as a way to promote the translation of a specific subset of transcripts.

In the past two decades there has been a growing appreciation that eIF4E1 is not the sole cap binding protein within cells. There is now evidence of two various homologous proteins of eIF4E1 called eIF4E2 (4EHP-4E homologous protein) and eIF4E3 in mammalian cells, as well as a eIF4E1 variant specific to plants called eIFiso4E (Browning & Bailey-Serres, 2015; Joshi, Cameron, & Jagus, 2004) (Table 1). It is believed that these eIF4E1 variants have all arisen from a single early eIF4E gene that underwent various gene duplication events generating multiple structural classes and variants (Joshi et al., 2005). In mammalian cells, neither eIF4E2 nor eIF4E3 can compensate for the loss of eIF4E. As such, neither can fully interact with the entire eIF4F complex and the regulatory 4E-BPs. eIF4E2 is 28-30% identical to eIF4E1 and is believed to be ubiquitously expressed across all tissue types in a similar manner to eIF4E1(Joshi et al., 2004). It is normally found in lower abundance than eIF4E1, however eIF4E2 retains the ability to π-π stack with the m^{7}G cap structure but cannot not retain the ability to interact or bind to eIF4G (Joshi et al., 2004). This lack of binding to eIF4G prevents translation of eIF4E2 bound transcripts under normal cellular conditions. However, it was recently proposed that under hypoxic conditions eIF4E2 can drive translation by being recruited by HIF-2α/RBM4 and subsequently interacting eIF4G3 and eIF4A to form a hypoxic eIF4F complex (eIF4FH) (Melanson, Timpano, & Uniacke, 2017). eIF4E3 has ~25% identity and ~50% similarity with the two other eIF4E family members and has been shown to have tissue specificity (Joshi et al., 2004). Though eIF4E3 can bind the 5' cap, this interaction fails to occur in the canonical fashion. Lacking one of the conserved amino acids (W102), eIF4E3 instead relies on electrostatic and Van der Waals interactions from the C terminal tail to stabilize its interaction with the cap (Osborne et al., 2013). eIF4E3 fails to retain any interaction with 4E-BPs and lacks the MNK phosphorylation site S209 (Volpon, Osborne, Culjkovic-Kraljacic, & Borden, 2013). It is currently supported that eIF4E3 can bind eIF4G as it retains a majority of the eIF4G binding site. The only contradiction in the literature is a study by Osborne in 2013 that could not identify this eFI4G interaction *in vivo* using NIH 3T3 cells(Landon et al., 2014; Osborne et al., 2013). There are various isoforms of eIF4E3 between mammals. In mice there is only one unique isoform of eIF4E3, whereas in humans there are two. The longer isoform of eIF4E3 in humans is more similar to mouse eIF4E3, but contains an N terminal expansion sequence as well as substitutions along the protein that introduce polar or charged amino acid residues (Frydryskova et al., 2016). The shorter isoform is significantly truncated and lacks many of the residues needed to maintain the eIF4G interaction (Frydryskova et al., 2016). In mice eIF4E3 has been shown to repress translation of bound transcripts and compete away eIF4E1 mRNAs (Osborne et al., 2013).

An additional unique eIF4E variant is observed in higher plant-based species. Here, eIFiso4E along with eIFiso4G form the eIFiso4F complex. eIFiso4E has 45–50% identity at the amino acid level to plant eIF4E, has similar biochemical properties to eIF4E, and there is evidence that it can support general translation in plants (Combe, Petracek, van Eldik, Meulewaeter, & Twell, 2005). Though there is currently very little known about eIFiso4E and its *in vivo* role, it has been suggested that eIF4E and eIFiso4E interact with cellular mRNAs at varying levels, potentially serving as a way for the cell to regulate the translation of mRNA subpopulations (Browning & Bailey-Serres, 2015; Combe et al., 2005).

This cap binding protein diversity extends beyond eIF4E homologs. A prime example of this is LARP1, La-related protein 1, which has been shown to regulate the translation of specific transcripts during stress conditions in a cap dependent manner. Upon nutrient starvation conditions, normally inactive LARP1 dissociates from mTORC1 and interacts with 5' terminal oligopyrimidine (5' TOP) mRNAs, repressing their translation (Lahr et al., 2017). These TOP motifs are defined by a cytosine immediately downstream of the 5' m^7G cap followed by and additional track of 7-14 oligopyrimidine residues (Meyuhas, 2000). 5' TOP mRNAs primarily encode ribosomal proteins, translation factors, and RNA binding proteins. LARP1 recognizes and binds the 5' m^7G cap and the immediately adjacent 5' TOP motif (Lahr et al., 2017). This binding serves as a structural hindrance preventing the assembly of eIF4E and the rest of the eIF4F complex on the mRNA, ultimately preventing translation. However, this is not the only proposed role of LARP1 in translation. Contrary to serving as a translation repressor, LARP1 has also been shown that in cancerous cells to actually interact and promote the translation of non-TOP mRNAs in a poorly understood manner (Berman et al., 2020).

Non-Canonical translation initiation

Under cellular stress, canonical translation is generally restricted in order to save resources and energy. Current estimates suggest that translation itself accounts for 50% of the cell's energy usage (Godet et al., 2019). This general repression of translation in response to stress is usually governed by two main pathways: the mTOR/4E-BP pathway and integrated stress response pathway involving eIF2α. Under nutrient-deplete stress conditions mTOR is inactivated and no longer able to hyper-phosphorylate 4E-BP (Saxton & Sabatini, 2017). This allows 4E-BP to bind to eIF4E and displace eIF4G, ultimately limiting the amount of free and functional eIF4E to promote cap-dependent translation (Z. Wang et al., 2019). A wide range of stress conditions activate the integrated stress response, which phosphorylates eIF2α through an extensive signal cascade. This phosphorylation event catalyzed by four serine/threonine (S/T) eIF2α kinases blocks the exchange of GDP to GTP in eIF2 (Pakos-Zebrucka et al., 2016). Because eIF2:GDP can no longer be properly recycled and incorporated into a new ternary complex, global translation is severely diminished.

Stress resulting from nutrient depletion, hypoxia, and viral infection, among many other stimuli, each drastically alters the gene expression landscape. However, not all translation is down-regulated by these conditions. These variations in the translatome

provide insight into alternate methods of translation that either modify traditional cap-dependent processes or in fact completely bypass the need for the cap. While there are many mRNA-specific mechanisms to regulate translation, I will be focusing on IRESs (Internal Ribosome Entry Sites) and eIF3-based translation. These two mechanisms regulate the docking of the 40S ribosome onto mRNA transcripts in a manner completely distinct from canonical translation

IRES translation

First discovered in viral transcripts, IRESs are highly structured *cis*-acting elements found most prevalently in the 5' UTRs of transcripts and serve as a site of internal ribosome recruitment (Godet et al., 2019; Jang et al., 1988). When these sites are present, translation initiation is not dependent on 5' m^{7}G cap recognition. Since their initial discovery IRESs have been identified in many other viral transcripts. These elements in viral transcripts allow translation of these typically uncapped RNAs to proceed when the host's general cap dependent translation has been shut down. Currently there is no identified universal IRES motif (Martinez-Salas, Francisco-Velilla, Fernandez-Chamorro, & Embarek, 2017). Diversity in IRES sequences could contribute to the various assortment of pathways that lead to 40S docking. The exact mechanism of function of an IRES is usually determined by its structural organization and can vary significantly between different types of IRESs. The two common methods for ribosomal docking occur through either RNA-RNA interactions directly between the 40S ribosome and the IRES or by RNA-protein interactions (Martinez-Salas et al., 2017). These proteins can be eukaryotic translation initiation factors or other RNA binding proteins (RBPs) that can then recruit and position the 40S internally on the transcript. Once the 40S is anchored on the mRNA there is usually very little to no scanning before it identifies the appropriate start codon(Godet et al., 2019; Martinez-Salas et al., 2017). The exception to this is the case of IV or Intergenic region (IGR) IRESs (Godet et al., 2019). These were originally identified in cricket paralysis virus (CrPV) transcripts and do not require the presence of a start codon or initiator Met-tRNA for 80S assembly (Godet et al., 2019).

More recently IRES-like elements have been identified in cellular transcripts. It has been proposed that upwards of 10% of cellular transcripts can undergo cap-independent translation (Gritsenko et al., 2017). Cellular IRESs similarly do not contain any identifiable motifs (Godet et al., 2019). They tend to be less structured than viral IRESs and fail to contain enough similarity to even group into classes. Unlike most viral IRES-containing transcripts, the cellular mRNAs that feature IRESs are capped (Godet et al., 2019; Leppek, Das, & Barna, 2018). The prevailing theory behind this dual ribosome recruitment potential is that translation occurs in a traditional cap dependent manner under normal conditions, but under various developmental, tissue specific, or stress conditions, the 40S is recruited internally to maintain ribosome assembly and protein production of a subset of key genes (Godet et al., 2019; Leppek et al., 2018). Immunoglobulin heavy chain-binding protein (BiP) was the first cellular transcript reported to have an IRES. BiP is involved in binding and scavenging misfolded proteins as well as aiding in promoting proper protein folding (Cho et al., 2007). This *BiP* IRES

was shown to maintain BiP translation under viral infection and heat stress (Macejak & Sarnow, 1991). Cellular IRESs have been shown to be crucial to development. Four *HOX* mRNAs, belonging to a family of homeobox genes, were identified to contain these internal ribosome recruitment sites. These genes are master regulators of development and tissue patterning. Knockout studies in mice involving the systematic removal of these IRES elements resulted in developmental defects (Xue et al., 2015). It was also shown that the HOX IRESs were coupled with translation inhibitory elements (TIEs) in this system (Xue et al., 2015). These elements impede and circumvent cap dependent translation allowing for this IRES-based translation to occur. There are many examples master regulator proteins such as VEGF and cMYC that have identified IRESs as well (Huez et al., 1998; Stoneley, Paulin, Le Quesne, Chappell, & Willis, 1998; Weingarten-Gabbay et al., 2016). Though cellular IRESs are not the sole method of translation initiation in eukaryotes, unlike viral IRESs, they rather act as a 'fail-safe' mechanism promoting translation in specific cellular conditions (Xue et al., 2015).

eIF3 and its contribution to specialized translation

Recently it has been appreciated that translation initiation factors themselves can contribute to specialized translation. eIF3 is the largest of the translation initiation factors at approximately 800 kD and composed of 13 subunits (eIF3a-m) in mammalian cells (Cate, 2017). eIF3 had previously been thought to serve solely a scaffolding role in translation initiation, organizing other initiation factors and the 40S for their recruitment to eIF4F-bound mRNAs (Hinnebusch, 2006). However, studies have now shown that eIF3 can go beyond this role as a scaffolding protein, and directly initiate and regulate the translation of a subset of cellular mRNAs (Figure 2).

eIF3 was initially shown to interact directly with RNA in the context of viral IRES translation. During HCV IRES translation, eIF3 serves to directly interact with the highly structured IRES itself recruiting the ribosome to the transcript and bypassing the need for the cap and the eIF4F complex (Collier et al., 2002). This capability of eIF3 to bind the viral IRES RNA is essential and relies upon a helix-loop-helix (HLH) motif in eIF3a (Sun et al., 2013). This suggested the possibility that direct RNA binding by eIF3 might also be feasible with cellular mRNAs. In a study done by Amy Lee in 2015, a genome-wide photoactivatable ribonucleoside-enhanced crosslinking and immunoprecipitation (PAR-CLIP) experiment demonstrated this to be the case (Lee, Kranzusch, & Cate, 2015). Four of the 13 eIF3 subunits (eIF3a, eIF3b, eIF3d, and eIF3g) were identified to cross link and directly interact with roughly 500 cellular mRNAs with functions ranging from the promotion of cellular proliferation to apoptosis (Lee et al., 2015). All of the various permutations of the four subunits binding to a single transcript were evident across the various mRNAs. This subset of transcripts predominantly contained eIF3-interacting regions within the 5' UTR (Lee et al., 2015). Following functional validation of two of the most significant PAR-CLIP hits (*c-JUN* and *BTG1*), eIF3 was shown to either activate or repress the translation of these mRNAs in a transcript-specific and cap-dependent manner (Lee et al., 2015). The cap dependence makes regulation by eIF3 on cellular mRNAs functionally distinct from viral IRES-like mechanisms highlighted in HCV IRES translation. Regulation by eIF3 has since been shown to be important for

ferritin light chain translation (FTL), cell cycle-dependent translation of polypyrimidine tract-binding proteins (PTBPs) isoforms, and the activation of T cells (Arake de Tacca, Pulos-Holmes, Floor, & Cate, 2019; De Silva et al., 2020; Pulos-Holmes et al., 2019).

Subsequent work investigating eIF3-based activation of c-JUN led to the novel discovery that eIF3d possesses cryptic cap binding activity that can promote translation independent of eIF4E. Activation of c-JUN by eIF3 was shown to be cap dependent, but upon further analysis of the 48S composition, there was a surprising absence of the eIF4F complex (Lee, Kranzusch, Doudna, & Cate, 2016). Additionally, c-JUN translation was not inhibited with the mTOR inhibitor INK128, which would hinder translation of eIF4E-sensitive transcripts (Lee et al., 2016). Using both biochemical and structural analysis it was identified that eIF3d was able to interact with a mature methylated cap structure through a complex cup-shaped fold containing a positively-charged RNA-binding tunnel and a 'RNA gate' (Lee et al., 2016). This RNA gate structure forms an insertion that blocks the RNA binding tunnel. It is only after the full eIF3 complex has been recruited to the mRNA via specific stem loop structures that eIF3d can be put in an active cap-binding confirmation. This mechanism provides for an eIF3 specialized pathway for the translation of a specific subset of transcripts, and demonstrates another instance where canonical eIF4E binding is inhibited by cis-acting RNA structures.

eIF3 was also shown to promote cap-independent translation by binding N^6-methyladenosine (m^6A) containing 5'-UTRs under stress conditions. This reversible m^6A modification can be found throughout mRNA transcripts, and is the most abundant internal modification in mammals (Desrosiers, Friderici, & Rottman, 1974; X. Wang et al., 2015). In the context of the 3'-UTR and stop codons, these modifications were thought to both decrease mRNA stability through interactions with YTHDF2 (a m^6A reader) and also increase translation by promoting the closed loop formation through the RNA-independent recruitment of eIF3 by YTHDF1 (Sheth & Parker, 2003; X. Wang et al., 2014). However, in the specific context of the 5'-UTR, these modifications do not require recognition by YTH domain proteins to be acted upon, and eIF3 can instead serve as a direct reader. This eIF3: m^6A interaction, which requires only a single m^6A modification, is sufficient to recruit the 43S complex to the mRNA and drive translation (X. Wang et al., 2015; Wolf et al., 2020). These m^6A-induced ribosome engagement sites (MIRES) provide an additional mechanism to sufficiently promote translation in cap and eIF4F independent context, in addition to serving as a dynamic mechanism to rapidly respond to stress conditions via alterations in the translatome (Knuckles & Buhler, 2018).
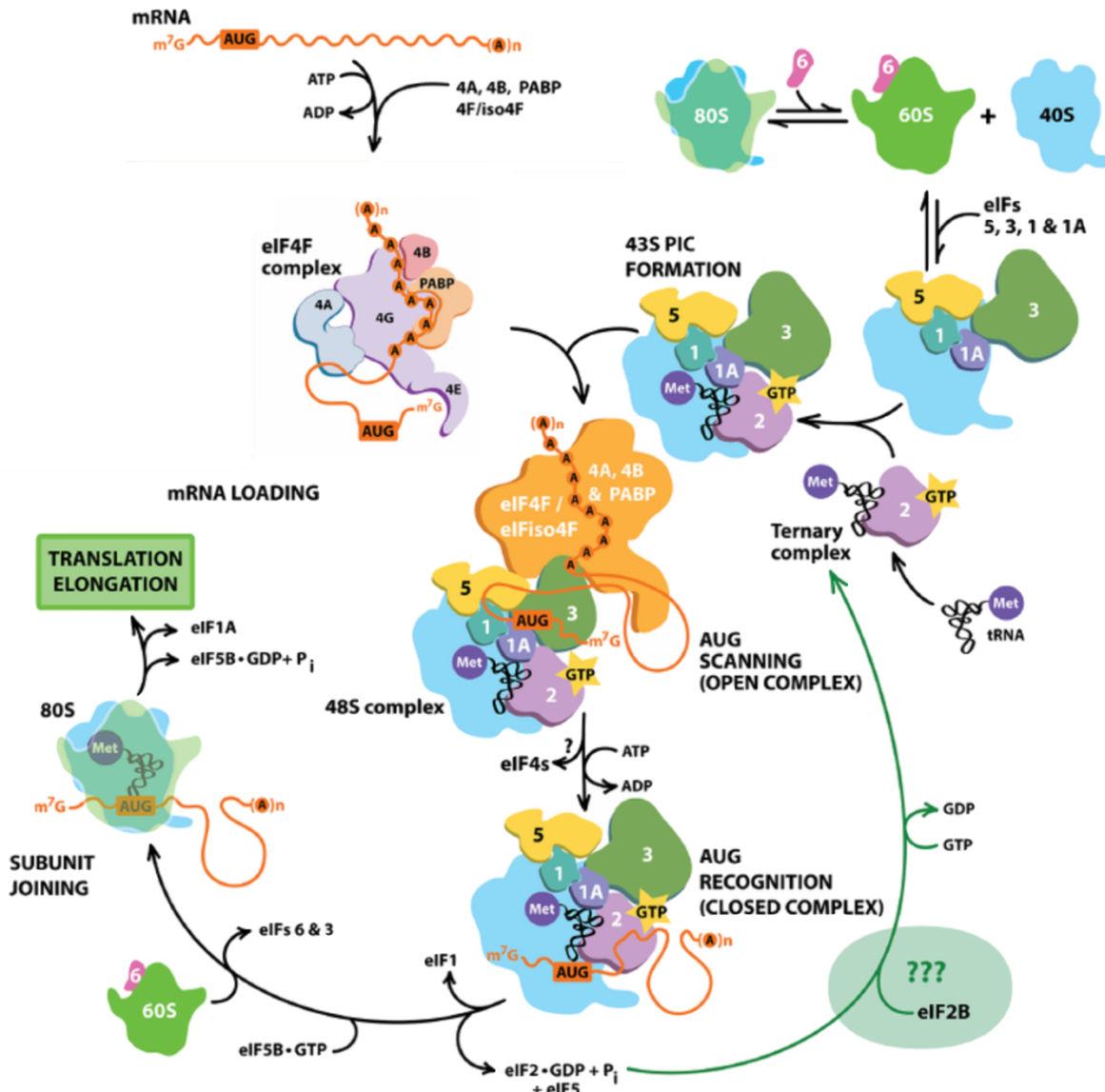
Figure 1. Eukaryotic translation initiation pathway. Figure adapted from (Browning & Bailey-Serres, 2015). Assembled 43S pre-initiation complex (PIC) binds to eIF4F complex bound mRNAs. Scanning proceeds across the mRNA until AUG recognition. Upon recognition, there is a release of multiple initiation factors from the complex that then facilitates the joining of the 60S subunit and the assembly of the 80S complex

Table 1: Functional and structural comparison of eIF4E1 and its homologs

| Member	Cap binding	Tissue expression	Percent identity to eIF4E1	Can interact with		Differences from eIF4E1
				eIF4G1	4E-BPs	
eIF4E1	π-π Stacking	Ubiquitous	100%	Yes	Yes	—————
eIF4E2	π-π Stacking	Ubiquitous	28-30%	No	Yes	• Can drive translation during hypoxia
eIF4E3	Van der Waals	Specific	~25%	Yes	No	• Has been shown to both repress and promote select translation • Levels have been reported to fluctuate with eIF4E1 activation
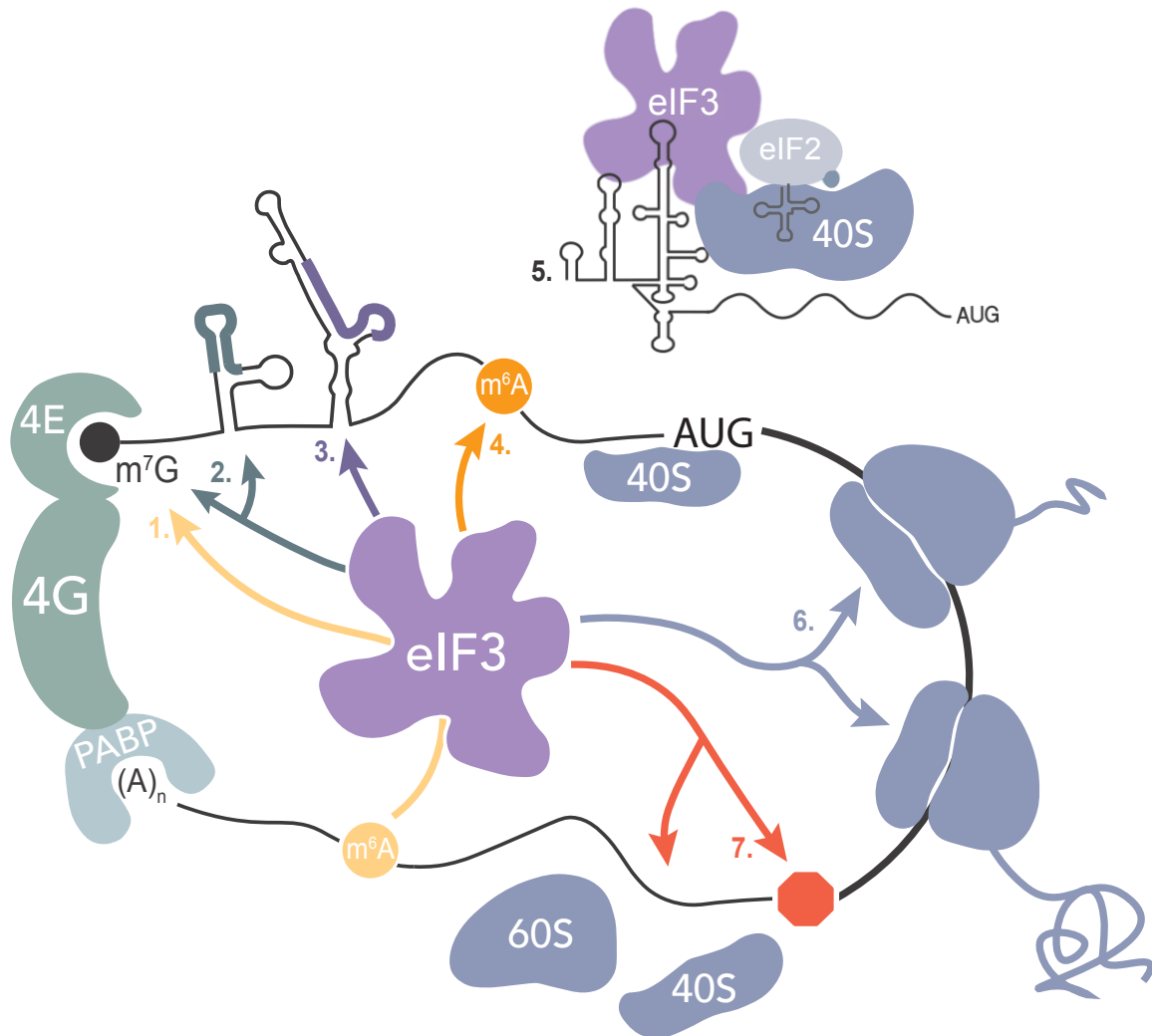
Figure 2: The roles of eIF3 during canonical and non-canonical forms of translation Figure adapted from (Wolf et al., 2020) This schematic represents seven different roles eIF3 serves during various forms of translation. (1) eIF3 recruitment driven by m6A recognition in the 3' UTR aids in the generating the closed loop formation. (2) eIF3 promotions the translation of a subset of transcripts through the direct interaction of eIF3 with the 5' m⁷G cap and highly structured regions in the 5' UTR (3) The interaction of eIF3 with highly structured regions in the 5' UTR can also function to repress the translation of a select mRNA transcripts. (4) eIF3 recruitment driven by m6A recognition in the 5' UTR promotes non-IRES cap-independent translation initiation. (5) eIF3 is vital for translation of certain viral mRNAs as eIF3 can directly interact with highly structured IRESs and promote translation initiation. (6&7) The role of eIF3 in translation extends beyond translation initiation and has been shown to directly interact with elongating 80S ribosomes and has been implicated in having roles in read-through events as well as and ribosome recycling.

Chapter 2: Repression of ferritin light chain translation by human eIF3

Pulos-Holmes MC, Srole DN**,** Juarez MG, Lee ASY, McSwiggen DT, Ingolia NT, Cate JHD. (August 2019) "Repression of ferritin light chain translation by human eIF3." *eLIFE* doi: 10.7554/eLife.48193

Abstract

A central problem in human biology remains the discovery of causal molecular links between mutations identified in genome-wide association studies (GWAS) and their corresponding disease traits. This challenge is magnified for variants residing in non-coding regions of the genome. Single-nucleotide polymorphisms (SNPs) in the 5' untranslated region (5'-UTR) of the ferritin light chain (*FTL*) gene that cause hyperferritinemia are reported to disrupt translation repression by altering iron regulatory protein (IRP) interactions with the *FTL* mRNA 5'-UTR. Here, we show that human eukaryotic translation initiation factor 3 (eIF3) acts as a distinct repressor of FTL mRNA translation, and eIF3-mediated *FTL* repression is disrupted by a subset of SNPs in *FTL* that cause hyperferritinemia. These results identify a direct role for eIF3-mediated translational control in a specific human disease.

Introduction:

Iron is essential for a spectrum of metabolic pathways and cellular growth. However, if not properly managed, excess iron catalyzes the production of reactive oxygen species (ROS). When iron is in the presence of oxygen, reactions such as the Fenton reaction: $Fe^{2+} + H_2O_2 \rightarrow Fe^{3+} + OH^- + OH$ can occur (Torti & Torti, 2002). The generated radicals then lead to lipid peroxidation, protein and DNA damage, and ultimately cell death (Palmer, Roberts, & Bero, 1994). To safeguard against these toxic effects, cells sequester iron in ferritin, a cage-like protein complex composed of a variable mixture of two structurally similar but functionally distinct subunits, the ferritin heavy chain (FTH) and the ferritin light chain (FTL) (Harrison & Arosio, 1996; Knovich, Storey, Coffman, Torti, & Torti, 2009). The FTH subunit catalyzes the simultaneous oxidization of two Fe^{2+} into two Fe^{3+}. The FTL subunit serves to stabilize the complex and maintain long-term storage of iron (Torti & Torti, 2002). This storage provides protection against the production of insoluable ferric oxide as well as preventing Fe^{2+} from reacting with oxygen species in the cell. Though ferritin is expressed in all mammalian tissues, the FTH: FTL ratio changes drastically between the different tissue types. The FTH:FTL ratio generally matches the requirement for iron mineralization and metabolism in each specific cell type. For example, tissues with low iron levels, such as the heart, are FTH rich with ratios centering around 10 FTH to 1 FTL, whereas tissues that manage high iron levels, such as the liver, are generally FTL rich with ratios around 1 FTH to 7 FTL (Harrison & Arosio, 1996).

To maintain iron homeostasis, the expression of both ferritin subunits in mammals is regulated post-transcriptionally by iron regulatory proteins (IRP1 and IRP2) that bind a highly conserved RNA hairpin called the iron responsive element (IRE), located in the 5'-UTRs of *FTL* and *FTH1* mRNAs (Figure 1A and B) (Theil, 1994; Wilkinson & Pantopoulos, 2014). Under low iron conditions IRP1 and IRP2 bind the IRE, causing a structural hinderance that prevents association of the 40S, and ultimately inhibit translation. In response to high iron conditions or an increase in the LIP, binding of these IRP proteins to the IRE is blocked and translation can occur normally (Gregory J. Anderson, 2012). Under these high iron conditions, IRP1 is bound by an iron sulfur cluster generated in the mitochondria and serves its moonlighting role as cytosolic aconitase while IRP2 is targeted for proteasomal degradation. It has also been proposed that Fe^{2+} can directly interact with the IRE and cause a dynamic shift in the 5'-UTR structure, ultimately altering the ability of IRP to bind to the IRE (Khan, Walden, Theil, & Goss, 2017; Ma et al., 2012).This has yet to be demonstrated *in vivo*. This is SNPs or deletions in the 5'-UTR that disrupt IRP- IRE interactions are thought to be the primary cause of hereditary hyperferritinemia cataract syndrome, a condition involving an abnormal buildup of serum ferritin in the absence of iron overload (Cazzola et al., 1997).

Although the IRP-IRE interactions have been considered to be the sole post-transcriptional means of regulating ferritin expression, recent studies have provided strong evidence that other presently unknown factors may provide another layer of regulation during *FTL* translation. For example, the *FTL* subunit composition of ferritin is

altered in response to environmental factors such as hypoxia (Sammarco, Ditch, Banerjee, & Grabczyk, 2008). We recently found that eIF3 can function beyond its scaffolding role in general translation initiation by acting as either an activator or repressor of translation in a transcript-specific manner (Lee et al., 2015; Lee et al., 2016).This regulation occurs through interactions with primarily 5'-UTR RNA structural elements (Lee et al., 2015). Notably, we found that *FTL* mRNA cross-links to eIF3 (Lee et al., 2015), but the role eIF3 plays in regulating *FTL* translation has not been established.

Here, we report a previously unknown mode of *FTL* translation regulation with a direct link to disease-related genetic mutations. We show that eIF3 binds to human *FTL* mRNA by means of sequences in the 5'-UTR immediately adjacent to the IRE, and provides additional regulation of *FTL* translation independent of IRP-IRE. After using CRISPR-Cas9 genome editing to delete the endogenous eIF3 interaction site in *FTL*, we monitored direct phenotypic responses of cells under normal and iron modulated conditions. Lastly, we used competitive IRP binding assays to explore the potential role of eIF3 in hyperferritinemia. These experiments reveal that eIF3 acts as a repressor of *FTL* translation, and disruption of eIF3 interactions with *FTL* mRNA due to specific SNPs in the *FTL* 5'- UTR likely contributes to a subset of hyperferritinemia cases.

Results

Identification of the eIF3-FTL mRNA interaction site

      In order to understand the functional effect of the interaction between eIF3 and *FTL* mRNA, we utilized Renilla luciferase (rLuc) reporter mRNAs in which the 5'-UTR from *FTL* was placed upstream of the Renilla coding sequence (Figure 1C). To measure the importance of the *FTL* mRNA region identified by PAR-CLIP, various mutations were introduced into the *FTL* 5'-UTR to disrupt eIF3 binding (Lee et al., 2015). The eIF3 binding site on the 5'-UTR of *FTL*, as determined by PAR-CLIP, spans a 24 nucleotide sequence that overlaps with the last five nucleotides of the annotated sequence of the *FTL* IRE (Figure 1—figure supplement 1). Notably, no eIF3 cross-linking site was observed in the 5'- UTR of the mRNA encoding *FTH1*, which shares the structurally conserved IRE, but not adjacent sequence features (Figure 1—figure supplement 1B) (7). The removal of the eIF3 interaction site dramatically increased translation of rLuc when compared to the full length wild type *FTL* 5'-UTR, 38-fold when the PAR-CLIP defined sequence was deleted (ΔPAR, nucleotides 53–76) and six fold in a deletion that maintained the full IRE sequence (eIF3 repressive element, Δ3RE, nucleotides 58–90) (Figure 1D and E, Figure 1—figure supplement 1D) (Theil, 2015). These results suggest that eIF3 binding to the *FTL* 5'-UTR represses *FTL* translation.
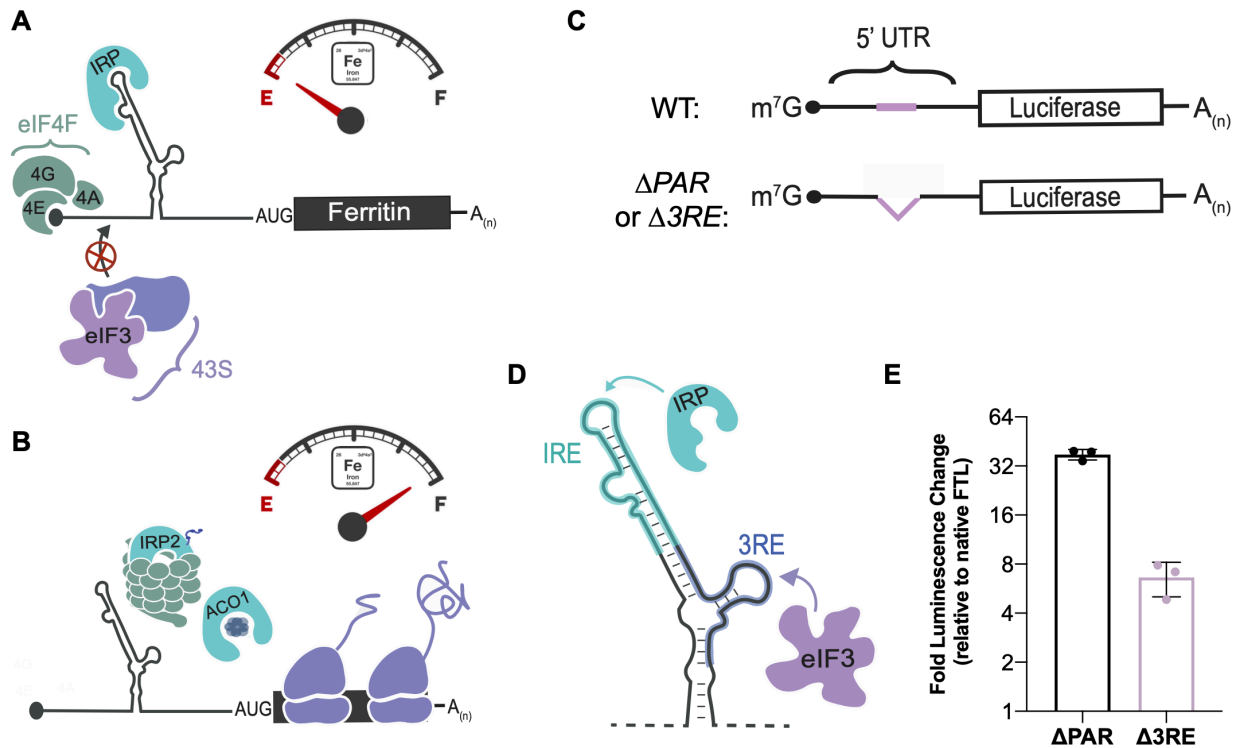
Figure 1. Post-transcriptional regulation of *FTL* mRNA.

(A, B) Iron-responsive regulation mediated by binding of Iron Response Proteins (IRPs) to Iron Response Element (IRE) RNA structures in the 5'-UTR in (A) low-iron conditions and (B) high-iron conditions. In high iron, IRP2 is degraded by the proteasome, whereas IRP1 binds an iron-sulfur cluster to form the enzyme Aconitase (ACO1). (C) General schematic of the luciferase reporter mRNAs. The eIF3 PAR-CLIP site in *FTL* mRNA spans nucleotides 53–76 (Lee et al., 2015) and the 3RE region spans nucleotides 58–90. (D) Schematic of the IRP and eIF3 interaction sites on the experimentally-determined secondary structure of *FTL* mRNA (Martin et al., 2012). (E) Luciferase activity in HepG2 cells transfected with luciferase reporter mRNAs 6 hr post transfection, normalized to luciferase luminescence from mRNA with wild-type *FTL* 5'-UTR. The results are for three biological replicates with error bars representing the standard deviation of the mean.
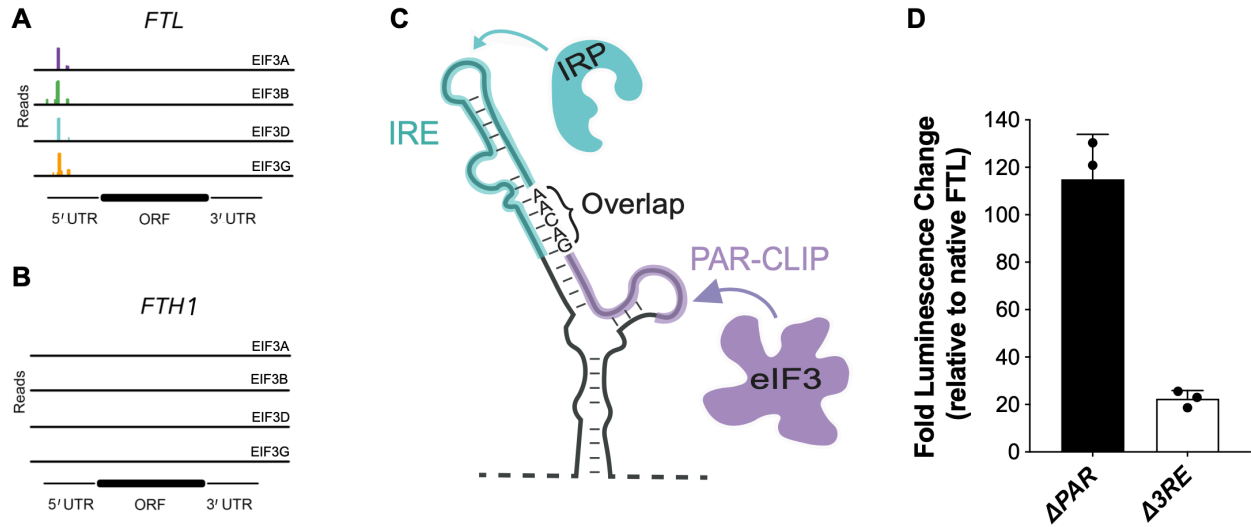
Figure 1—figure supplement 1 Sites of eIF3 interaction with *FTL* and *FTH1* mRNAs.

(**A, B**) eIF3 PAR-CLIP cluster identified for (**A**) *FTL* but missing in (**B**) *FTH1* (Lee et al., 2015). (**C**) Mapping of the IRP and PAR-CLIP derived eIF3 interaction sites on the secondary structure of the 5'-UTR in *FTL* mRNA, determined by chemical probing (Martin et al., 2012). The overlap of the extended IRE and the PAR-CLIP site spans nucleotides 53–57. (**D**) Luciferase activity in HepG2 cells transfected with luciferase reporter mRNAs 12 hr post transfection, normalized to luciferase luminescence from mRNA with wild-type *FTL* 5'-UTR. The results are of three biological replicates with error bars representing the standard deviation.

Decoupling the repressive role of eIF3 on *FTL* mRNA from that of IRP

Due to the close proximity between the eIF3 interaction site and the *FTL* IRE, accompanied by the fact that the 5'-UTR of *FTL* is prone to large-scale structural rearrangements (Martin et al., 2012), we tested whether the derepression observed in the ΔPAR and Δ3RE mRNAs is a direct result of altering eIF3 binding and not due to disrupting the IRE-IRP interaction. To evaluate the effect of the deletions (ΔPAR, Δ3RE) on IRP binding, we carried out RNA-electrophoretic mobility shift assays with near-IR-labeled *FTL* 5'-UTR RNA and recombinant IRP1. As expected, IRP1 bound to the wild type 5'-UTR of *FTL* (Figure 2A). IRP1 also bound the Δ3RE RNA, but failed to bind efficiently to the ΔPAR RNA (Figure 2A). The loss of IRP1 binding to ΔPAR RNA could be attributed to disrupted RNA folding, or to the importance of the region of overlap between the IRE and the PAR-CLIP defined eIF3-binding site (Figure 1—figure supplement 1C). We further quantified IRP binding to the Δ3RE 5'-UTR using RNA binding competition assays (Figure 2B and C, Figure 2—figure supplement 1). IRP1 had only slightly attenuated binding to the Δ3RE 5'-UTR RNA when compared to the wild-type *FTL* 5'-UTR, suggesting that the alleviation of repression observed in the luciferase translation experiments for the Δ3RE mRNA (Figure 1E, Figure 1—figure supplement 1D) could be due to disruption of eIF3 binding.

To further ensure that the alleviation of repression of *FTL* translation by the Δ3RE mutation results primarily from disruption of eIF3-FTL binding and not IRE-IRP interactions, we modulated the location of the IRE in the 5'-UTR of *FTL*. It had been shown previously that moving the IRE in the *FTH1* 5'-UTR further than 60 nucleotides from the 5' m^{7}G-cap partially relieves IRP-dependent inhibition of *FTH1* translation (Goossen & Hentze, 1992). Inhibition is lost because bound IRP can no longer fully sterically block the assembly of the 43S preinitiation complex on the mRNA (Muckenthaler, Gray, & Hentze, 1998; Paraskeva, Gray, Schlager, Wehr, & Hentze, 1999). To further investigate if this holds for *FTL* mRNA, we used the *FTL* and Δ3RE luciferase reporter constructs and placed the characteristic C bulge of the IRE either 32 nucleotides away (native) or 70 nucleotides away (extended) from the 5'-cap (Figure 2D). As with *FTH1* mRNA (Goossen & Hentze, 1992), moving the IRE further from the 5'-cap partially derepressed translation of the *FTL*-based luciferase reporter (Figure 2E). Notably, overall translation was much higher from both Δ3RE mRNAs, even with partial removal of IRP-dependent repression due to the distance from the 5'-cap (Figure 2E). This cap position-independent derepression is unique to *FTL* as the 3RE region is not conserved in the *FTH1* 5'-UTR. Furthermore, combining the Δ3RE mutation with a mutation that disrupts IRP binding to the IRE entirely (Loop) (Cazzola et al., 1997) synergistically derepressed luciferase reporter translation (Figure 2F, compare Double to Loop and Δ3RE). We verified the mRNAs were equally stable during the 6 hr time courses (Figure 2—figure supplement 2), ensuring the observed phenotypic changes are caused by changes in translational regulation. The slight inconsistency in the amount of derepression observed with the double mutation (Figure 2F) and the extended Δ3RE mRNA (Figure 2E) may be due to the fact that the extension of the 5'-UTR from its native state does not completely abolish the repression of *FTL* mRNA translation by IRP, in contrast to the loop mutation which abolishes IRP binding

(Cazzola et al., 1997). Furthermore, it is not clear how the distance from the 5'-cap affects repression mediated by eIF3. Taken together, these results indicate that IRP-mediated inhibition of translation is maintained in the Δ3RE mRNA, and that eIF3 confers an additional level of repression beyond that which can be provided by IRP.

We used the luciferase reporter results in Figure 2F to formulate a mathematical model to determine whether eIF3 and IRP can bind and regulate *FTL* mRNA simultaneously (See Materials and methods for details). Such a model would be useful in conditions with different extents of iron-response regulation. We defined a system in which IRP and eIF3 do not bind the same mRNA. This leaves three possible states in which the *FTL* mRNA could exist: the fraction bound solely by IRP (x_1), the fraction bound solely by eIF3 (x_2), and the remainder of the mRNA which is unbound by either factor (x_3) (Figure 2—figure supplement 3). We further elaborated this model to include translation efficiency (y). Here we assume the mutations do not affect the translation efficiency of the unbound species (x_3), while the other two populations (x_1 and x_2) have translational efficiencies (y_1 and y_2) scaled between full repression ($y_n = 0$) and no repression ($y_n = 1$). Lastly, we assumed the mutations that disrupt binding shift the equilibrium of the total mRNA population between bound and unbound fractions of the alternate factor by some amount, either a for those affecting eIF3 binding or b for IRP binding. Using the translational output determined in Figure 2F, we find that the data are inconsistent with the model that eIF3 and IRP cannot bind the same mRNA. Rather, the data indicate that IRP and eIF3 likely act in cis on at least a fraction of the *FTL* mRNA.
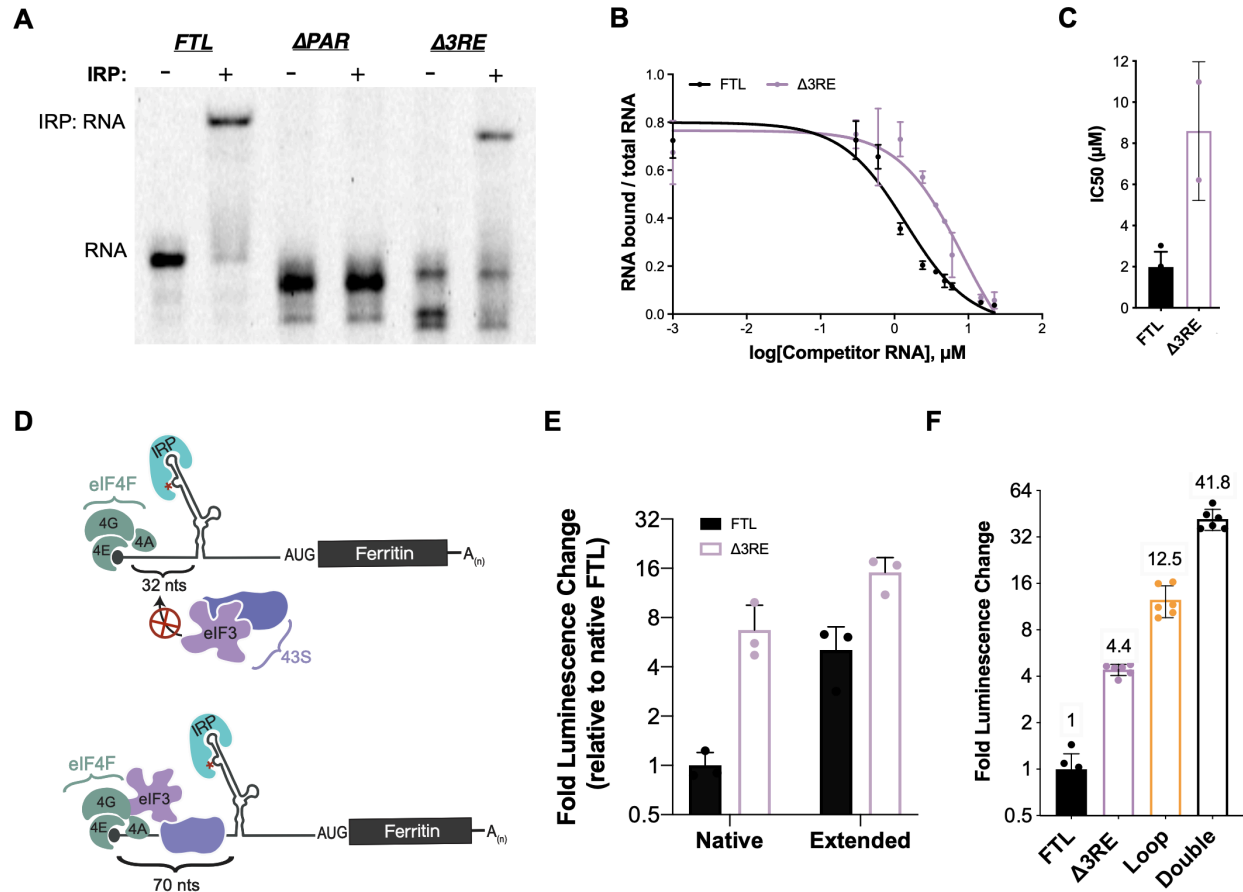
Figure 2. Maintenance of 5'-cap and IRP-dependent regulation of 3RE deletions in the *FTL* 5'-UTR.

(A) Representative native RNA gel shift showing recombinant IRP1 binding activity. Near IR (NIR) labeled RNAs corresponding to the full-length WT *FTL* 5'-UTR and the *FTL* 5'-UTR with deletions of the predicted eIF3 interaction site were incubated with recombinant IRP1 and resolved on a native polyacrylamide gel. (B) Dose-response curve of two RNA competition assays, based on gel shifts of NIR-labeled WT IRE-containing RNA, with WT or Δ3RE RNAs serving as cold competitors. Fold excess of competitors extended up to 75,000x. Error bars represent standard deviations for each concentration of competitor. (C) Calculated IC_{50} values using Prism 7 of the various competitor RNAs, based on the data in (B), with error bars representing the standard deviation from the mean IC_{50} value. N.A., the IC_{50} value could not be determined for the Loop mutant due to lack of any detectable competition. (D) Schematics showing the effect of increasing the distance of the IRE from the 5'-cap on IRP regulation of translation initiation (Goossen & Hentze, 1992; Muckenthaler et al., 1998). The characteristic C (C18 in the wild-type context) is denoted by an asterisk. (E) The luciferase activity of HepG2 cells transfected with mRNAs containing the native and extended spacing between the 5'-cap and IRE, with or without the 3RE site, normalized to the luciferase luminescence of cells transfected with WT *FTL* mRNA with native spacing from the 5'-cap. The values are from cells that have been harvested 6 hr post-

transfection. The results are from three biological replicates, with error bars representing the standard deviation of the mean. (F) The luciferase activity of HepG2 cells transfected with mRNAs containing the native and various combinations of eIF3 (Δ3RE) and IRP (Loop, A15G/G16C) disrupting mutations in HepG2 cells, normalized to the luciferase luminescence of cells transfected with WT *FTL* mRNA with native spacing from the 5'-cap. Double represents an mRNA construct that contains both the Loop and Δ3RE mutations. The results are from six independent transfections, with error bars representing the standard deviation of the mean.
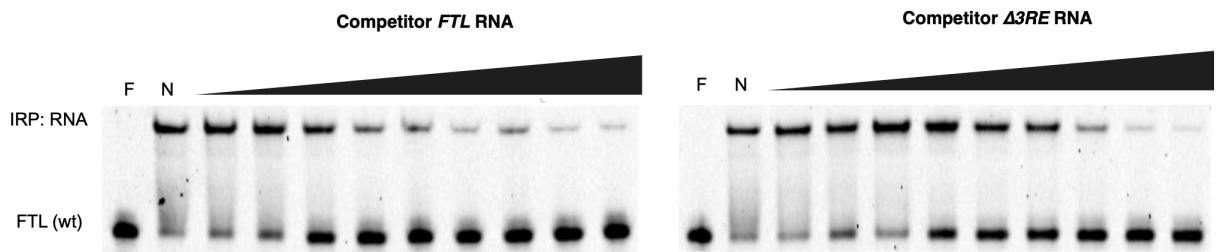
Figure 2—figure supplement 1 Native gels resolving RNA-IRP1 complexes formed after competition experiment.

Near IR (NIR) labeled RNA corresponding to the full-length WT *FTL* 5'-UTR were incubated with recombinant IRP1 and increasing molar excess concentrations of unlabeled competitor *FTL* or Δ*3RE* RNA (1000x, 2000x, 4000x, 8000x, 12,000x, 16,000x, 20,000x, 50,000x, 75,000x), as indicated. F, lane with only NIR-labeled *FTL* RNA; N, no addition of competitor RNA to the NIR-RNA-IRP1 complex.
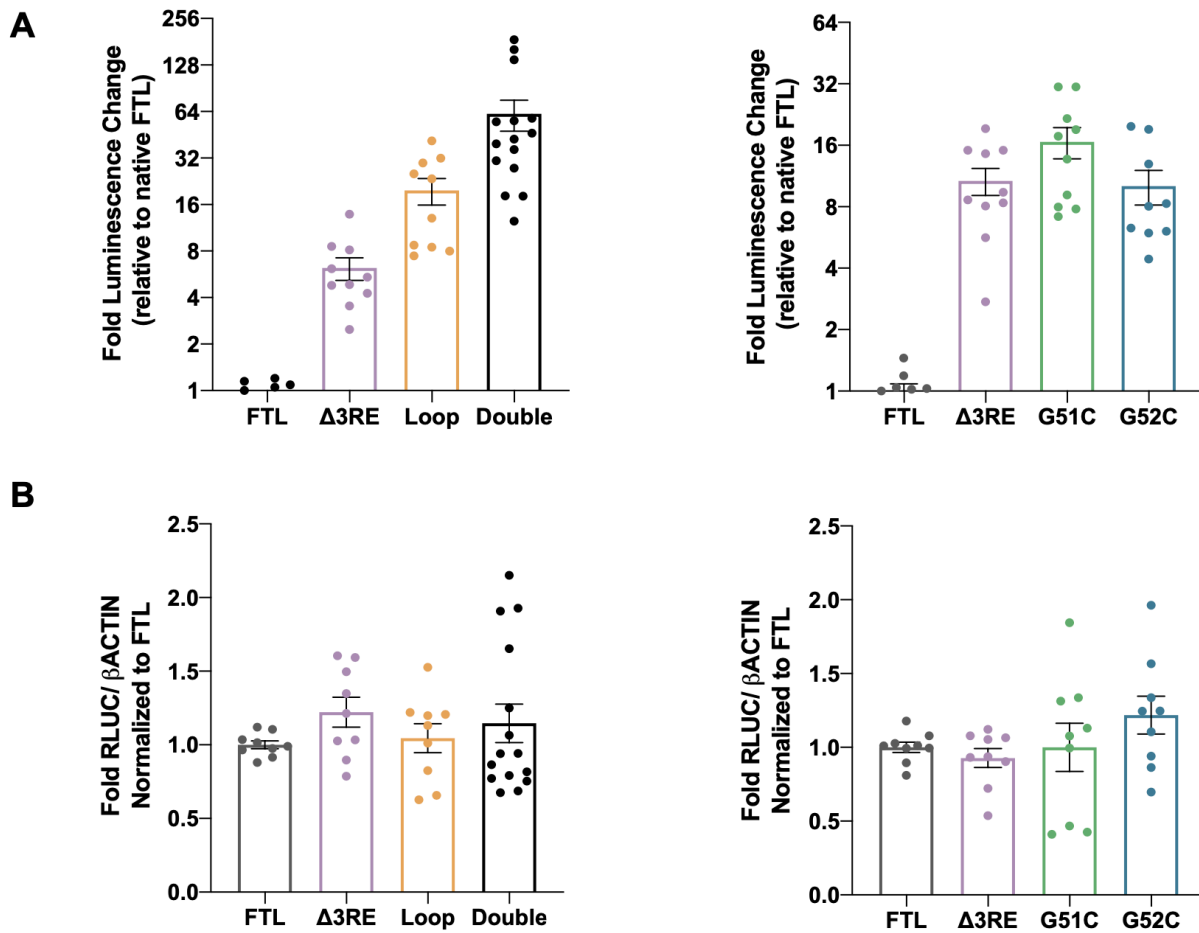
Figure 2—figure supplement 2 Luciferase readouts and mRNA stability during 6 hr mRNA transfections.

(A) Luciferase activity of HepG2 cells transfected with mRNAs encoding the WT *FTL* 5'-UTR or various mutant mRNAs. The first graph shows experiments with the Δ3RE, Loop (A15G/G16C), and Double mutants, while the second graph shows experiments with the hyperferritinemia mutations (G51C and G52C), normalized to WT *FTL* reporter luciferase luminescence. The results are from nine biological replicates with error bars representing the standard error of the mean. (B) RNA extraction and RT-qPCR of cells harvested at 6 hr post-transfection with the various luciferase reporters.
The *ACTB* mRNA was used as a control to normalize across samples. Error bars represent the standard error of the mean for three biological replicates, with three technical replicates each.
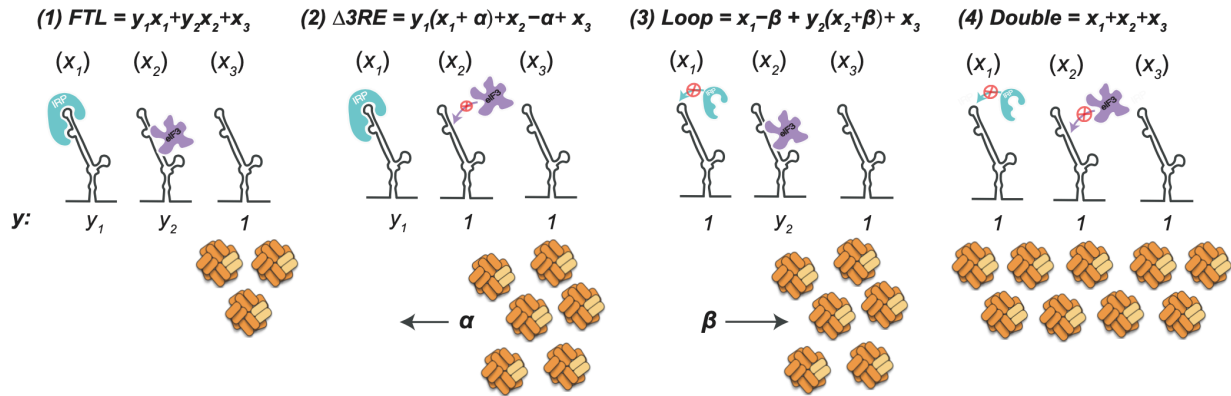
(1) FTL = $y_1x_1+y_2x_2+x_3$ **(2) Δ3RE = $y_1(x_1+\alpha)+x_2-\alpha+x_3$**   **(3) Loop = $x_1-\beta + y_2(x_2+\beta)+x_3$**   **(4) Double = $x_1+x_2+x_3$**

(x_1) (x_2) (x_3) (x_1) (x_2) (x_3) (x_1) (x_2) (x_3) (x_1) (x_2) (x_3)

y: y_1 y_2 1 y_1 1 1 1 y_2 1 1 1 1

Figure 2—figure supplement 3 Mathematical modeling of IRP and eIF3 co occupancy on *FTL* mRNA.

Schematic for mathematical modeling based on luciferase activity shown in Figure 2F which demonstrates that IRP and eIF3 seem to work synergistically rather than exclusively. x_1 represents the fraction of *FTL* mRNA bound by IRP. x_2 represents the fraction of *FTL* mRNA bound by eIF3. x_3 represents the fraction of unbound *FTL* mRNA. The orange complexes at the bottom of the figure represent the ferritin complexes produced by the various mRNA pools. α and β represent a fraction of the previously bound mRNA populations x_2 and x_1 respectively.

Physiological response to loss of eIF3-dependent repression

To investigate the physiological response to the loss of eIF3-based repression, we genetically engineered either HEK293T or HepG2 cells to generate the Δ3RE mutation in the 5'-UTR in the FTL gene (Figure 3—figure supplement 1A–1C). Notably, we found that the Δ3RE mutation abolished the preferential interaction of eIF3 with *FTL* mRNA (Figure 3E,F). Furthermore, FTL protein production increased dramatically in the Δ3RE cell lines, as expected from removing the predicted eIF3 repressive element (Figure 3A, Figure 3—figure supplements 1D, 4A and 5A). Importantly, the increase in FTL protein levels was not due to increases in mRNA levels (Figure 3—figure supplement 2A), indicating that the derepression occurs post-transcriptionally. Interestingly, the increase in FTL levels occurs with a concurrent reduction in FTH levels (Figure 3B, Figure 3—figure supplements 4C and 5A). The decrease in FTH protein levels is also not due to changes in *FTH1* mRNA levels (Figure 3—figure supplement 2B).

To test whether IRP maintains its ability to dynamically regulate *FTL* translation, we treated the cell lines with either ferric ammonium citrate (FAC), an iron donor, or desferoxamine (DFO), an iron chelator, to increase or decrease iron levels, respectively. (Figure 3—figure supplement 3, Figure 3—figure supplement 4B and D, Figure 3—figure supplement 5A and B) (Schneider & Leibold, 2003). FTL levels in the Δ3RE cell lines responded to FAC and DFO treatment in a comparable manner to the unedited (WT) cell lines (Figure 3C–D, Figure 3—figure supplement 4B and D, Figure 3—figure supplement 5A and B), showing that the Δ3RE transcript retains IRP-dependent translational regulation in cells. This iron-responsive regulation is maintained even though the basal levels of FTL protein are much higher in the Δ3RE compared to WT cells (Figure 3D). FTH levels also respond to iron levels in both the WT and Δ3RE cells (Figure 3—figure supplement 3, Figure 3— figure supplement 4D, Figure 3—figure supplement 5B), with basal FTH levels reduced in the Δ3RE compared to WT cells.

To further ensure that IRP-mediated repression was maintained in the Δ3RE cell lines, we transiently transfected the WT and Δ3RE cell lines with plasmids encoding C-terminally FLAG-tagged IRP1. We then used FLAG immunoprecipitation followed by qPCR to determine whether IRP is bound to the edited *FTL* and other IRE containing mRNAs in vivo. We found that FLAG-tagged IRP bound *FTL* mRNA similarly in the wild type and Δ3RE cell line (Figure 3G). Intriguingly, *FTH1* mRNA was recovered at a considerably higher level in the Δ3RE cell line compared to wild-ßtype cells (Figure 3G), suggesting increased IRP binding. This increased binding of IRP to *FTH1* mRNA may explain the concurrent decrease in FTH abundance seen in Figure 3B. Notably, this increase in IRP binding to *FTH1* mRNA does not appear to be a simple mass action effect, as ferroportin levels–also regulated by an IRP-IRE interaction (Gregory J. Anderson, 2012)- are not altered in the Δ3RE cell line (Figure 3—figure supplement 5C). Taken together, these data further support the hypothesis that the observed derepression in the Δ3RE cells is due to the modulation of eIF3-based regulation of *FTL* translation, and not due to disruption of IRP-mediated regulation.

We proceeded to investigate whether the lack of eIF3-based repression of FTL translation and concomitant decrease in FTH protein levels had any effects on the assembled ferritin complexes. We purified the ferritin complexes from either wild-type HepG2 cells or the Δ3RE cell line using a fractional methanol precipitation protocol (Cham, Roeser, Nikles, & Ridgway, 1985). We observed that the ferritin complex in the Δ3RE cell line was far more stable than that isolated from wild-type cells. Without ferric ammonium citrate (FAC) treatment to stabilize the complex (Linder, 2013), ferritin purified from WT cells consistently degraded, unlike the stable complexes from the Δ3RE cell line (Figure 3—figure supplement 6). This implicates eIF3 in regulating the dynamics and stability of the ferritin complex, as FTL-enriched ferritin complexes have been shown to be more stable under a wide array of denaturing condition (Santambrogio et al., 1992). Taken together, these results support the hypothesis that removal of the eIF3 interaction site in the 5'-UTR of the FTL mRNA derepresses *FTL* translation and can have a dramatic effect on ferritin subunit composition in the cell.
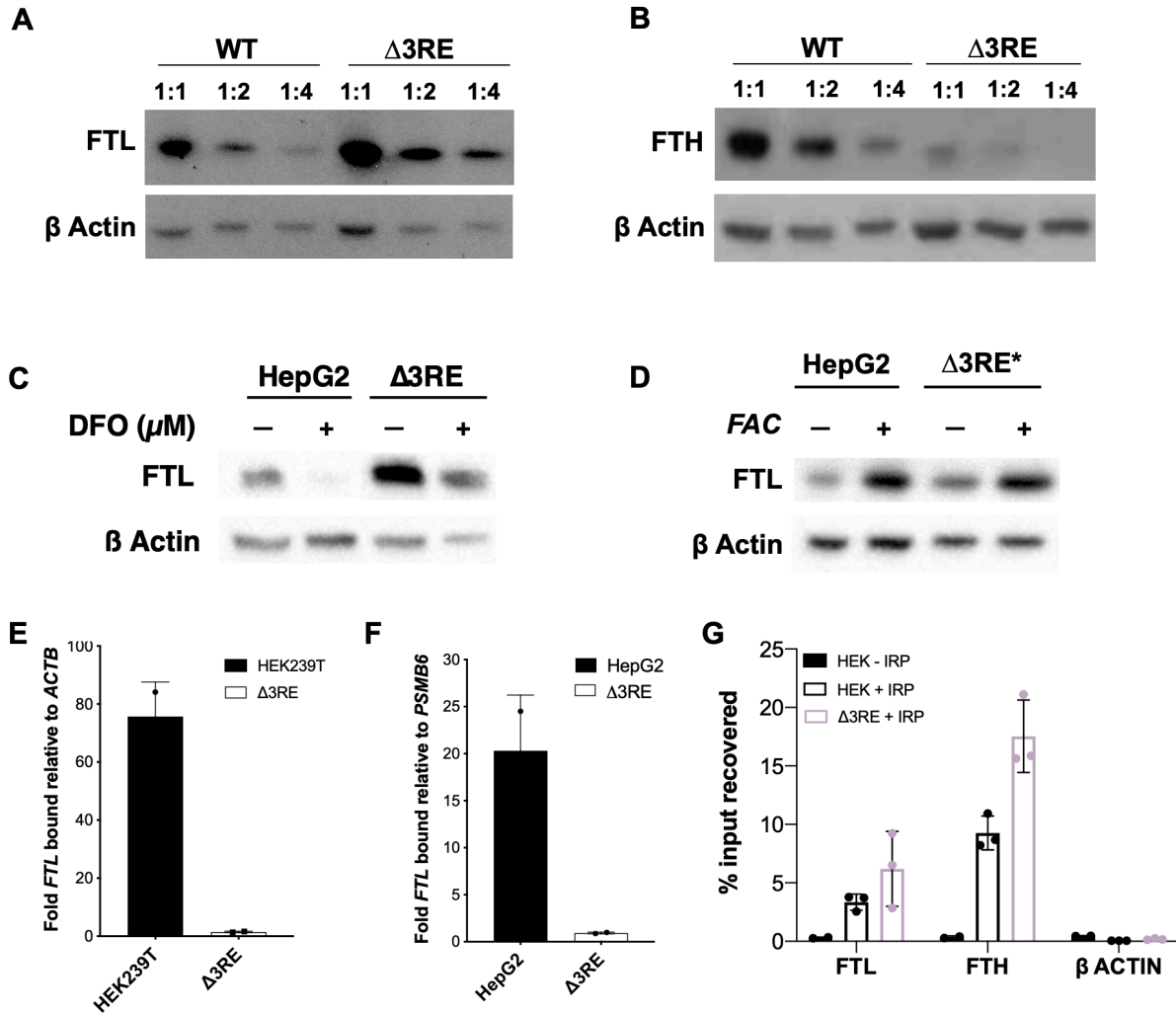
Figure 3. Physiological effects of the endogenous removal of the 3RE repressive element.

(A,B) Representative western blots of (A) FTL and (B) FTH levels in the edited (Δ3RE) and WT HepG2 cells under normal iron conditions. Serial dilutions were used in order to better visualize the significance of the changes in FTL and FTH protein abundance. (C, D) Representative western blots of FTL levels in the edited (Δ3RE) and WT HepG2 cells under high- or low-iron conditions. Iron donor treatment with FAC at 50 mg/mL for 24 hr, and Iron chelation treatment with DFO at 50 mM for 48 hr. The asterisk (*) indicates that lysate from Δ3RE cells were diluted two-fold, due to the higher overall levels of FTL in these cells. All FTL blots are representative of three or more replicates. (E, F) Determination of the preferential binding of eIF3 to *FTL* mRNA via EIF3B immunoprecipitation (IP) followed by RNA extraction and RT-qPCR in both (E) HEK293T and (F) HepG2 cell lines. Control mRNAs used to normalize IPs were PSMB6 and ACTB. Error bars represent the standard deviation of duplicate qPCR measurements from representative IP reactions. (G) Determination of IRP1 binding to *FTL* mRNA in WT (HEK + IRP) and Δ3RE (Δ3RE + IRP) HEK293T cells via FLAG

immunoprecipitation (IP) followed by RNA extraction and RT-qPCR. The ACTB mRNA was used to control for nonspecific binding to FLAG-tagged IRP. HEK – IRP reflects cells that were not transiently transfected, but were carried through the IP and following experiments. Error bars represent the standard deviation for triplicate measurements from representative IP reactions.
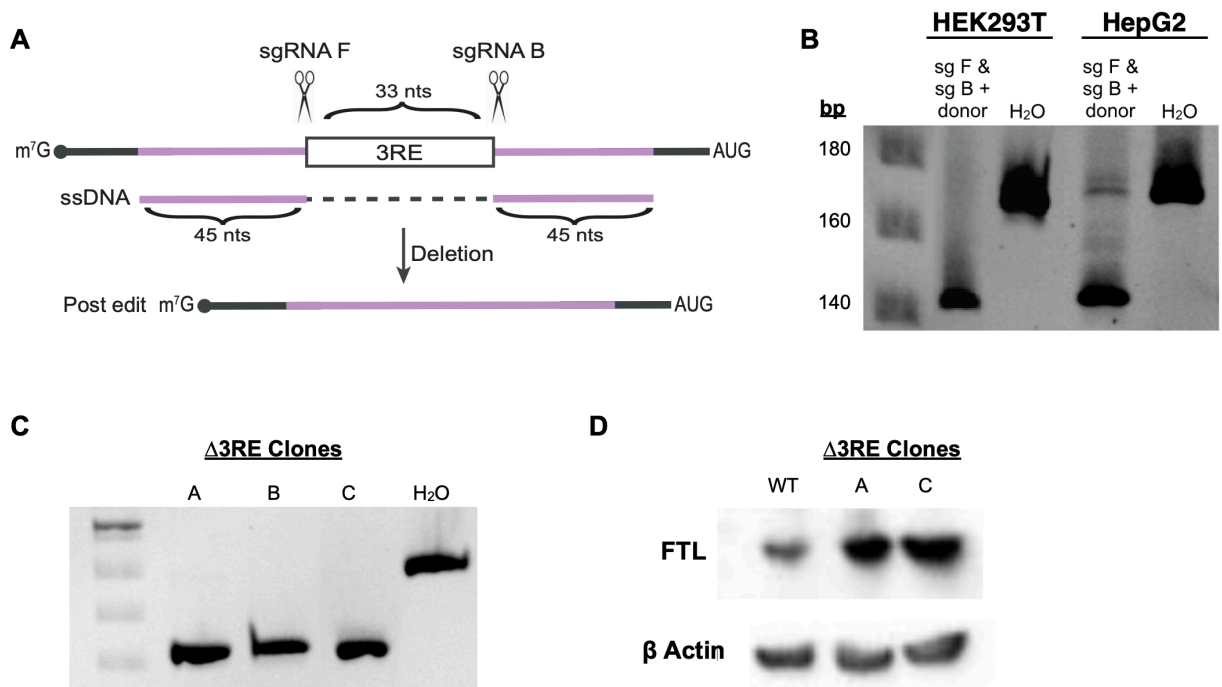
Figure 3—figure supplement 1 CRISPR-Cas9 editing to remove the proposed eIF3-*FTL* interaction site.

(**A**) CRISPR-Cas9 RNP editing schematic in which two sgRNAs target sequences immediately adjacent to the 3RE. Reactions were supplemented with 90-nt ssDNA that had full homology to the intended edited sequence. (**B**) Editing efficiency in both HEK293T and HepG2 cells, based on PCR of the region of interest and analysis on a native polyacrylamide gel. (**C**) Three successfully edited HepG2 clonal populations, as determined by sequencing the *FTL* locus. H_2O represents cells nucleofected without sgRNA. These should represent fully wild-type cells. (**D**) Representative Western blots FTL in two of the edited (Δ3RE) lines compared to WT HepG2 cells under normal iron condition.
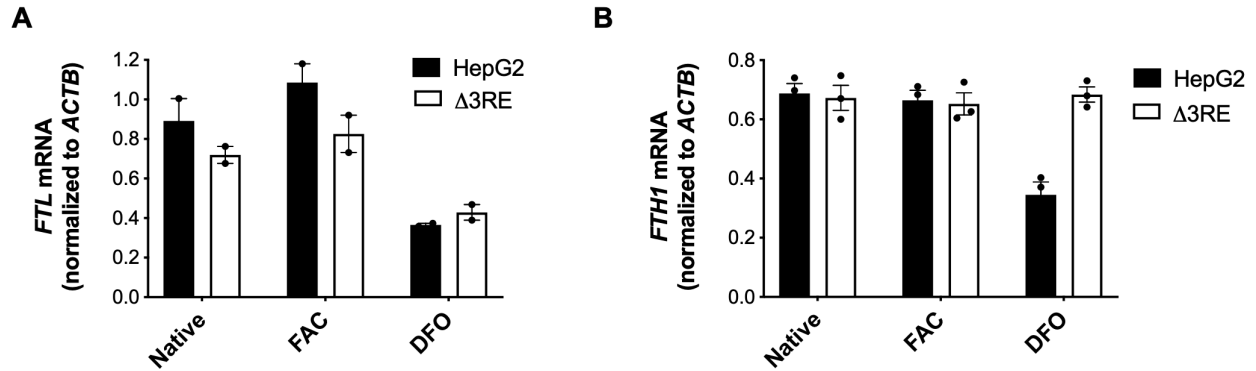
Figure 3—figure supplement 2 mRNA levels in edited cell lines.

(A, B) mRNA levels of either **(A)** *FTL* or **(B)** *FTH1* as determined by RNA extraction from HepG2 (solid black bars) or HepG2 Δ3RE (black outlined bars) cells and RT-qPCR. The mRNA levels for *FTL* and *FTH1* were normalized to *ACTB* mRNA. Cells were grown in normal media, 50 µg/mL FAC treatment for 24 hr (FAC), or 200 µM DFO treatment for 24 hr (DFO). The results are from two or three technical replicate qPCR readouts, respectively, that reflect the data from two biological replicates, with error bars representing the standard deviation of the mean.
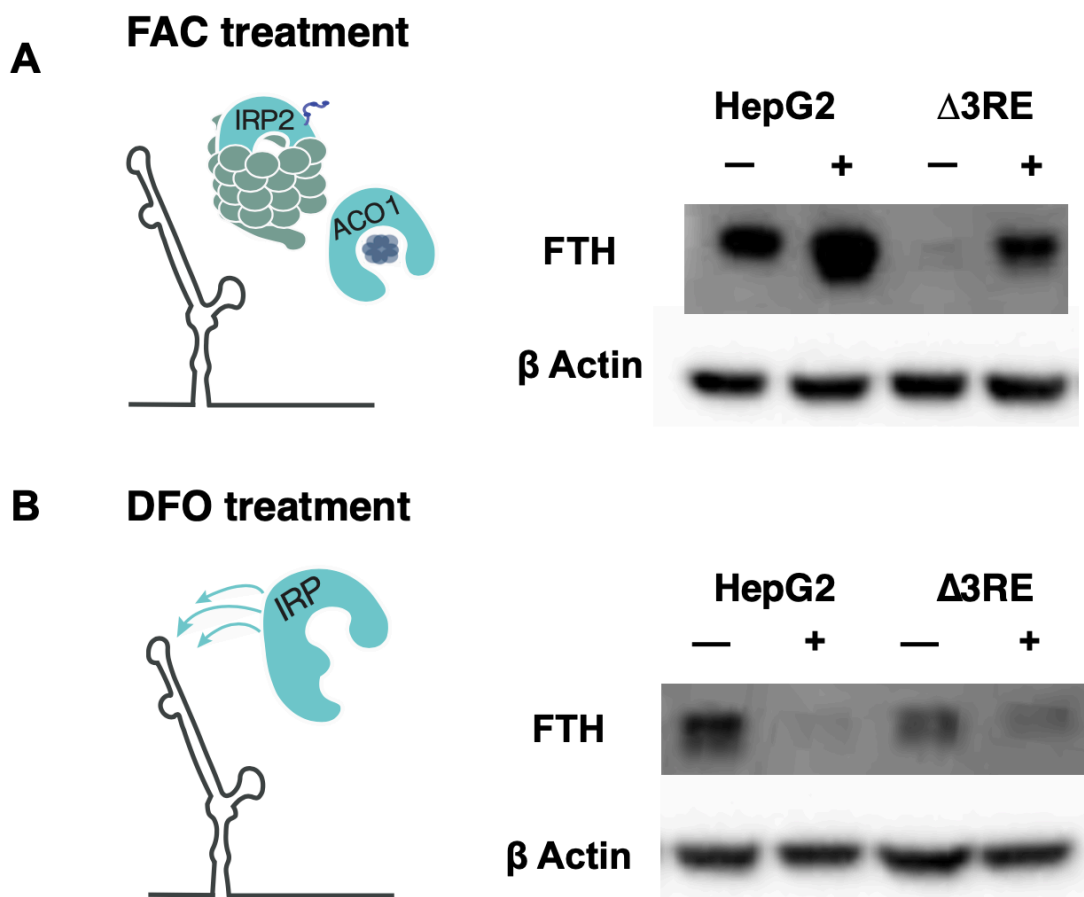
Figure 3—figure supplement 3 Physiological effects of the endogenous removal of the 3RE on FTH protein levels.

(**A, B**) Representative western blots of FTH levels in the edited (Δ3RE) and WT HepG2 cells under various iron conditions. (**A**) Iron donor treatment with FAC at 50 μg/mL for 24 hr; (**B**) Iron chelation treatment with DFO at 200 μM for 24 hr.
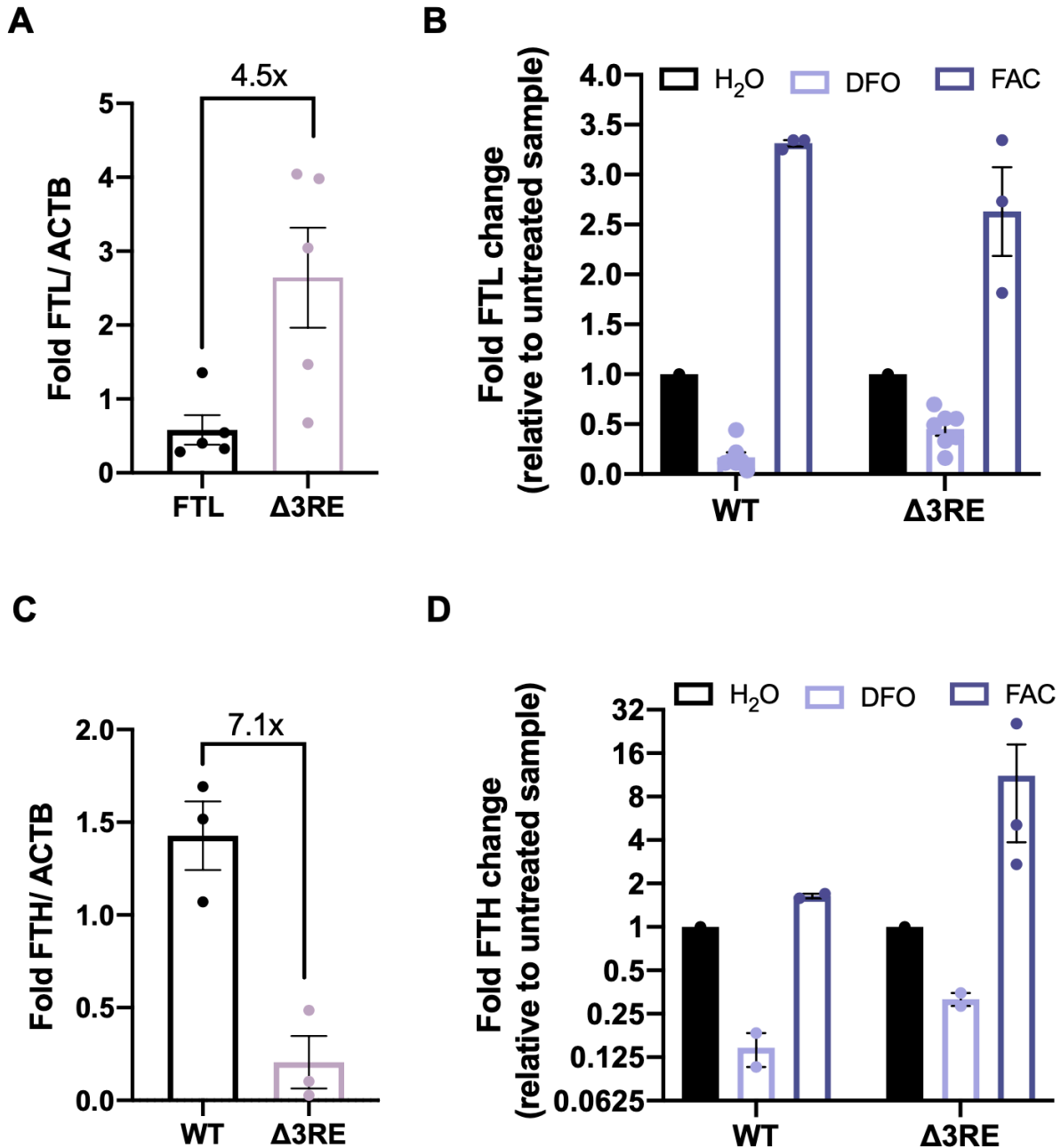
Figure 3—figure supplement 4 Quantification of FTL and FTH protein levels in HepG2 cells.

(**A**) Quantification of western blots comparing the levels of FTL in wild-type vs Δ3RE HepG2 cells. Five biological replicates are represented with error bars representing standard error of the mean. (**B**) Quantification of western blots comparing the levels of FTL in wild-type vs Δ3RE HepG2 cells under various iron conditions. Iron donor treatment with 50 μg/mL FAC for 24 hr or iron chelation treatment with 200 μM DFO at for 24 hr. Three biological replicates are represented for FAC treatment and six biological replicates are represented for DFO treatment. Error bars represent standard

error of the mean. (**C**) Quantification of western blots comparing the levels of FTH in wild-type vs Δ3RE HepG2 cells. Three biological replicates are represented with error bars representing standard error of the mean. (**D**) Quantification of western blots comparing the levels of FTH in wild-type vs Δ3RE HepG2 cells under various iron conditions. Iron donor treatment with 50 µg/mL FAC for 24 hr or iron chelation treatment with 200 µM DFO for 24 hr.
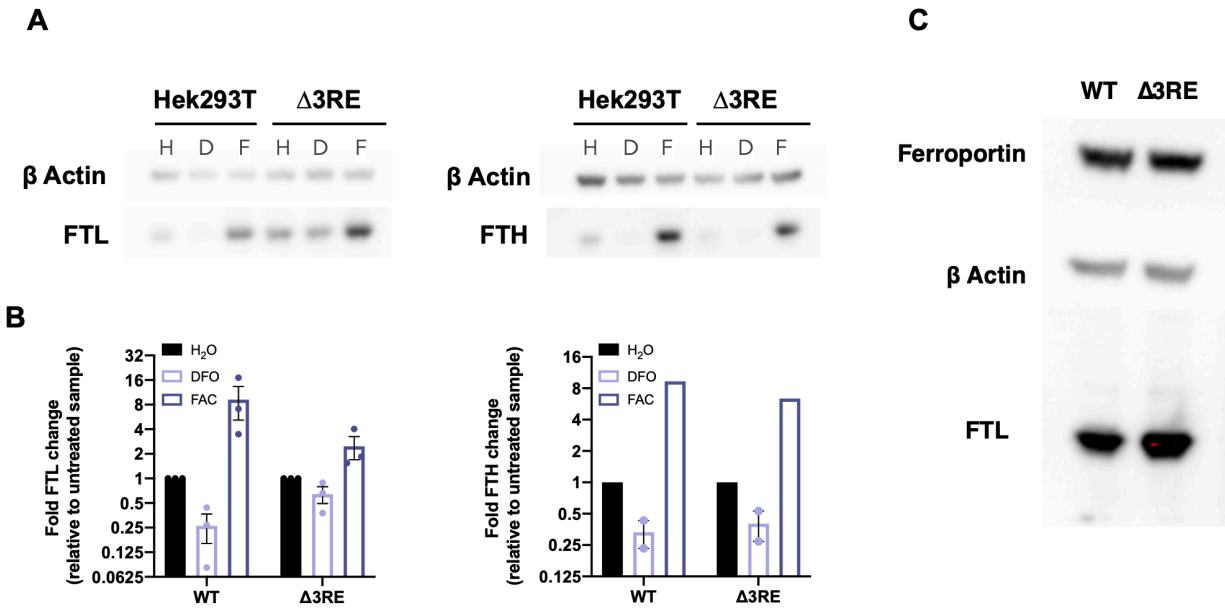
Figure 3—figure supplement 5 Quantification of FTL and FTH protein levels in HEK293T cells.

(**A**) Representative western blots comparing the levels of FTL and FTH in wild type vs Δ3RE under different iron treatment conditions. Iron donor treatment with FAC at 50 μg/mL for 24 hr or iron chelation treatment with DFO at 200 μM for 24 hr. (**B**) Quantification of western blots comparing the levels of FTL and FTH in wild type vs Δ3RE HEK293T cells. Three biological replicates are shown with error bars representing standard error of the mean for both of the FTL data sets. There are two biological replicates for FTH levels under DFO treatment and error bars represent standard error of the mean. There was only one quantifiable replicate for the Δ3RE FAC treatment. (**C**) Representative western blots comparing the levels of ferroportin in wild type vs Δ3RE (HepG2) cells under various iron conditions.
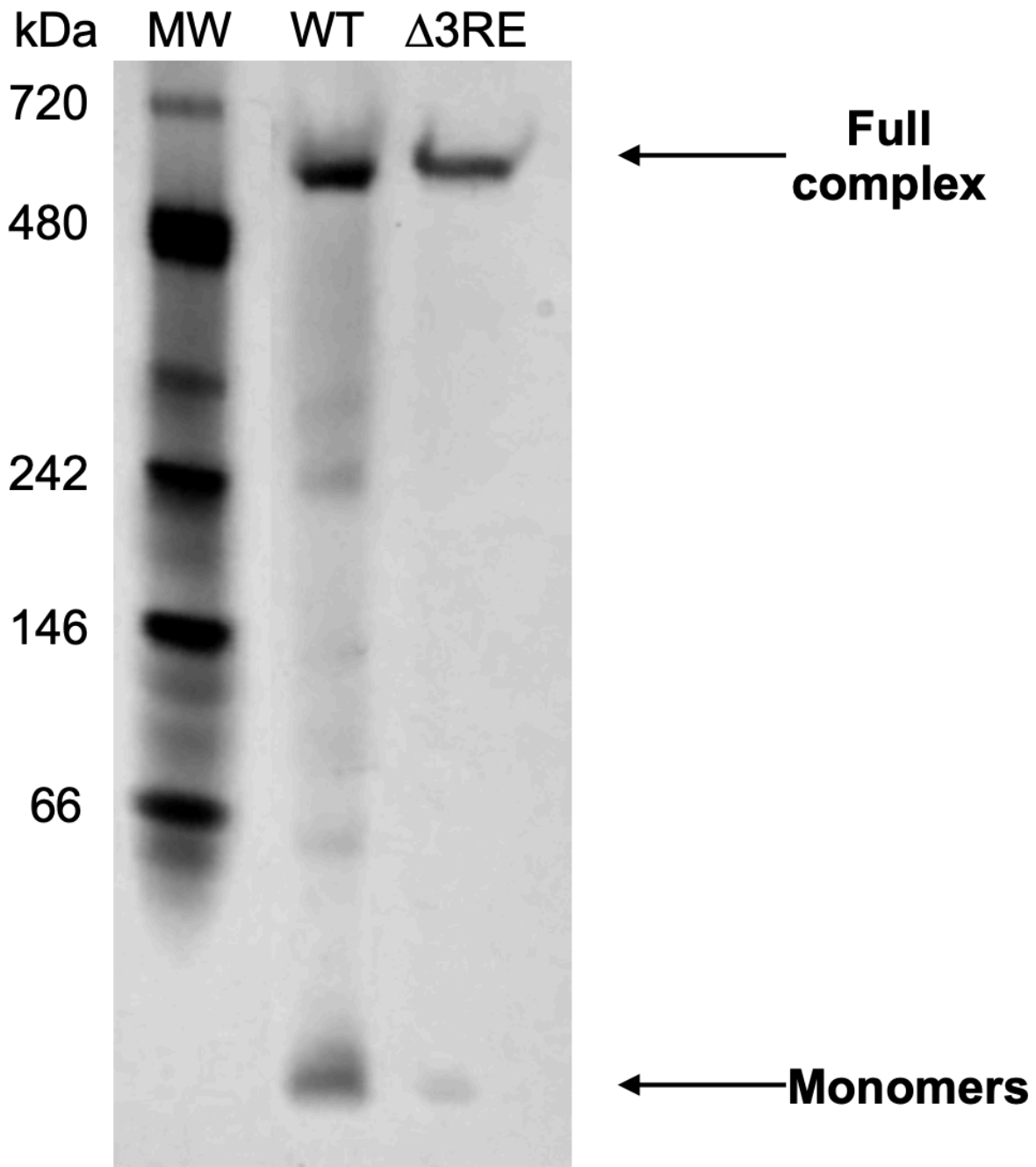
Figure 3—figure supplement 6 Analysis of the ferritin complex upon deletion of the 3RE in FTL mRNA.

Representative Coomassie stained native 4–12% gradient Tris-Glycine gel resolving ferritin complexes purified using methanol, from either 8 × 15 cm dishes of WT HepG2 cells treated with 50 µg/mL FAC for 24 hr or a single 15 cm dish of Δ3RE HepG2 cells under normal media conditions. An equal amount of protein was loaded for each sample.

SNPs in FTL that cause hyperferritinemia

Although the Δ3RE mutation in *FTL* revealed eIF3-dependent repression of *FTL* translation, it is not clear what role eIF3 may play in ferritin homeostasis in humans. The human genetic disease hereditary hyperferritinemia cataract syndrome (HHCS) is an autosomal dominant condition that primarily results in early onset of cataracts due to ferritin amassing in the lens (Millonig, Muckenthaler, & Mueller, 2010). HHCS arises from SNPs or deletions in the 5'-UTR of *FTL*, which are thought to disrupt the IRP-IRE interaction leading to increased *FTL* translation. For example, mutations observed in the apical loop of the IRE directly disrupt critical contacts essential for IRP binding to the IRE (Figure 4A) (5). Interestingly, two SNPs identified in certain patients with hyperferritinemia, G51C and G52C, disrupt the nucleotides one and two bases upstream of the annotated eIF3 PAR-CLIP site (Figure 4A) (Camaschella et al., 2000) (Luscieti et al., 2013). Although the PAR-CLIP methodology maps the region of interaction between an RNA and protein of interest, it does not always capture the full interaction site due to the requirement for 4-thiouridine cross-linking and subsequent RNase digestion to generate fragments for deep sequencing (Ascano, Hafner, Cekan, Gerstberger, & Tuschl, 2012) (Hafner et al., 2010). Thus, we wondered whether the G51C and G52C SNPs could potentially impact eIF3 repression of *FTL* mRNA translation, due to the proximity of the G51C and G52C mutations to the eIF3 PAR-CLIP site. We generated luciferase reporter constructs with either of the G51C and G52C SNPs, as well as a control with the previously described mutations in the IRE apical loop, and used mRNA transfections to test their effects on luciferase translation levels. All mutations led to an increase in luciferase levels, indicating that they alleviated translational repression (Figure 4B). We also observed that the G51C and G52C mRNAs do not interact with eIF3, based on eIF3 immunoprecipitations from transfected HEK293T cells (Figure 4C). Furthermore, the G51C and G52C SNPs maintained near wild-type IRP binding (Figure 4D and E), in stark contrast to the mutations in the IRE apical loop (Figure 4A), which completely abolished the interaction between IRP1 and the 5'-UTR element (Figure 4—figure supplement 1). Furthermore, using stable cell lines, we observe iron-responsive regulation of luciferase reporter mRNAs with G51C or G52C SNP-containing FTL 5' -UTRs, as well as IRP binding to these mRNAs (Figure 4—figure supplement 2). These results identify SNPs in *FTL* that cause hyperferritinemia likely due to disruption of eIF3-dependent repression of *FTL* translation.
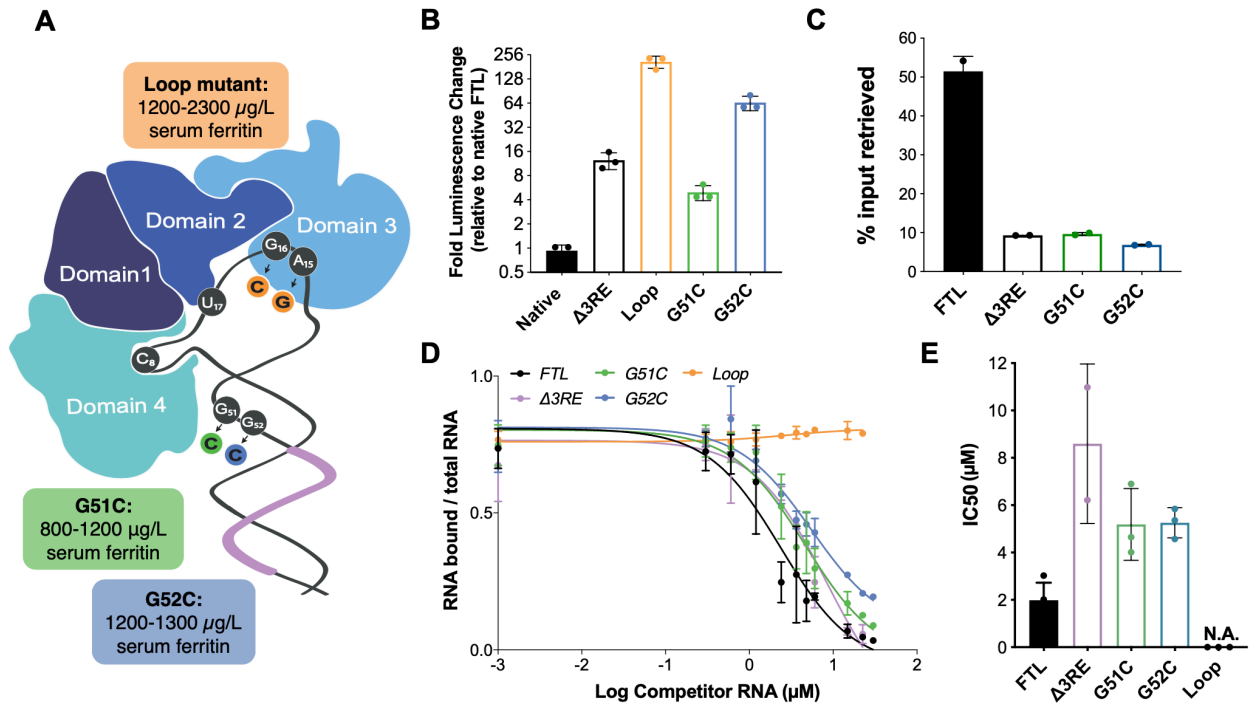
Figure 4. Role of eIF3 in select cases of hyperferritinemia.

(A) Diagram of IRP binding to the IRE in *FTL* mRNA (Gregory J. Anderson, 2012). Hyperferritinemia mutations are highlighted in orange (Cazzola et al., 1997), green (Camaschella et al., 2000), and blue (Luscieti et al., 2013) with their corresponding serum ferritin levels listed. Normal serum ferritin levels are under 300 mg/L. The 3RE is indicated in purple. Nucleotides that directly interact with the IRP are also identified (i.e. A15, G16, U17). (B) Luciferase activity of HepG2 cells transfected with mRNAs encoding the WT FTL 5'-UTR or various hyperferritinemia mutations (G51C, G52C, or Loop mutant (A15G/G16C)), normalized to WT FTL reporter luciferase luminescence. The results are from three biological replicates, with error bars representing the standard deviation of the mean. (C) Binding of eIF3 to luciferase reporter mRNAs with WT or mutant forms of the *FTL* 5'-UTR, using EIF3B immunoprecipitation (IP), followed by RNA extraction and RT-qPCR. Cells were harvested 8 hr post-transfection. Data are shown as the percent in the IP, compared to input levels. Error bars are the standard deviation of the mean of duplicate qPCR measurements from a representative IP. (D) Dose-response curve of RNA competition assays, based on gel shifts of NIR-labeled WT IRE-containing RNA, with WT, G51C, G52C, or Loop mutant (A15G/G16C) RNAs serving as cold competitors. Fold excess of competitor WT extended up to 100,000x. Recombinant IRP1 was used. Error bars represent standard deviations for each concentration of competitor. (E) The calculated IC_{50} values of the various competitor RNAs, based on the data in (D), with error bars representing the standard deviation from the mean IC_{50} value. N.A., the IC_{50} value could not be determined for the Loop mutant due to lack of any detectable competition. Note that the data for ∆3RE in panels

(D) and (E) are from Figure 2B and C, measured in duplicate. The remaining experiments in (D) and (E) were carried out in triplicate.
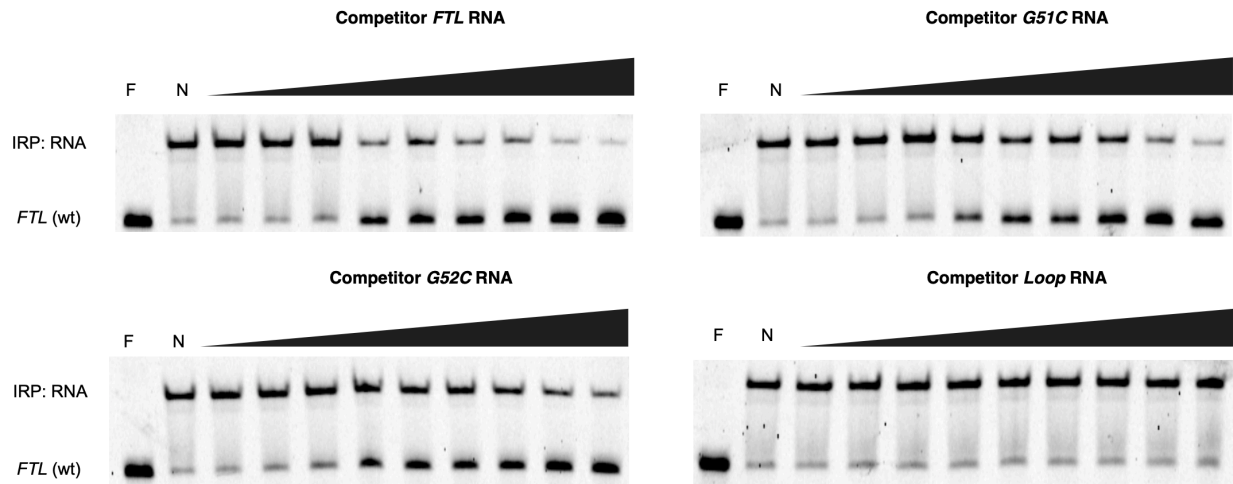
Figure 4—figure supplement 1 Native gels resolving RNA-IRP1 complexes formed after competition experiments with hyperferritinemia-related RNAs.

Near IR (NIR) labeled RNA corresponding to the full-length WT *FTL* 5'-UTR were incubated with recombinant IRP1 and increasing molar excess concentrations of unlabeled competitor RNAs (1000x, 2000x, 4000x, 8000x, 12,000x, 16,000x, 20,000x, 50,000x, 75,000x), as indicated. F, lane with only NIR-labeled *FTL* RNA; N, no addition of competitor RNA to the NIR-RNA-IRP1 complex.

Figure 4—figure supplement 2 Iron responsiveness of hyperferritinemia associated SNPs in the *FTL* 5'-UTR.

(**A**) Schematic of the stable lentivirus lines generated that contain the rLUC reporters. (**B**) Representative western blot demonstrating the inherent iron responsiveness in the generated cell lines vs wild-type cells. This experiment was done in biological triplicate. Iron donor treatment with FAC at 50 µg/mL for 24 hr or iron chelation treatment w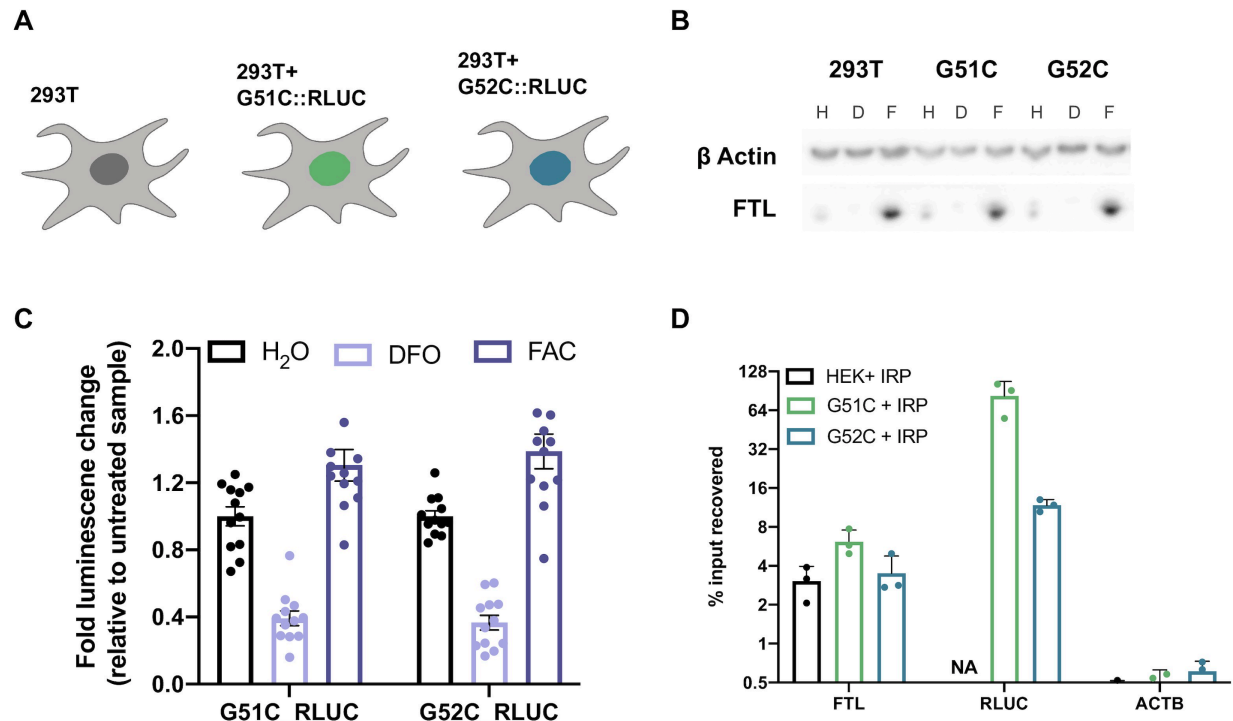ith DFO at 200 µM for 24 hr. (**C**) Luciferase activity of the stable hyperferritinemia reporter cell lines after iron treatment. This experiment was done with 12 biological replicates. Error bars represent standard error of the mean. (**D**) Determination of IRP1 binding to *FTL* mRNA in WT (HEK + IRP) and various SNP reporter mRNAs (G51C + IRP, G52C + IRP) in HEK293T cells via FLAG immunoprecipitation (IP) followed by RNA extraction and RT-qPCR. The *ACTB* mRNA was used to control for nonspecific mRNA binding to FLAG-tagged IRP or beads. HEK – IRP reflects cells that were not transiently transfected, but were carried through the IP and following experiments. Error bars represent the standard deviation for the experiment carried out in biological triplicate, with measurements from representative IP reactions carried out in technical triplicate.

Discussion:

We have shown that eIF3 represses the translation of *FTL* mRNA by binding a region of the *FTL* 5'- UTR immediately adjacent to the IRE. Upon disruption of eIF3 binding, the basal level of FTL production increases dramatically without affecting the iron-responsiveness of *FTL* translation (Figure 3), or binding of IRP to the remainder of the 5'-UTR containing the IRE (Figure 2, Figure 3, Figure 4). Taken together, these results expand the classical model of *FTL* mRNA post-transcriptional regulation by the iron-responsive IRP/IRE interaction to include a functionally distinct eIF3-dependent repressive mechanism (Figure 5). The physiological need for a dual repressive system involving IRPs and eIF3 in normal human health remains to be determined. Experiments combining the Δ3RE and apical loop mutations (Figure 2F, Figure 2—figure supplement 3) suggest that eIF3 and IRP can act simultaneously to repress *FTL* translation. Due to the close proximity of the IRE and eIF3 binding sites, and as suggested by our mathematical modeling (Figure 2—figure supplement 3), it may be possible that eIF3 physically interacts with IRP when they bind to the 5'-UTR in *FTL* mRNA in certain tissue or cellular contexts. Although we have identified a role for eIF3 in *FTL* mRNA translation regulation, it is still unclear what role eIF3 may play in response to iron level modulation, a key question to answer in the future. It is possible that both eIF3 and IRP are required for the proper iron responsiveness of *FTL* translation.

Our present findings also provide the first molecular evidence for the direct involvement of eIF3 in a human disease caused by SNPs in the human population. We found that disruption of eIF3-mediated regulation of *FTL* translation could serve as the dominant cause of certain cases of hyperferritinemia. The specific genetic mutations we analyzed (G51C, G52C) map to the less-conserved lower stem of the IRE, and are predicted to have no direct physical interaction with IRP1 (PDB: 3SNP) (Walden et al., 2006). Here, we establish that these mutations minimally interfere with IRP's interaction with the IRE, whereas they greatly impact the eIF3-based interaction and *FTL* translational repression (Figure 4C–E). This work highlights how even highly clustered SNPs can contribute to disease through divergent molecular mechanisms. In the case of *FTL*, these clustered SNPs can disrupt three different aspects of translation regulation: IRP binding, eIF3 binding, or RNA folding (Figure 5).

While our results connect eIF3 translational control to specific examples of hyperferritinemia, they also suggest a broader role for eIF3 in other hyperferritinemias and ferritin-related diseases. For example, we observed that derepression of *FTL* translation by disruption of the eIF3 interaction site leads to a concomitant decrease in FTH levels, driving an overall increase in ferritin complex stability (Figure 3—figure supplement 6). Ferritin is a known mediator of inflammatory responses, raising the question of whether eIF3 may contribute to ferritin's role in inflammation (Morikawa, Oseko, & Morikawa, 1995; Recalcati, Invernizzi, Arosio, & Cairo, 2008). Our results provide new insights that should help connect molecular mechanisms of translational control to disease-associated SNPs identified in ever expanding genomic databases.
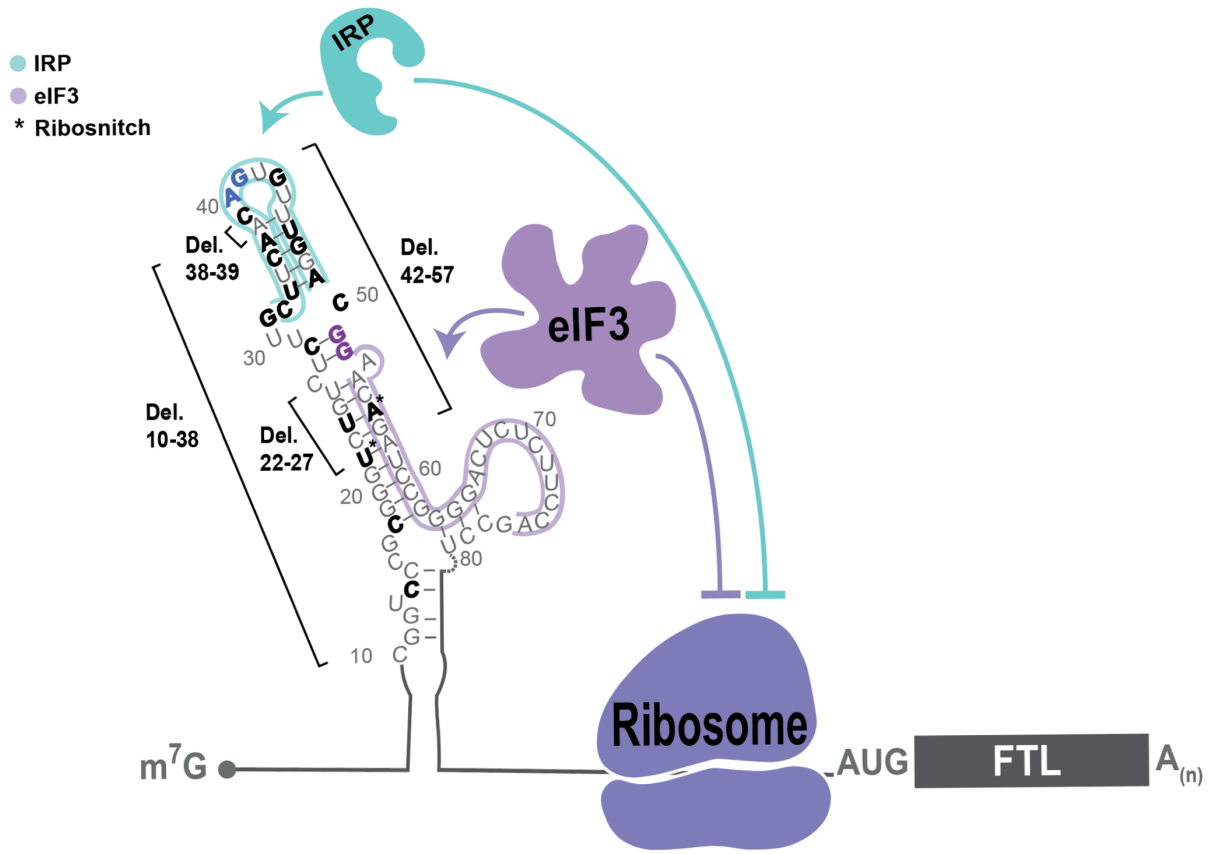
Figure 5. Model of post-transcriptional regulation of FTL mRNA.

IRPs repress *FTL* mRNA translation in an iron-dependent manner, whereas eIF3 represses FTL translation in an iron-independent manner. Coordination between IRP repression and eIF3 repression may differ by cell and tissue context. Various hyperferritinemia mutations (bolded) listed in the literature are mapped on the experimentall -determined secondary structure of the *FTL* mRNA 5'-UTR (Luscieti et al., 2013; Martin et al., 2012). The minimal annotation of the IRE is denoted by with a blue outline and the eIF3 PAR-CLIP defined interaction site is denoted with a purple outline. Mutations that disrupt IRP binding used in this study and determined here to disrupt eIF3 binding are bolded in blue and purple, respectively. (*) indicates nucleotides identified as ribosnitches (Martin et al., 2012).

Methods:

Plasmids

The FTL 5'-UTR was amplified from human cDNA, and cloned into the pcDNA4 vector with a modified Kozak sequence (Kranzusch et al., 2014), by using In-Fusion HD Cloning Kit (Takara, Cat.# 638911) to generate the starting luciferase reporter plasmids. The FTL transcription start site is derived from the FANTOM5 database (Lizio et al., 2015). Additional mutations were generated through around-the-horn cloning using either blunt primers for deleting regions or primers with overhangs to introduce single or double nucleotide mutations. The IRP1 protein expression plasmid was generated by amplifying the human IRP1 sequence from human cDNA and inserting it into the 2B-T vector (Addgene, plasmid # 29666) following a His6 tag and TEV protease cleavage site. The IRP-FLAG construct was generated by inserting a 1X FLAG tag at the C-terminal end of IRP in the pCMV6-XL4 backbone (OriGENE, SC126974).

In vitro transcription

RNAs were transcribed using T7 RNA polymerase prepared in-house. For luciferase reporter mRNAs, 5'-capping and 3'-polyadenylation were performed co-transcriptionally by including $3'$-O-Me-m^{7}G $(5')$ppp$(5')$G RNA Cap Structure Analog (NEB, Cat.# S1411L) and using linearized plasmid template that had a sequence encoding a poly-A tail. Non-labeled RNAs for the IRP1 electrophoresis mobility shift assays were generated in the same manner, except the templates were not polyadenylated. Additionally, RNAs with the 38-nucleotide extension between the 5' -cap and IRE were constructed using a random nucleotide sequence. The exact nucleotide composition 5' of the IRE was previously reported to not significantly impact IRP binding (Goossen & Hentze, 1992). RNAs were purified after DNA template digestion by phenol-chloroform extraction and ethanol precipitation.

For genome editing, we used tandem CRISPR-Cas9 enzymes programmed with single-guide RNAs (sgRNAs) targeting the FTL gene, along with a single-stranded DNA (ssDNA) oligonucleotide homologous to the regions spanning the deleted 3RE sequence (Figure 3—figure supplement 1). sgRNAs were designed using the CRISPR.MIT.EDU program from the Feng Zhang Lab, MIT. CRISPR-Cas9-sgRNA was assembled as RNA-protein complexes (RNPs) (Kim, Kim, Cho, Kim, & Kim, 2014). The DNA for transcription was synthesized by appending the sgRNA sequence downstream of a T7 RNA polymerase promoter. The DNA was then purified using phenol-chloroform extraction followed by isopropanol precipitation. After transcription, the RNA products were treated with DNase I (Promega, Cat.# M6101), run on a 10% denaturing polyacrylamide gel (6 M urea), and extracted from the gel using the crush and soak method and ethanol precipitation.

Luciferase reporter transfections

Human HepG2 cells were maintained in DMEM (Invitrogen 11995–073) with 10% FBS (Seradigm) and 1% Pen/Strep (Gibco, Cat.# 15140122). Transfections of the luciferase reporter mRNAs were done using the Mirus TransIT-mRNA Transfection Kit (Cat.# MIR 2250), with the following protocol modifications. The day prior to transfection, HepG2 cells were seeded into opaque 96-well plates so that they would reach 80% confluence at the time of transfection. At this point, 200 ng of 5'-capped and 3'-polyadenylated mRNA was added at room temperature to OptiMEM media (Invitrogen, Cat. # 31985–088) to a final volume of 10 mL. All mRNA concentrations were determined using a Nanodrop, and were validated by running samples on an agarose gel. Bands on the gel were quantified to properly ensure all constructs were transfected at equal amounts. Then, 0.6 mL of both Boost reagent and TransIT mRNA reagent were added to the reaction and left to incubate at room temperature for 3 min. The TransIT-mRNA Reagent:mRNA Boost:RNA complex was distributed to the cells in a drop wise manner. Luciferase activity was assayed either 6 hr, or 12 hr post-transfection using the Renilla Luciferase assay kit (Promega, Cat.# E2820) and a Microplate Luminometer (Veritas). We used 6 hr incubation times for these experiments in order to keep readouts for various mutant constructs in a linear range (Bert, Grepin, Vadas, & Goodall, 2006).The only transfection not shown at 6 hr (Figure 4B) was also carried out for 6 hr in Figure 2—figure supplement 3. In all experiments, we define biological replicates as cells cultured in separate wells, and technical replicates as multiple measurements from cells from the same well.

In order to monitor the stability of transfected mRNAs during the timecourse of the luciferase reporter experiments, these 750 ng of each mRNA was transfected into HEK293T cells at 80% confluency well in a 24-well plate. After 6 hr, the cells were collected, pelleted, and then the RNA was extracted using the Directzol RNA Mini prep kit (R2051). cDNA was the prepared using 250 ng of RNA and Superscript IV (Thermo Fisher scientific, Cat. # 18091050). qPCR was carried out with the primers to the luciferase coding sequence with run conditions as described below in the methods for determination of transcript level abundance. We note that a completely accurate quantification of accessible mRNAs in the cell is limited due to technical complications inherent with mRNA transfection protocols and mechanisms (Kirschman et al., 2017).

Cell line generation

Cell lines (HEK293T and HepG2) were obtained from the University of California Berkeley Cell Culture Facility, validated by STR analysis, and confirmed to be mycoplasma-free by the facility. To generate FTL-eIF3 interaction site null cell lines (Δ3RE), we used tandem CRISPR-Cas9 enzymes programmed with single-guide RNAs (sgRNAs) targeting the FTL gene, along with a single-stranded DNA (ssDNA) donor with homology to the regions spanning the deleted Δ3RE sequence. The sgRNAs were generated as described above, and targeted regions on both sides of the eIF3 interaction site (Figure 2A). The RNP complex was generated by incubating 100 pmol Cas9 with the two sgRNAs at a 1:1.2 Cas9 to total sgRNA ratio. This mixture was heated to 37℃ for 10 min and then kept at room temperature until use. The ssDNA donor was 90 nucleotides long, with 45-nucleotide homology on either side of the

predicted double-strand cut sites allowing it to have perfect homology to the predicted edited sequence.

The Cas9-sgRNA RNP complexes, along with 500 pmol of the ssDNA donor, were transfected into either 5 x 10^5 HEK293T or HepG2 cells using the Lonza 96-well shuttle system SF kit (Cat. # V4SC-2096). The nucleofection programs used were as follows: CM-130 for HEK293T and EH-100 for HepG2. The transfected cells were left to incubate for either 48 hr for HEK293T cells or 72 hr for HepG2 cells before harvesting and extracting gDNA using QuickExtract (Epicentre: QE09060). The editing efficiency of individual Cas9-sgRNA RNPs was determined using a T7 endonuclease one assay (Reyon et al., 2012).The efficiency of the dual-sgRNA editing approach was determined by PCR-amplifying a 180-base pair region around the eIF3 interaction site, and analyzing the resulting products on a 6% non-denaturing 29:1 polyacrylamide gel. This method achieved an editing efficiency of nearly 100% in HEK293T cells and roughly 85% in HepG2 cells (Figure 3—figure supplement 1B). Monoclonal populations of edited cells were sorted using FACS, screened, and the final edited sequence was determined using TOPO TA cloning (Ramlee, Yan, Cheung, Chuah, & Li, 2015).

Transcript level abundance

Total transcript abundance was determined by lysing 1.25 x 10^6 cells with Qiazol lysis buffer followed by using the Directzol RNA extraction kit (Zymo Research, Cat. # R2061), according to the manufacturer's instructions. The cDNA was generated by reverse transcription using 350 ng of RNA, random hexamers, and Superscript IV (Thermo Fisher scientific, Cat. # 18091050). Primers for the qPCR were as follows: FTL forward: 5' -ACCTCTCTGGGCTTCTAT-3', FTL reverse: 5' -AGCTGGC TTCTTGATGTCCT-3' (Cozzi et al., 2004), ACTB forward: 5'-CTCTTCCAGCCTTCCTTCCT-3', ACTB reverse: 5'-AGCACTGTGTTGGCGTACAG-3' (Chen et al., 2008), PSMB6 forward: 5'-GGACTCCAGAACAACCACTG-3', PSMB6 reverse: 5'-CAGCTGAGCCTGAGCGACA-3' (Mokany, Tan, Bone, Fuery, & Todd, 2013), FTH1 forward: 5'-CGCCAGAACTACCACCA-3', FTH1 reverse: 5'-TTCAAAGCCACATCATCG-3' (Liu et al., 2013), 18S forward: 5'-GGCCCTGTAATTGGAATGAGTC-3', 18S reverse: 5'-CCAAGA TCCAACTACGAGCTT-3' (Lee et al., 2016), RLUC forward: 5'-GGAATTATAATGCTTATCTACG TGC-3', RLUC reverse: 5'-CTTGCGAAAAATGAAGACCTTTTAC-3' (Kong et al., 2008). Run conditions were: 95℃ for 15 s, followed by 40 cycles of 95℃ for 15 s, 60℃ for 60 s, 95℃ for 1 s.

RNA immunoprecipitation and qPCR

The EIF3B-RNA immunoprecipitations were adapted from Ramlee et al. (2015) with the following modifications. One 15 cm plate of either HEK293 or HepG2 cells was used to prepare cell lysate using a NP40 lysis buffer (50 mM HEPES-KOH pH 7.5, 150 mM KCl, 2 mM EDTA, 0.5% Nonidet P-40 alternative, 0.5 mM DTT, 1 Complete EDTA-free Proteinase Inhibitor Cocktail tablet per 50 mL of buffer). The lysate was precleared with 15 mL of Dynabeads preloaded with rabbit IgG (Cell Signaling, Cat. # 2729) for one

hour at 4℃. The lysate was collected and then incubated with a fresh 15 mL aliquot of Dynabeads and 7.5 mL of anti-EIF3B antibody (Bethyl A301-761A) for two hours at 4℃. Preparation of cDNA and qPCR primers are described and listed above.

For EIF3B immunoprecipitations of transfected mRNAs, 2.15 µg of mRNA was transfected into 1 well of either HEK293T or HepG2 cells in a 12-well plate using the protocol above. Cells were then left to incubate for 8 hr before harvesting. The cells were lysed using the NP40 lysis buffer listed above (Lee et al., 2015), and precleared with 2 µL of rabbit IgG-coated Dynabeads for one hour at 4℃. The lysate was collected and then incubated with a fresh 2 µL aliquot of Dynabeads and 4 µL of anti-EIF3B antibody (Bethyl A301-761A) for 2 hr at 4℃. RNA was collected, cDNA prepared and

qPCR carried out with the primers and run conditions as described in the methods for transcript level abundance.

For FLAG-tagged IRP1 immunoprecipitations, 2.2 mg of plasmid DNA was transfected into a 10 cm dish of 80% confluent HEK239T WT cells or HEK293T Δ3RE mutant cells. Cells were then left to incubate for 24 hr before harvesting. The cells were lysed using the NP40 lysis buffer as described in Ramlee et al. (2015) and then further diluted 3x with the lysis buffer lacking DTT. The lysate was collected and then incubated with pre-equilibrated anti-FLAG antibody conjugated agarose beads (Sigma A2220) for two hours at 4℃. The beads were then washed with a high salt wash buffer (50 mM HEPES-KOH pH 7.5, 300 mM KCl, 2 mM EDTA, 1% Nonidet P-40 alternative) three times. The protein was eluted from the beads using two washes with 1X FLAG peptide for 30 min each at 4℃. The RNA was collected using phenol/chloroform extraction followed by ethanol precipitation. cDNA was prepared using Superscript IV (Thermo Fisher scientific, Cat. # 18091050) and qPCR carried out with the primers and run conditions as described above in the methods for determination of transcript level abundance.

Iron level modulation

In order to modulate the iron levels in cells, HepG2 and HEK293T cells were treated with a final concentration of either 50 mg/mL of ferric ammonium citrate (FAC) (an iron donor) for 24 hr or either 200 mM for 24 hr or 50 mM for 48 hr of desferoxamin (DFO) (an iron chelator) before harvesting.

For the iron treatment of cells with the stably integrated luciferase reporters harboring the FTL 5'UTR SNPs, either H_2O, 200 mM of DFO, or 50 ug/mL of FAC was added to an individual 96 well of 80% confluent cells. The cells were allowed to incubate for 24 hr before taking the luminescence reading. BioRender was used for the cell schematic in Figure 4—figure supplement 2A.

IRP1 purification

IRP1 was purified based on the protocols in Carvalho and Meneghini (2008), Basilion et al. (1994) with modifications (Carvalho & Meneghini, 2008) (Basilion, Rouault, Massinople, Klausner, & Burgess, 1994). The IRP1-encoding 2B-T plasmid was transformed into chemically-competent BL21 Rosetta pLysS E. coli, using heat shock at 42°C, and grown on Ampicillin plates. A single colony was used to inoculate a 5 mL LB culture containing Ampicillin, which was then used to inoculate a 50 mL starter culture that was allowed to reach saturation overnight. Approximately 4 x 10 mL of the overnight culture was used to inoculate 4 x 1L cultures using ZY5052 media lacking the 1000x trace metal mix (30 mM HEPES, 5% glycerol, 43 mM KCl, 0.5 mM EDTA, 0.5 mM DTT) (Studier, 2005) plus Carbomicillin. The 1 L cultures were grown at 37°C to OD_{600} = 0.36, at which point the temperature was lowered to 18°C, and allowed to grow at 18°C for 36 hr prior to harvest.

Pelleted E. coli cells were lysed using sonication in lysis buffer (30 mM HEPES pH = 7.5, 400 mM KCl, 5% Glycerol and 1 mM DTT) along with Protease inhibitor (Roche, Cat. # 5056489001) tablets. Lysate was loaded on a 5 mL Ni-NTA pre-packed HiTrap column (GE, Cat. # 17-5248-02), allowed to incubate at 4°C for 1 hr, before eluting using 600 mM imidazole in the same buffer as above. Pooled fractions from the elution were then dialyzed overnight into ion-exchange (IEX) buffer (30 mM HEPES pH 7.5, 1 mM DTT, 5% Glycerol, and 1 mM EDTA), for subsequent purification using a 5 mL HiTrap Q-column (GE, Cat. # 17-1154-01). Samples were then loaded on a Q column using IEX buffer, and the column was washed with eight column volumes of IEX buffer without KCl. IRP1 was eluted using 800 mM KCl in IEX buffer.

IRP1 electrophoresis mobility shift assays

To detect IRP1 binding by native gel shifts, RNA samples were transcribed using the Atto-680 RNA Labeling Kit (Jena Bioscience, FP-220–680) and subsequently purified using RNA Clean and Concentrator-25 columns (Zymo, R1018). This form of labeling has been shown not to disrupt protein-RNA interactions (Kohn, Lederer, Wachter, & Huttelmaier, 2010). Unlabeled RNA was transcribed and purified as described above.

Binding experiments were carried out with a final concentration of 300 pM of labeled RNA and 225 nM of recombinant human IRP1, which facilitated a 1:1 ratio of RNA binding to IRP1. We first ensured the RNA competition experiments reached equilibrium – which required at least 11 hr of incubation – by measuring the approximate dissociation rate constant (k_{off}) of WT FTL 5'-UTR from IRP1. Heparin was included at the beginning of the reaction at a final concentration of 4.5 mg/mL. The initial binding reaction was carried out in a 1x RXN buffer (40 mM KCl, 20 mM Tris-HCL, pH 7.4, 2 mM $MgCl_2$, 2 mM DTT, and 5% Glycerol) for 30 min at room temperature (Goforth et al., 2010), (Fillebeen, Wilkinson, & Pantopoulos, 2014). For competition experiments, unlabeled RNA was then added in concentrations 1000x-100,000x that of the labeled RNA. In preliminary experiments, we found the k_{off} to be roughly 0.006 min^{-1} using an 8 hr incubation time course with competitor. We then tested the fraction of IRP bound after 11 hr and 18 hr incubations with competitor FTL RNA and observed no changes in the residual fraction of IRP bound to RNA (~15%), indicating the reactions had reached

equilibrium. Thus, subsequent experiments with competitor RNAs were carried out for 18 hr, after the first 30 min pre-incubation in the absence of competitor. The reactions were resolved on Tris-glycine gels (Thermo Fisher Scientific, Cat.# XP04122BOX) and gels was visualized using an Odyssey Licor set to 700 nM wavelength and an intensity of 6.5. Band intensity quantification was carried out using Image Studio (Licor). The IC_{50} values for each competitor RNA was determined using Graph Pad Prism 7 (Graph Pad Software) from a set of triplicate experiments, except for the Δ3RE competitor RNA, which was tested in duplicate.

Ferritin complex purification

The ferritin complex purification procedure was adapted from Cham et al. (1985), with slight modifications. Either one 15 cm dish of Δ3RE cells grown in normal media or eight 15 cm dishes of wild-type HepG2 cells that had been treated with 50 ng/mL FAC for 24 hr were harvested, weighed, and lysed in 4x weight/volume NP40 lysis buffer (50 mM HEPES-KOH pH = 7.5, 150 mM KCl, 2 mM EDTA, 0.5% Nonidet P-40 alternative, 0.5 mM DTT, 1 Complete EDTA-free Protease Inhibitor Cocktail tablet per 10 mL of buffer). Samples were incubated on ice for ten minutes and then centrifuged for 10 min at 21,000xg at 4℃. Samples were diluted in 1:2 phosphate buffered saline (PBS), and methanol was added to the diluted lysate to a final concentration of 40% (v/v). The sample was then heated to 75℃ for 10 min. After cooling on ice for 5 min, the samples were centrifuged in a microfuge 20R at 1251xg RPM for 15 min at 4℃. The resulting supernatant was collected and concentrated using a 100 k MW cutoff Amicon filter (Cat.# UFC510024) by centrifugation for 10 min at 14000xg. The sample was washed once with PBS and spun for an additional 4 min at 14000xg. The sample was then collected by inverting the column and centrifuging the sample for 2 min at 1000xg at 4℃. All samples collected were brought to a final volume of 80 mL with PBS. The purity of the sample was determined by running the sample on a native gel (Thermo Fisher Scientific, Cat.# XP04200BOX) followed by Coomassie staining.

Western blots

The following antibodies were used for Western blot analysis: anti-EIF3B (Bethyl A301-761A) at 1:1000; anti-FTL (Abcam, ab69090) at 1:800; anti-FTH (Santa Cruz, sc-25617) at 1:400; anti-IRP1 (Abbexa, abx004618) at 1:400; anti-IRP2 (Abcam, ab129069) at 1:800; and anti-b-Actin (Abcam, ab8227) at 1:1000, anti-Ferroportin (Novus, NBP 1–2150255) at 1:300.

Lentiviral transduction

The G51C and G52C Renilla luciferase reporters were cloned into the NLV103 plasmid. Virus was generated using LentiX cells in a 10 cm dish format and TransIT-LT1 transfection reagent. Virus was harvested and filtered after 48 and 72 hr. Total virus was pooled and 500 mL of fresh virus was added to 10^6 HEK293T cells along with 10 mg/mL of polybrene (Millipore). Cells were left to incubate for 48 hr before a 4 day

selection process with 4 mg/mL of puromycin. Cells were split in non-selective media once before use.

Mathematical modeling of IRP and eIF3 co-occupancy on FTL mRNA

We tested a mathematical model in which IRP and eIF3 do not bind simultaneously to the same *FTL* mRNA. This model thus includes three possible states of the *FTL* mRNA: the fraction bound solely by IRP (x_1), the fraction bound solely by eIF3 (x_2), and the remainder of the mRNA, which is unbound by either factor (x_3) (Figure 2 – figure supplement 2). The model also assumes that the mutations introduced into *FTL* mRNA do not affect the translational efficiency of unbound mRNA species, i.e. translation of x_3 is identical for all 4 mRNAs. The translational efficiency of IRP-bound mRNA (y_1) and eIF3-bound mRNA (y_2) ranges from fully repressed $(y = 0)$ to completely unbound and derepressed $(y = 1)$. Thus, the translational efficiency for the bound populations $(x_1$ and $x_2)$ is less than 1, while the translational efficiency of x_3 is equal to 1. We also include the parameters α and β to account for changes in the distribution, or shifts, of previously bound mRNA $(x_2$ and $x_1)$ to new populations $(0 \leq \alpha + \beta \leq 1)$. Taken together, 4 overall equations can then represent the luciferase output of each *FTL* mRNA:

(1) FTL = $y_1 x_1 + y_2 x_2 + x_3$
(2) Δ3RE = $y_1 (x_1 + \alpha) + x_2 - \alpha + x_3$
(3) Loop = $x_1 - \beta + y_2 (x_2 + \beta) + x_3$
(4) Double = $x_1 + x_2 + x_3$

Here, FTL represents the luciferase readout of wild-type *FTL* mRNA, Δ3RE the luciferase readout of *FTL* mRNA with the Δ3RE mutation, Loop the luciferase readout of *FTL* mRNA with the IRE loop mutation, and Double the luciferase readout of FTL mRNA with both the Δ3RE and Loop mutations. In order to solve this system of equations we proceeded to use experimentally determined values as seen in Figure 2F. We assume the Δ3RE and Loop mutations disrupt regulation by the respective factor (IRP or eIF3) completely, consistent with the biochemical results in Figure 4. In these cases, both y_1 and y_2 revert to a value of 1, i.e. the same translational efficiency of x_3.

To reduce the number of variables, we rearranged equation (1) with normalized luciferase values $(x_3 = 1 - y_1 x_1 - y_2 x_2)$ and substituted it into equations (2) through (4)

(5) Δ3RE = $y_1 (x_1 + a) + x_2 - \alpha + 1 - y_1 x_1 - y_2 x_2 \rightarrow 1 + y_1 \alpha - \alpha + (1 - y_2) x_2$
(6) Loop = $x_1 - \beta + y_2 (x_1 + \beta) + 1 - y_1 x_1 - y_2 x_2 \rightarrow 1 + y_2 \beta - \beta + (1 - y_1) x_1$
(7) Double = $x_1 + x_2 + 1 - y_1 x_1 - y_2 x_2 \rightarrow 1 + (1 - y_1) x_1 + (1 - y_2) x_2$

Further rearrangement and substitution of Δ3RE and Loop into equation (7) yields:

(8) $(1 - y_2) x_2 = $ Δ3RE $- 1 - y_1 \alpha + \alpha$
(9) $(1 - y_1) x_1 = $ Loop $- 1 - y_2 \beta + \beta$
(10) Double = Loop + Δ3RE + $(\alpha + \beta - y_1 \alpha - y_2 \beta - 1)$

Given the measured luciferase values (Figure 2F), the above model, which assumes IRP and eIF3 do not bind simultaneously to the same *FTL* mRNA, is inconsistent with the data, even accounting for measurement error.

Refer to equation (10):

$$41.8 \ (\pm 6.5) \ > \ 12.5 \ (\pm 2.9) \ + \ 4.4 \ (\pm 0.4) \ + (\alpha + \beta - y_1\alpha - y_2\beta - 1)$$
$$41.8 \ (\pm 6.5) \ > \ 16.9 \ ((\pm 2.9)) + (\alpha + \beta - y_1\alpha - y_2\beta - 1)$$

Thus, IRP and eIF3 likely can act in *cis* on *FTL* mRNAs.

Chapter 3: Foundational modeling for understanding the dynamics between eIF4E1 and eIF4E3 throughout tumor progression

Abstract:

Dysregulated translation promotes tumorigenesis, cancer progression, and metastasis. One key point of translational control often perturbed in cancer is dysregulation of eIF4E1, the canonical mRNA cap-binding protein. The over-expression of this initiation factor has been well-documented in a broad spectrum of cancers varying from non-Hodgkin's lymphomas, to cancers of the colon, breast, bladder, prostate and gastrointestinal tract (Graff & Zimmer, 2003). Recently eIF4E3 has been implicated in altering the translation of cancer specific transcripts potentially acting in an eIF4E1-competitive manner. It is most likely the case that like eIF4E1, eIF4E3 levels are heavily modulated over the progression of a cancer. However, clarity on the exact role eIF4E3 serves during tumor progression as well as its dynamics response to eIF4E1 remains to be fully investigated. Here, we establish a system to disentangle the roles and interplay between eIF4E3 and eIF4E1 during tumor progression, at both phenotypic and molecular levels.

Introduction:

Cancer progression and metastasis is sustained in part by a global increase in protein synthesis accompanied with specific alterations to a subset of the translatome. This raises fundamental interests into how this specific dysregulation is achieved. Normally transcript selection is discerned by the eukaryotic translation initiation factor 4E1 (eIF4E1). One of the three main proteins that compose the eIF4F complex, eIF4E1 directly binds the 5'-methylguanosine cap found on virtually all cellular mRNAs (Sonenberg & Hinnebusch, 2009). This cap recognition allows for the appropriate identification and recruitment of translation machinery onto specific transcripts. However, eIF4E1 has been shown to be misregulated in up to 30% of human tumors and malignancies (Mamane et al., 2004).

Normally, eIF4E1 abundance is low, and the translation initiation factor is isolated from the rest of the eIF4F complex by its interactions with 4E-BPs. This regulation limits the pool of mRNAs that are being translated at any one time. But upon transformation, key oncogenic pathways such as PI3K/Akt/mTOR and MAPK/Mnk upregulate the availability and activity of eIF4E1, ultimately increasing protein synthesis (Furic et al., 2010; Sonenberg & Hinnebusch, 2009). As a downstream result of PI3K/Akt activation, 4E-BP becomes hyperphosphorylated, freeing eIF4E1 to assemble with the rest of the eIF4F complex (Hsieh et al., 2012; Thoreen et al., 2012). Furthermore, upon the binding of eIF4E1 to eIF4G, eIF4E1 is phosphorylated at S209 by MNK, placing eIF4E1 in an active state. While this phosphorylation has been demonstrated to be non-essential in supporting normal translation, it is crucial for cellular transformation (McKendrick, Morley, Pain, Jagus, & Joshi, 2001; T. Ueda, Watanabe-Fukunaga, Fukuyama, Nagata, & Fukunaga, 2004; Wendel et al., 2007). This activation removes transcript competition for the initiation machinery and disproportionally promotes the translation of transcripts with highly structured 5' UTRs. These include oncogenic transcripts such as c-MYC, VEGF, and cyclin D1 (Mamane et al., 2004). Additionally, work by the Ruggero group has shown that this eIF4E1 over-abundance is accompanied by translational reprogramming to promote the translation of mRNAs containing certain cytosine-enriched (CERT) motifs in their 5'UTR (Truitt et al., 2015). Since eIF4E1 is such a potent oncogene, it has been evaluated as a potential target for cancer therapeutics. Controlling the eIF4E1 dosage in cells has shown to be an effective way to mitigate cellular transformation. It has been demonstrated in both cultured cells and in eIF4E1 haploinsuficient mice (eIF4E1^{+/-}), that limiting eIF4E1 expression increased resistance to cellular transformation without negatively impacting general protein synthesis (Truitt et al., 2015). There are also currently therapies in clinical trials that target MNK and its ability to phosphorylate eIF4E1 (Reich et al., 2018).

Subsequent to the discovery of eIF4E1, two eIF4E homologs have been identified: eIF4E2, and eIF4E3 (Joshi et al., 2004; Joshi et al., 2005). These proteins alter translation and subsequently protein expression under different physiological stress conditions. eIF4E3 is the least studied of the eIF4E family, and the few reports that exist have conflicting results. eIF4E3 was originally proposed to act in opposition of eIF4E1. Looking specifically at a selected few oncogenic transcripts, such as VEGF and

c-MYC, eIF4E3 was shown to be able to interact with their 5' m^{7}G cap but fail to promote their translation (Osborne et al., 2013). This observation, along with the fact that eIF4E3 does not associate with 4E-BPs, led the field to identify eIF4E3 as a tissue-specific tumor suppressor and potential competitor of eIF4E1 (Joshi et al., 2004; Osborne et al., 2013; Volpon et al., 2013). Additionally, a computational study of RNA-binding proteins in the cancer genome atlas identified consistent down regulation of eIF4E3 across roughly 6700 clinical samples and 16 human cancer types (Zhang et al., 2018). This was soon challenged by a study focused on understanding the effects of MNK inhibition (Landon et al., 2014). They demonstrated that in the absence of eIF4E1 phosphorylation of S209, physiological levels eIF4E3 increase and eIF4E3 supports tumor persistence by regulating the translation of a unique set of transcripts (Landon et al., 2014). These conflicting studies fail to provide clarity on whether eIF4E3 acts in a pro- or anti-oncogenic manner.

In order to address this ambiguity, we have developed a system in which we can assess the role of eIF4E3 during the tumor life cycle. Through modeling various eIF4E3 states and grafting these syngeneic tumor cells on mice, we are able to monitor physiological tumor progression in a natural tumor microenvironment as well as the corresponding translatome. We hypothesize that eIF4E3 activity is modulated over the progression of a cancer, and in implementing this system we aim to uncover the true mechanism of action of eIF4E3. Elucidating this role of eIF4E3 may provide insight into how it can serve as an effective target for anti-cancer therapy as well as having implications for current therapies targeting eIF4E1
.

Results:

Generating the appropriate model for eIF4E3 CRISPR-Cas9 knockout and add back cells

In order to assess the phenotypic effects of eIF4E3 level modulation during cancer progression, we genetically engineered a set of cell lines: an eIF4E3 knockout cell line (ΔeIF4E3), a line with wild type eIF4E3 (eIF4E3^{WT}) restored or overexpressed, and line with the cap binding null version of eIF4E3 (eIF4E3$^{\Delta cap}$) restored or overexpressed to be grafted in mice. The cap binding null version of eIF4E3 contains a mutation at position 98 in which a key cap interacting aromatic amino acid tryptophan is mutated to alanine (Osborne et al., 2013). These foundational sets of cell lines were generated in both LSL4 and B16-F10 cells. LSL4 cells are a mouse soft tissue sarcoma line derived from leg muscle (Dodd et al., 2015; DuPage, Dooley, & Jacks, 2009). eIF4E3 was originally identified to be expressed in a tissue specific manner with predominant expression occurring in muscle tissues, making the LSL4 line an optimal choice. B16-F10 cells are a mouse skin melanoma cell line that is reliably used for synergistic grafting experiments (Potez et al., 2018). eIF4E3 expression in both LSL4 and B16-F10 cells was confirmed through western blot analysis. We proceeded to use a dual-guide CRISPR-Cas9 approach supplemented with a single stranded DNA donor, having complete homology to the intended repair sequence, to remove the first exon of eIF4E3 in the LSL4 cell line (Figure 1A). This method was proven to be successful and we were able to obtain ΔeIF4E3 clonal cell lines with verified sequence junction (Figure 1B,C). Lack of eIF4E3 expression in these LSL4 based cell lines was confirmed on a transcript level via RT-qPCR and on a protein level via western blotting (Figure 1D,E). It was previously reported that alterations in eIF4E1 levels and functionality has a consequential effect on the abundance of eIF4E3. Interestingly, we fail to observe any significant change in eIF4E1 protein levels in our ΔeIF4E3 lines (Figure 1F). We then restored expression of wild-type or Δcap eIF4E3 in this background by lentiviral transduction. Clonal populations were obtained of both eIF4E3^{WT} and eIF4E3$^{\Delta cap}$ and validated for rescue expression of eIF4E3 via western blotting (Figure 2A,B).

Due to the extensive use of B16-F10 cells in grafting experiments we deemed these cells as an apt system to attempt to make a more complete knock out and remove the full eIF4E3 genomic sequence. We optimized our CRISPR-Cas9 genomic engineering approach by assessing three different editing strategies. Similar to eIF4E1, the genomic sequence of eIF4E3 is replete with introns and spans a ~ 40 kb region. This expansive length poses technical challenges when attempting to achieve a complete homozygous knock out. Our first approach is consistent with what was performed in the LSL4 line, in which solely the first exon is removed (Figure 3A). Though this fails to remove the full genomic sequence, it had been demonstrated to efficiently excise the first exon and inhibit eIF4E3 production. The second set up aims to remove the full 40 kb region and using similar dual-guide CRISPR-Cas9 approach supplemented with a single stranded DNA donor; however, these guides flank the full genomic eIF4E3 sequence (Figure 3A). The third and final approach is a hybrid of the previous two. Here we use a tri-guide CRISPR-Cas9 approach with the three guides

targeting upstream of eIF4E3, immediately downstream of the first exon, and downstream of the eIF4E3 genomic sequence (Figure 3A). This was also supplemented with the ssDNA donor corresponding to the full gene removal sequence used in the second approach. It has been shown that longer deletions have a higher chance of being sporadically reincorporated back into the genome. We anticipate that this additional and third cleavage event will mitigate reincorporation.

In all three cases we see evidence of the desired editing outcomes (Figure 3—figure supplement 1). Single cell clonal populations were obtained from each of these three editing strategies in B16-F10 cells and confirmed to be homozygous eIF4E3 knockouts (Figure 3B,C). Interestingly, upon RT-qPCR validation, we see about 20% *eIF4E3* mRNA expression remaining despite no detectable protein expression in cell lines derived from the dual-guide whole gene deletion strategy (Figure 3C). This potentially could be attributed to sequence reincorporation elsewhere in the genome, as this same phenomenon is not observed with the tri-guide approach. Additionally, across all of the edited cell lines, there was an upregulation of unidentifiable protein species as evident by the upper and lower bands on our western blots (Figure 3—figure supplement 2). In an attempt to determine whether these were alternate eIF4E3 isoforms or completely unique protein species, we carried out immunoprecipitation to purify from lysate anything that bound to the same antibody used in the western blot analysis, followed by mass spectrometry. Upon review of the resulting peptide fragments we were unable to identify anything that had homology to eIF4E3. Further optimization of this protocol is needed in order to capture and identify these protein species.

Both eIF4E3^{WT} and eIF4E3$^{\Delta cap}$ add back cell lines were generated in these various B16-F10 ΔeIF4E3 lines using the previous lentiviral approach. Clonal populations were obtained for both and validated for rescue expression of eIF4E3 via western blotting (Figure 4). In contrast to the LSL4 cell lines, we did not see as strong over-expression of eIF4E3. It is currently unclear why we are observing this reduced expression of eIF4E3. We confirmed by transient DNA transfections of the plasmids encoding eIF4E3^{WT} and eIF4E3$^{\Delta cap}$ that the cells can sustain higher expression of eIF4E3 than observed in the clonal add back lines (Figure 4E).
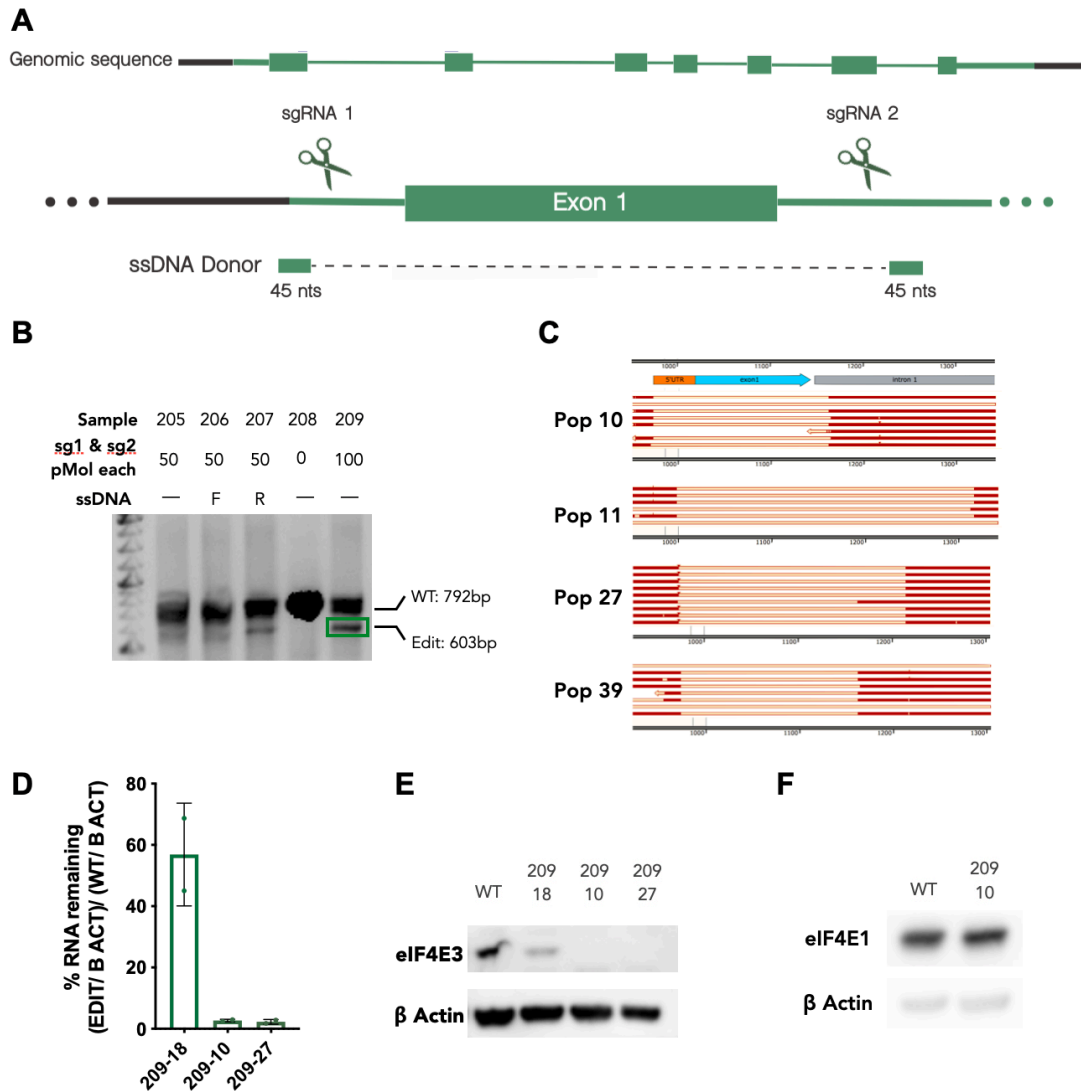
Figure 1: CRISPR-Cas9 editing to excise exon1 of eIF4E3 in LSL4 cells.

(A) CRISPR-Cas9 RNP editing schematic in which two sgRNAs target sequences immediately adjacent to exon 1 of eIF4E3. Reactions were supplemented with 90-nt ssDNA that had full homology to the intended edited sequence. **(B)** Editing efficiency in LSL4 cells at the population level, based on PCR of the region of interest and analysis agarose gel. Efficiency for multiple variations of the experimental set up are demonstrated. **(C)** Sanger sequencing of TOPO cloned gDNA amplified of from edited, clonal populations. Four successfully edited LSL4 clonal populations are shown. **(D)** mRNA levels of *eIF4E3* as determined by RNA extraction from WT LSL4 and LSL4 ΔeIF4E3 cells and RT-qPCR. The mRNA levels for eIF4E3 were first normalized to *ACTB* mRNA. **(E)** Representative western blots of eIF4E3 in three of the edited (ΔeIF4E3) lines compared to WT LSL4 cells under normal conditions. **(F)** Representative western blots of eIF4E1 in an edited (ΔeIF4E3) line compared to WT LSL4 cells under normal conditions.
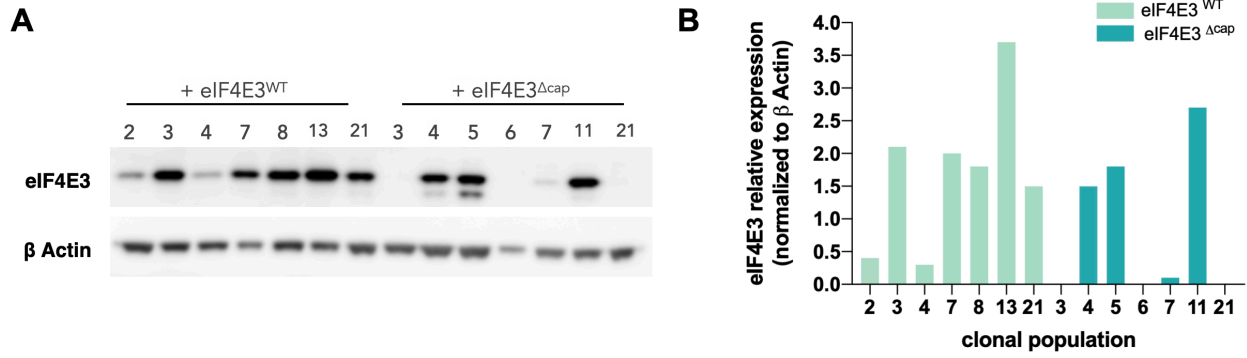
Figure 2: Lentiviral based generation of WT or cap binding null versions of eIF4E3 add backs.

(A) Representative western blots of eIF4E3 levels in add back of eIF4E3^{WT} or eIF4E3$^{\Delta cap}$ in LSL4 ΔeIF4E3 line. **(B)** The quantification of the abundance of the various forms of eIF4E3 seen in the western blot **(A)** after normalization to β Actin.
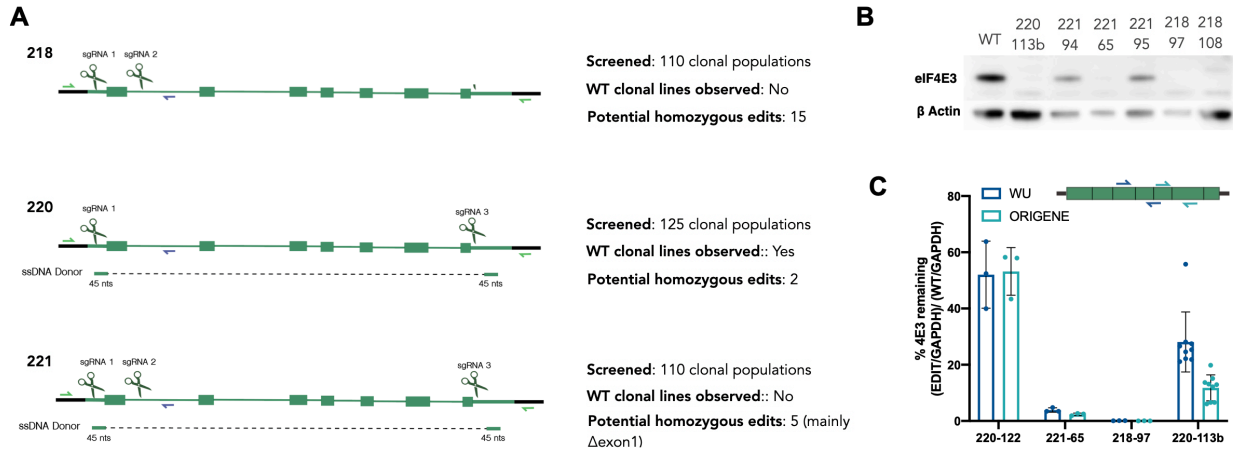
Figure 3: CRISPR-Cas9 based removal of eIF4E3 in B16-F10 cells.

(A) CRISPR-Cas9 RNP editing schematic in which two or three sgRNAs target sequences immediately adjacent to exon 1 or the full genomic sequence of eIF4E3. Adjacent to each set up is information about editing efficiency observed during clonal population screening. **(B)** Representative western blots of eIF4E3 in various edited (ΔeIF4E3) clonal lines compared to WT B16-F10 cells under normal condition. **(C)** mRNA levels of *eIF4E3* as determined by RNA extraction from WT B16-F10 and ΔeIF4E3 clonal cells and RT-qPCR. The mRNA levels for eIF4E3 were first normalized to *GAPDH* mRNA. Two qPCR primers sets were used and are referenced as WU or Origene based on where the primer sequences were obtained.
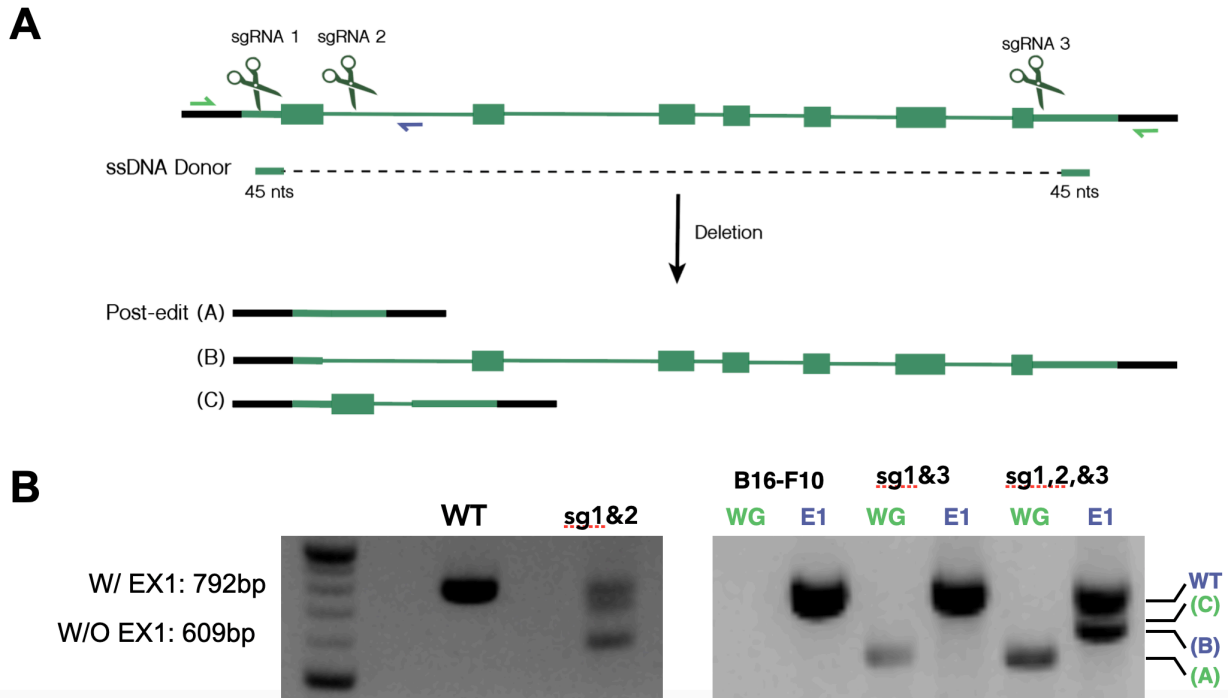
Figure 3 supplement 1: CRISPR-Cas9 editing strategy to excise eIF4E3 in B16-F10 cells.

(A) CRISPR-Cas9 RNP editing schematic demonstrating the various predicted editing results using three sgRNAs target sequences immediately adjacent to Exon 1 or the full genomic sequence of eIF4E3. Reactions were supplemented with 90-nt ssDNA that had full homology to the intended edited sequence. Post-edit (A) represents a full gene deletion of eIF4E3. Post-edit (B) represents an eIF4E3 exon 1 deletion. Post-edit (C) represents the deletion of the full eIF4E3 gene except for exon1. **(B)** Editing efficiency in B16-F10 cells at the population level, based on PCR of the region of interest and analysis agarose gel. WG represents a PCR with primers upstream and downstream of the full eIF4E3 genomic sequence. This should not amplify in the WT context due to extreme length of product. E1 is a PCR amplifying the region encompassing exon 1. This serves as a representative for WT sequence in the population. The (A) (B) and (C) identified bands correspond to the potential post-edit populations diagramed earlier in the figure **(A)**.
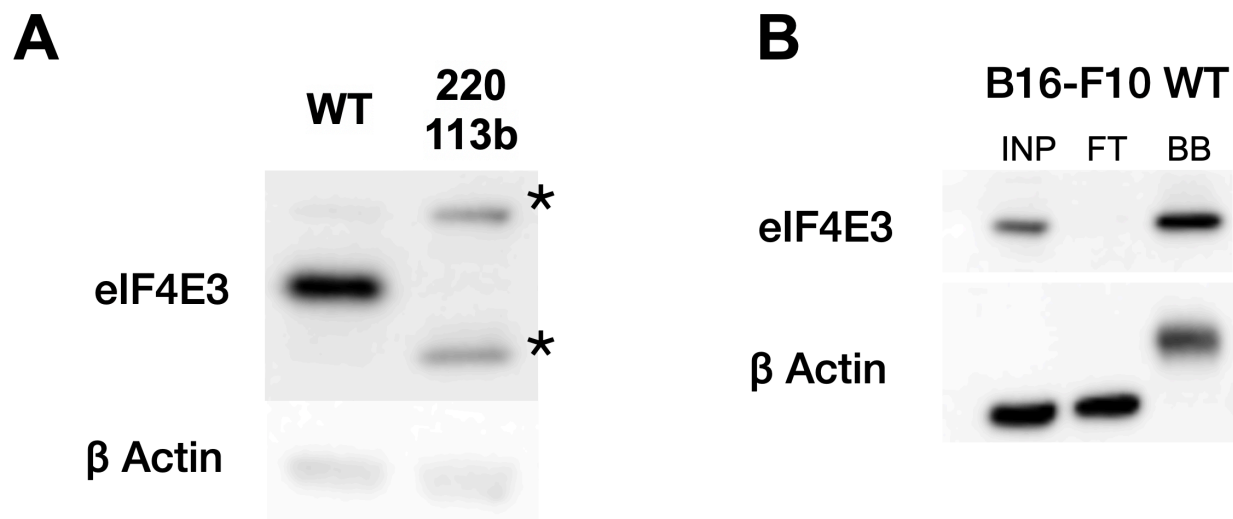
Figure 3 supplement 2: eIF4E3 Immunoprecipitation to identify upregulated and unidentified protein species in the eIF4E3 knock out population

(A) Representative western blot of eIF4E3 levels WT or eIF4E3 knock out B16-F10 cells. * indicates the bands corresponding to proteins of unknown identity that consistently are found upregulated in the eIF4E3 knock out cell lines. **(B)** Representative western blots showing the eIF4E3 immunoprecipitation efficiency. INP represents the input fraction, FT represents flow through, and BB represents the sample collected post bead boil. The upshifted band in the BB lane of the actin panel can be attributed to the recognition of the antibody used for the IP.
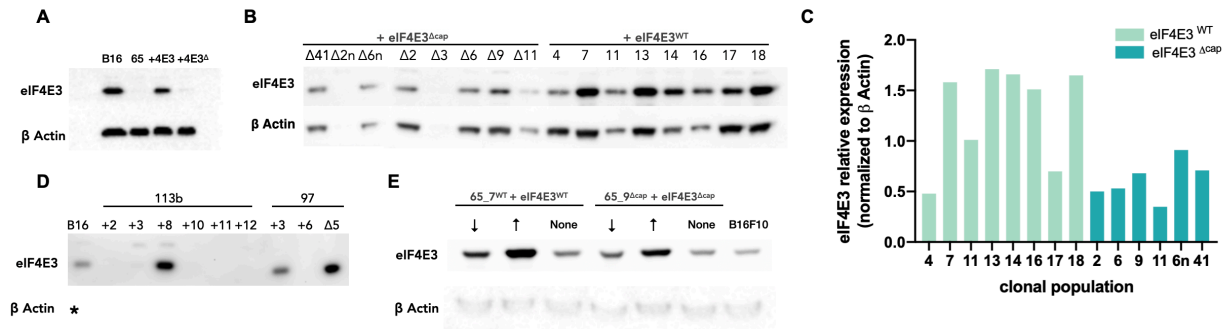
Figure 4: Lentiviral based generation of WT or cap binding null versions of eIF4E3 add backs in B16-F10 cells.

(A) Representative western blots at the population levels of eIF4E3 in add back of eIF4E3^{WT} or eIF4E3$^{\Delta cap}$ in to one of the ΔeIF4E3 clonal lines and comparing the levels of the various forms of eIF4E3 relative to WT B16-F10 cells. **(B)** Representative western blots of eIF4E3 levels in add back eIF4E3^{WT} or eIF4E3$^{\Delta cap}$ in B16-F10 clonal ΔeIF4E3 line #65 **(C)** Quantification the western blot in Figure **(B)**. **(D)** Representative western blots of eIF4E3 levels in add back eIF4E3^{WT} or eIF4E3$^{\Delta cap}$ in B16-F10 clonal ΔeIF4E3 line #113b or #97. * indicates the lack of a successful β Actin blot **(E)** Western blots of transiently transfected eIF4E3^{WT} or eIF4E3$^{\Delta cap}$ at various amounts to monitor eIF4E3 overexpression.

Preliminary phenotypic assessment of eIF4E3 level modulation on tumor progression

In order to gain a deeper understanding of how eIF4E3 affects oncogenic transformation, we directly monitored the physiological characteristics of grafted tumors in mice. Initial grafting experiments of our LSL4 cell line set (ΔeIF4E3 and eIF4E3^{WT}) showed no difference between the eIF4E3 knock out and add-back lines. Upon grafting of these cells, we observed an inherent rapid tumor growth rate which appeared to confound any meaningful changes that could be attributed to eIF4E3 expression differences (data not shown). This inherent rapid growth rate and the adept ability of these cells to recover from stress was also observed in cell culture.

However, after following the B16-F10 based tumors for 25 days in our pilot run, we did observe a potential difference between the two lines (Figure 5A). Contrary to initial reports that suggested eIF4E3 to be a tumor suppressor, we observed that in the absence of eIF4E3 expression there was a reduction in tumor growth compared to the eIF4E3^{WT} line. We do not attribute these results to be directly related to an initial difference in eIF4E1 levels between the cell lines. eIF4E1 protein expression was assessed through western blotting before grafting and no changes in overall eIF4E1 levels was observed amongst the cell types (Figure 5B). This experiment needs to be duplicated to achieve greater statistical power.

.
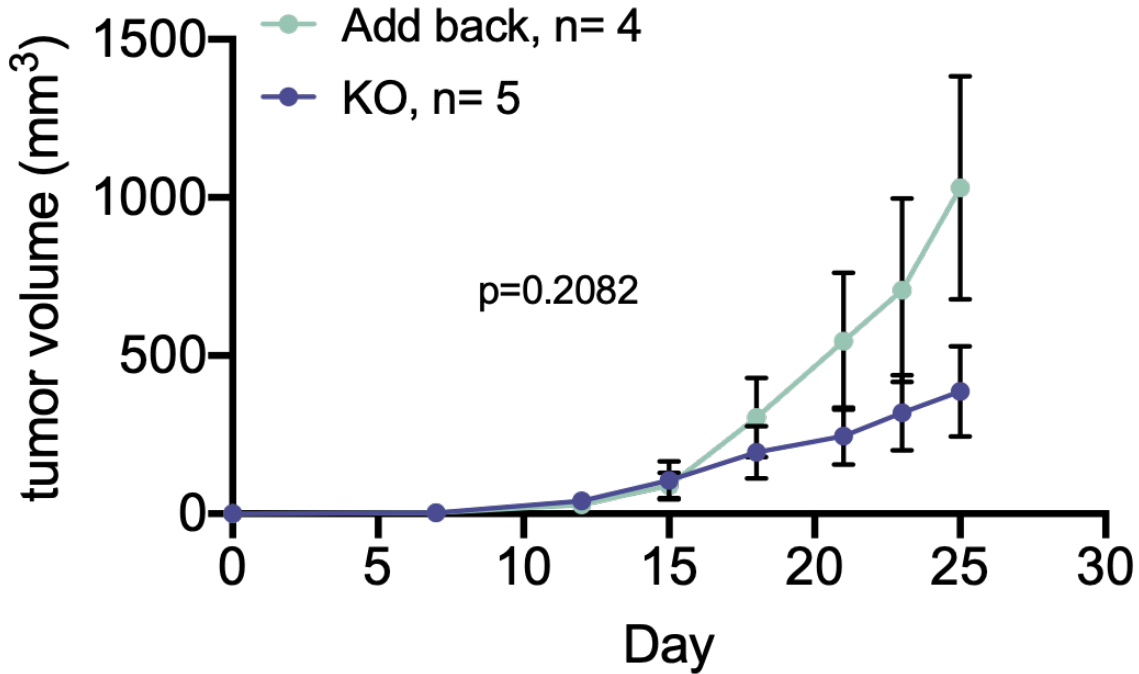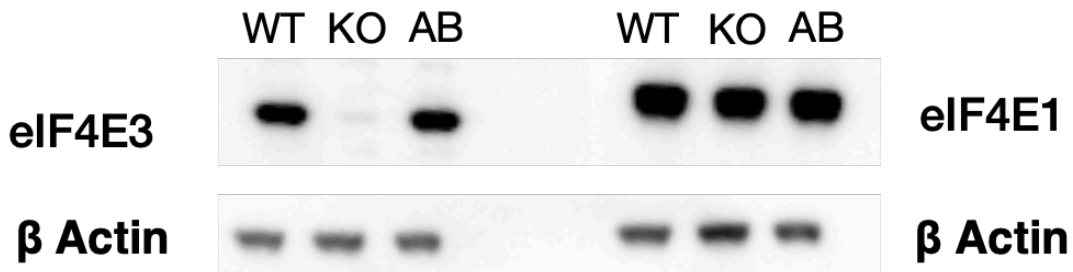
Figure 5: Tumor growth comparison across various eIF4E3 levels.

(A) C57BL/6J mice were injected subcutaneously with B16-F10 eIF4E3 knock out or addback lines. These tumors were allowed to progress for 25 days before harvesting. The data is representative of two independent experiments. *n* = 4 to 5. Tumor volume and analyzed with two way ANOVA

(B) Representative western blots of eIF4E3 and eIF4E1 levels in the of the cells. WT indicates non-edited B16-F10 cells. KO indicates a clonal population of eIF4E3 knock out cells. AB indicated a population of cells in which eIF4E3 has been added back to the KO cells.

Discussion:

Using genome editing, we have established a foundational system to investigate the potential roles of eIF4E3 in oncogenesis. We have observed in this pilot study that eIF4E3 expression can impact tumor progression, with eIF4E3 knockout cell lines showing slower growth. Our eIF4E3-modulated cell lines consistently fail to show any significant changes in eIF4E1 global protein levels. This challenges the findings presented in by Landon et. al. 2014, in which they observed a dynamic interplay between eIF4E3 and eIF4E1 expression levels. This could indicate that eIF4E3 expression is altered by eIF4E1 and this regulation is not reciprocated in the reverse context. Further experiments testing whether levels of phosphorylated eIF4E1 at position S209 are altered in these cell lines might suggest a more subtle form of feedback of activated eIF4E1 governed by eIF4E3 levels.

Through further experimentation we expect these cell lines to provide insight into novel mechanisms of translational regulation by eIF4E3 during the cancer lifecycle. Using genome-wide studies, we will identify novel networks and a broad collection of new factors involved in mediating eIF4E3's regulatory function. Currently, I have done initial transcriptional and translational profiling based experiments on these cells in culture, but further optimization is required to derive any meaningful insight into alterations in the translatome. Additionally, tumors from the mouse experiments in Fig 5 have been harvested and paired ribosome profiling with RNA-seq will be completed in the future. This comparison between tissue culture and *in vivo* samples will also provide information about how the natural tumor microenvironment alters any of these changes observed in the translatome.

Additionally, variations have accumulated between mouse and human eIF4E3 over the course of evolution. To address any functional differences that might arise and confirm conservation of regulatory networks, we have started engineering paired (primary and secondary) human colon adenocarcinoma cancer cell lines that overexpress the long isoform of human eIF4E3. This type of cancer had been previously identified to have decreased expression of eIF4E3 (Zhang et al., 2018). With this overexpression line, we once again hope to monitor changes in the translatome as well as in cellular phenotypes. We expect these longer-term studies to identify larger networks involved in the eIF4E3-based response to cancer, and potentially offer future therapeutic targets aimed to inhibit cancer progression.

Methods:

Plasmids

The Mouse eIF4E3 CDS sequence was obtained from cDNA derived from C2C12 cells and subcloned using In-Fusion HD Cloning Kit (Takara, Cat.# 638911) into MCSV IRES based plasmid backbone to generate an eIF4E3 CDS flanked by NotI restriction digest sites. This was then cloned into the nLV103 vector, using restriction digest cloning with Not1 as the primary restriction enzyme. Cap binding mutations, in which the key cap interacting aromatic amino acid tryptophan 98 was mutated to alanine, were generated in the subcloned plasmid through around-the-horn cloning using primers with overhangs to introduce the single codon mutation (Osborne et al., 2013). The human eIF4E3 construct was ordered from vectorbuilder and contained a Puro:GFP coding sequence on an alternate promoter. The RFP-Puro plasmid was generously provided by Ryan Muller from the Ingolia lab.

In vitro transcription

For genome editing, we used tandem or triple CRISPR-Cas9 RNPs programmed with single-guide RNAs (sgRNAs) targeting the eIF4E3 gene, along with a single-stranded DNA (ssDNA) oligonucleotide homologous to the regions spanning the deleted eIF4E3 sequence (Figure1A and Figure 3A). sgRNAs were designed using the CRISPR.MIT.EDU program from the Feng Zhang Lab, MIT. CRISPR-Cas9-sgRNA was assembled as RNA-protein complexes (RNPs) (Kim et al., 2014). The DNA for transcription was synthesized by appending the sgRNA sequence downstream of a T7 RNA polymerase promoter. The DNA was then purified using phenol-chloroform extraction followed by isopropanol precipitation. After transcription, the RNA products were treated with DNase I (Promega, Cat.# M6101), run on a 10% denaturing polyacrylamide gel (6 M urea), and extracted from the gel using the crush and soak method and ethanol precipitation. Guides were also treated with rSAP to reduce immunogenicity.

Cell line generation

Cell lines (LSL4 and B16-F10) were obtained from the Raulet lab and the University of California Berkeley Cell Culture Facility respectively, validated by STR analysis, and confirmed to be mycoplasma-free. To generate eIF4E3 knockouts, we used tandem CRISPR-Cas9 enzymes programmed with single-guide RNAs (sgRNAs) targeting the eIF4E3 gene, along with a single-stranded DNA (ssDNA) donor with homology to the regions spanning the deleted sequence. The sgRNAs were generated as described above, and targeted regions on both sides of either the first exon or the whole gene region of eIF4E3 (Figure 3A). The RNP complex was generated by incubating 100 pmol Cas9 with the two sgRNAs at a 1:1.2 Cas9 to total sgRNA ratio. This mixture was heated to 37 °C for 10 min and then kept at room temperature until use. The ssDNA donor was 90 nucleotides long, with 45-nucleotide homology on either side of the

predicted double-strand cut sites allowing it to have perfect homology to the predicted edited sequence.

The Cas9-sgRNA RNP complexes, along with 500 pmol of the ssDNA donor, were transfected into either 5×10^5 LSL4 and B16-F10 cells using the Lonza 96-well shuttle system SF kit (Cat. # V4SC-2096). The nucleofection programs used were as follows: CD-137 for LSL4 and DJ-110 for B16-F10. The transfected cells were left to incubate for 72 hr before harvesting and extracting gDNA using QuickExtract (Epicentre: QE09060). The efficiency of the dual or tri-sgRNA editing approach was determined by PCR-amplifying a 792-base pair region around exon 1 (forward primer 5'-GGACTTTGAGACTCCATCCGCACTGATCCAT-3', reverse primer 5'-GAAGTTTCTATTTTGGAGAGGGATCTGAGACCTCACAGAGG-3', ™= 66°, 5x KAPA GC buffer) or a ~40,500 base pair region (forward primer 5'-GGACTTTGAGACTCCATCCGCACTGATCCAT-3', reverse primer 5'-CCCTGAATAAGGAATCTTATGGGGAGGGGAAGAGTG -3',™= 66°, 5x KAPA HIFI buffer) around the full eIF4E3 genomic sequence, and analyzing the resulting products on a 1.5% agarose gel. Monoclonal populations of edited cells were sorted using FACS, screened, and the final edited sequence was determined using TOPO TA cloning (Ramlee et al., 2015).

Transcript level abundance

Total transcript abundance was determined by lysing 1.25×10^6 cells with Qiazol lysis buffer followed by using the Directzol RNA extraction kit (Zymo Research, Cat. # R2061), according to the manufacturer's instructions. The cDNA was generated by reverse transcription using 350 ng of RNA, random hexamers, and Superscript IV (Thermo Fisher scientific, Cat. # 18091050). Primers for the qPCR were as follows: eIF4E3 (WU) forward: 5'-AGACCAGCCTGCCTTTGAGAT-3', eIF3 (WU) reverse: 5'-TTCCAAACTGTGGACGTGCT-3' (Ruibin et al., 2018), eIF4E3 (Origene) forward: 5'-GTTAGCGACCATTGGAGAGCAG-3', eIF4E3 (Origene) reverse: 5'-TGAGGCGTTGACATTCCACACC-3' (CAT#: MP204425)
ACTB forward: 5'- CCTTCTTGGGTATGGAATCCTGT -3' ACTB reverse: 5' -CACTGTGTTGGCATAGAGGTCTTTAC -3' (Gong et al., 2016), GAPDH forward: 5'-TGCACCACCAACTGCTTAG -3', GAPDH reverse: 5'- GGATGCAGGGATGATGTTC -3' (Gong et al., 2016). Run conditions were: 95 °C for 15 s, followed by 40 cycles of 95 °C for 15 s, 60 °C for 60 s, 95 °C for 1 s.

RNA immunoprecipitation and Mass spectrometry:

The eIF4E3-RNA immunoprecipitations were adapted from Landon et al., 2014 with the following modifications. One 10 cm plate of B16-F10 cells was used to prepare cell lysate using 200 µl of NP40 lysis buffer listed in Chapter 2 (Lee et al., 2015). The lysate was incubated with 13 µg eIF4E3 antibody overnight at 4 °C. Both protein G agarose beads (Abcam, ab193258) and Dynabeads preloaded with rabbit IgG (Cell Signaling, Cat. # 2729) were shown to be effective for this protocol. The beads were pre-equalized by using one wash of 150mM KCl+ Tris wash for the protein G agarose beads or a PBS

tween wash for the Dynabeads followed by two washes with NP40 lysis buffer without DTT or a protease tablet. The lysate antibody mix was then added to the beads and allowed to incubated for two hours at 4 °C. The Lysate-bead mixture was washed three times using the following wash buffer (50 mM HEPES pH 7.5, 150 mM KCl, 1 mM EDTA, 1% Triton X-100, 0.5% Nonidet-40, 1X protease inhibitor). Sample was collected by boiling the beads at 95 °c for 5 minutes in 30µL of 2x loading dye and wash buffer mix.

An abbreviated version of this IP provides comparable results. Here the beads are pre-bound to the eIF4E3 antibody at the same time the lysate is pre-cleared by incubating it with beads. Both of steps have a 2 hour incubation period at 4 °C. All mass spectrometry samples were collected and analyzed according to the UC Berkeley mass spectrometry facilities' protocol.

Western blots:

The following antibodies were used for Western blot analysis: anti-EIF4e3 (proteintech, 17282-1-AP) at 1:300; anti-eIF4E1 (Abcam, ab76256 and Santa Cruz Biotechnology, sc-9976) at 1:600; and anti-b-Actin (Abcam, ab8227) at 1:1000.

Transient plasmid transfection:

Mouse B16-F10 cells were maintained in DMEM (Invitrogen 11995–073) with 10% FBS (Seradigm) and 1% Pen/Strep (Gibco, Cat.# 15140122). Transfections of the various eIF4E3 NLV103 plasmids were done using the Muris transIt 2020 kit Transfection Kit (Cat.# MIR 5400), with the following protocol modifications. The day prior to transfection, eIF4E3^{wt} or eIF4E3$^{\Delta cap}$ cells were seeded into a 6-well of plate so that they would reach 70% confluence at the time of transfection. Either high levels (3750 ng) or low levels (1250 ng) of plasmid DNA was added at room temperature to 250µL OptiMEM media (Invitrogen, Cat. # 31985–088) and 7.5 µL TransIt 2020 reagent and left to incubate at room temperature for 25 min. The TransIT 2020 Reagent:OptiMEM:DNA complex was distributed to the cells in a drop wise manner. Cells were harvested 72 hr post transfection and western blots were performed to assess eIF4E3 protein abundance.

Lentiviral transduction:

The eIF4E3 mouse and human plasmids listed above were used to generate the add back/ over-expression cell lines. Virus was generated using LentiX cells in a 10 cm dish format and TransIT-LT1 transfection reagent. Virus was harvested and filtered after 48 and 72 hr. Total virus was pooled and 500 mL of fresh virus was added to 10^6 HEK293T cells along with 10 mg/mL of polybrene (Millipore). Cells were left to incubate for 48 hr before a 4-day selection process with 4 mg/mL of puromycin. Cells were split in non-selective media once before use.

Sleeping Beauty Transduction:

A PURO:RFP plasmid was stably integrated into either eIF4E3 KO or addback cell lines using sleeping beauty transduction. A one to one mix of 400 ng of the RFP: PURO plasmid along with 400ng of the sleeping beauty transposase plasmid was nucleofected into 5×10^5 cells. These cells were then plated in a 6-well plate and propagated for 1.5 weeks to ensure sufficient dilution of unincorporated plasmid. These cell lines were then bulk sorted for RFP expression using the Aria fusion sorter.

Mouse Grafting:

Mice were maintained at the University of California, Berkeley. These experiments were conducted by our collaborators in the Raulet lab. This procedure for these *in vivo* tumor growth experiments was adapted from Nicolai et al. (2020) with the following changes (Nicolai et al., 2020). 100,000 cells (B16-F10 ΔeIF4E3 clonal line and eIF4E3^{WT} population) were injected subcutaneously into the flank. Tumor growth was measured and assessed in the same manner using calipers and the ellipsoid formula: V=(π/6)ABC. Tumors were also harvested and immediately flash frozen for future experiments. All C57BL/6Jmice used were aged 8 to 30 weeks. All experiments were approved by the University of California (UC) Berkeley Animal Care and Use Committee.

Chapter 4: Conclusion and outstanding questions

Translation initiation provides a system of regulatory networks aiding in the management of appropriate protein synthesis. We have studied two components of this pathway with the capacity to selectively alter transcript selection and ultimately global protein expression. In our first study, we identify a counterintuitive role of eIF3, in the selective repression of *FTL* mRNA translation (Pulos-Holmes et al., 2019). This demonstrated new breath amongst the many functions of eIF3. In our second study we successfully establish a platform to gain a mechanistic understanding of the role of eIF4E3 during cellular transformation. Using this system, we have observed a potential phenotypic difference in *in vivo* tumor progression when eIF4E3 is no longer expressed in cells. This work needs to be further expanded upon to fully determine significance.

While this work has contributed to the larger understanding of specialized regulation of translation, questions still remain about the unique regulation these two translation initiation factors provide. With respect to eIF3 we have yet to identify what primes its repression of *FTL* translation. Currently, eIF3 has not been shown to have any innate environmental sensing capabilities. However, expression of FTL is strongly environmentally regulated by both iron abundance and tissue type (Gregory J. Anderson, 2012). We hypothesize that context-dependent regulation could arise through either interactions with other RNA binding proteins, potentially IRP, or through the addition of post-translational modifications (PTMs) to eIF3, context dependent regulation could be stimulated. It would be valuable to validate our mathematical model presented in chapter 2 and experimentally obtain evidence for the ability of eIF3 and IRP to concurrently interact with the 5' UTR of *FTL (Pulos-Holmes et al., 2019)*. Regardless of whether our model is supported or not, this would provide evidence regarding conditions where eIF3 can be recruited to *FTL* as well as potentially identifying a mechanism for eIF3 recruitment. Another potential way eIF3 could be recruited to *FTL* mRNA is through eIF3d cap binding activity (Lee et al., 2016). Further experimentation is needed to see whether the observed eIF3d:*c-JUN* interaction is recapitulated with respect to *FTL*. Additionally, it is key that we understand the impact eIF3 has on the regulating the ferritin complex composition and cellular iron abundance. We have observed that, in absence of repression of FTL by eIF3, there is a simultaneous change in FTH levels (Pulos-Holmes et al., 2019). Analyzing the ferritin complex composition under these circumstances would test whether eIF3 can in fact contribute to overall ferritin dynamics. Obtaining intracellular labile iron measurements with and without the presence of eIF3 based repression would inform us whether this regulation served as a fail-safe maintaining iron regulation or servers to a different function within the cell.

Furthermore, there remains much to be done with respect to eIF4E3. We have established a system to understand eIF4E3 driven translational control, but we have yet to fully make use of it. Initial attempts to understand the changes in the translatome across the various cell lines were conducted, but they still need further optimization before we can obtain reliable results. These RNA-seq and ribosome profiling experiments must be performed on cultured cells, and on harvested tumors as well.

This will allow us to identify individual transcripts as well as general processes that are eIF4E3 sensitive. The resulting data from these experiments can also be analyzed in comparison with published data identifying eIF4E1 sensitive transcripts. This will allow us to detect interactions between these alternative cap-binding proteins. Our system primarily focuses on mouse eIF4E3, which has only one reported isoform. It would be beneficial to see how our findings carry over and eIF4E3 serves similar functions across species. Lastly, understanding how eIF4E3 carries out these functions and what other complexes it interacts with will better allow us to appreciate the need for cap binding complex diversity. Through both of these projects presented we have gained insight into and have identified new avenues of study for the regulatory mechanisms controlling translation initiation and protein synthesis.

References

Altmann, M., Edery, I., Sonenberg, N., & Trachsel, H. (1985). Purification and characterization of protein synthesis initiation factor eIF-4E from the yeast Saccharomyces cerevisiae. *Biochemistry, 24*(22), 6085-6089. doi:10.1021/bi00343a009

Arake de Tacca, L. M., Pulos-Holmes, M. C., Floor, S. N., & Cate, J. H. D. (2019). PTBP1 mRNA isoforms and regulation of their translation. *RNA, 25*(10), 1324-1336. doi:10.1261/rna.070193.118

Ascano, M., Hafner, M., Cekan, P., Gerstberger, S., & Tuschl, T. (2012). Identification of RNA-protein interaction networks using PAR-CLIP. *Wiley Interdiscip Rev RNA, 3*(2), 159-177. doi:10.1002/wrna.1103

Basilion, J. P., Rouault, T. A., Massinople, C. M., Klausner, R. D., & Burgess, W. H. (1994). The iron-responsive element-binding protein: localization of the RNA-binding site to the aconitase active-site cleft. *Proc Natl Acad Sci U S A, 91*(2), 574-578. doi:10.1073/pnas.91.2.574

Berman, A. J., Thoreen, C. C., Dedeic, Z., Chettle, J., Roux, P. P., & Blagden, S. P. (2020). Controversies around the function of LARP1. *RNA Biol*, 1-11. doi:10.1080/15476286.2020.1733787

Bert, A. G., Grepin, R., Vadas, M. A., & Goodall, G. J. (2006). Assessing IRES activity in the HIF-1alpha and other cellular 5' UTRs. *RNA, 12*(6), 1074-1083. doi:10.1261/rna.2320506

Bohlen, J., Fenzl, K., Kramer, G., Bukau, B., & Teleman, A. A. (2020). Selective 40S Footprinting Reveals Cap-Tethered Ribosome Scanning in Human Cells. *Mol Cell*. doi:10.1016/j.molcel.2020.06.005

Bramham, C. R., Jensen, K. B., & Proud, C. G. (2016). Tuning Specific Translation in Cancer Metastasis and Synaptic Memory: Control at the MNK-eIF4E Axis. *Trends Biochem Sci, 41*(10), 847-858. doi:10.1016/j.tibs.2016.07.008

Browning, K. S., & Bailey-Serres, J. (2015). Mechanism of cytoplasmic mRNA translation. *Arabidopsis Book, 13*, e0176. doi:10.1199/tab.0176

Camaschella, C., Zecchina, G., Lockitch, G., Roetto, A., Campanella, A., Arosio, P., & Levi, S. (2000). A new mutation (G51C) in the iron-responsive element (IRE) of L-ferritin associated with hyperferritinaemia-cataract syndrome decreases the binding affinity of the mutated IRE for iron-regulatory proteins. *Br J Haematol, 108*(3), 480-482. doi:10.1046/j.1365-2141.2000.01920.x

Carvalho, H., & Meneghini, R. (2008). Increased expression and purification of soluble iron-regulatory protein 1 from Escherichia coli co-expressing chaperonins GroES and GroEL. *Braz J Med Biol Res, 41*(4), 270-276. doi:10.1590/s0100-879x2008005000009

Cate, J. H. (2017). Human eIF3: from 'blobology' to biological insight. *Philos Trans R Soc Lond B Biol Sci, 372*(1716). doi:10.1098/rstb.2016.0176

Cazzola, M., Bergamaschi, G., Tonon, L., Arbustini, E., Grasso, M., Vercesi, E., . . . Arosio, P. (1997). Hereditary hyperferritinemia-cataract syndrome: Relationship between phenotypes and specific mutations in the iron-responsive element of ferritin light-chain mRNA. *Blood, 90*(2), 814-821. doi:DOI 10.1182/blood.V90.2.814.814_814_821

Cham, B. E., Roeser, H. P., Nikles, A., & Ridgway, K. (1985). A procedure for the purification of ferritin from human liver by heating a methanol-treated homogenate. *Analytical Biochemistry, 151*(2), 561-565. doi:10.1016/0003-2697(85)90220-9

Chen, J. L., Lucas, J. E., Schroeder, T., Mori, S., Wu, J., Nevins, J., . . . Chi, J. T. (2008). The genomic analysis of lactic acidosis and acidosis response in human cancers. *PLoS Genet, 4*(12), e1000293. doi:10.1371/journal.pgen.1000293

Cho, S., Park, S. M., Kim, T. D., Kim, J. H., Kim, K. T., & Jang, S. K. (2007). BiP internal ribosomal entry site activity is controlled by heat-induced interaction of NSAP1. *Mol Cell Biol, 27*(1), 368-383. doi:10.1128/MCB.00814-06

Choi, J., Grosely, R., Prabhakar, A., Lapointe, C. P., Wang, J., & Puglisi, J. D. (2018). How Messenger RNA and Nascent Chain Sequences Regulate Translation Elongation. *Annu Rev Biochem, 87*, 421-449. doi:10.1146/annurev-biochem-060815-014818

Colgan, D. F., & Manley, J. L. (1997). Mechanism and regulation of mRNA polyadenylation. *Genes Dev, 11*(21), 2755-2766. doi:10.1101/gad.11.21.2755

Collier, A. J., Gallego, J., Klinck, R., Cole, P. T., Harris, S. J., Harrison, G. P., . . . Walker, S. (2002). A conserved RNA structure within the HCV IRES eIF3-binding site. *Nat Struct Biol, 9*(5), 375-380. doi:10.1038/nsb785

Combe, J. P., Petracek, M. E., van Eldik, G., Meulewaeter, F., & Twell, D. (2005). Translation initiation factors eIF4E and eIFiso4E are required for polysome formation and regulate plant growth in tobacco. *Plant Mol Biol, 57*(5), 749-760. doi:10.1007/s11103-005-3098-x

Cozzi, A., Corsi, B., Levi, S., Santambrogio, P., Biasiotto, G., & Arosio, P. (2004). Analysis of the biologic functions of H- and L-ferritins in HeLa cells by transfection with siRNAs and cDNAs: evidence for a proliferative role of L-ferritin. *Blood, 103*(6), 2377-2383. doi:10.1182/blood-2003-06-1842

De Silva, D., Ferguson, L., Smith, B. E., Chin, G. H., Apathy, R. A., Roth, T. L., . . . Cate, J. H. D. (2020). Dynamics of T cell activation mediated by eIF3 interactions with T cell receptor mRNAs. *bioRxiv*. doi:10.1101/2019.12.20.885558

Desrosiers, R., Friderici, K., & Rottman, F. (1974). Identification of methylated nucleosides in messenger RNA from Novikoff hepatoma cells. *Proc Natl Acad Sci U S A, 71*(10), 3971-3975. doi:10.1073/pnas.71.10.3971

Dodd, R. D., Ano, L., Blum, J. M., Li, Z., Van Mater, D., & Kirsch, D. G. (2015). Methods to generate genetically engineered mouse models of soft tissue sarcoma. *Methods Mol Biol, 1267*, 283-295. doi:10.1007/978-1-4939-2297-0_13

Doudna, J. A., & Rath, V. L. (2002). Structure and Function of the Eukaryotic Ribosome. *Cell, 109*(2), 153-156. doi:10.1016/s0092-8674(02)00725-0

DuPage, M., Dooley, A. L., & Jacks, T. (2009). Conditional mouse lung cancer models using adenoviral or lentiviral delivery of Cre recombinase. *Nat Protoc, 4*(7), 1064-1072. doi:10.1038/nprot.2009.95

Fillebeen, C., Wilkinson, N., & Pantopoulos, K. (2014). Electrophoretic mobility shift assay (EMSA) for the study of RNA-protein interactions: the IRE/IRP example. *J Vis Exp*(94). doi:10.3791/52230

Frydryskova, K., Masek, T., Borcin, K., Mrvova, S., Venturi, V., & Pospisek, M. (2016). Distinct recruitment of human eIF4E isoforms to processing bodies and stress granules. *BMC Mol Biol, 17*(1), 21. doi:10.1186/s12867-016-0072-x

Furic, L., Rong, L., Larsson, O., Koumakpayi, I. H., Yoshida, K., Brueschke, A., . . . Sonenberg, N. (2010). eIF4E phosphorylation promotes tumorigenesis and is associated with prostate cancer progression. *Proc Natl Acad Sci U S A, 107*(32), 14134-14139. doi:10.1073/pnas.1005320107

Godet, A. C., David, F., Hantelys, F., Tatin, F., Lacazette, E., Garmy-Susini, B., & Prats, A. C. (2019). IRES Trans-Acting Factors, Key Actors of the Stress Response. *Int J Mol Sci, 20*(4). doi:10.3390/ijms20040924

Gong, H., Sun, L., Chen, B., Han, Y., Pang, J., Wu, W., . . . Zhang, T. M. (2016). Evaluation of candidate reference genes for RT-qPCR studies in three metabolism related tissues of mice after caloric restriction. *Sci Rep, 6*, 38513. doi:10.1038/srep38513

Goossen, B., & Hentze, M. W. (1992). Position is the critical determinant for function of iron-responsive elements as translational regulators. *Mol Cell Biol, 12*(5), 1959-1966. doi:10.1128/mcb.12.5.1959

Graff, J. R., & Zimmer, S. G. (2003). Translational control and metastatic progression: enhanced activity of the mRNA cap-binding protein eIF-4E selectively enhances translation of metastasis-related mRNAs. *Clin Exp Metastasis, 20*(3), 265-273. doi:10.1023/a:1022943419011

Gregory J. Anderson, G. D. M. (2012). Iron Physiology and Pathophysiology in Humans. *Springer*, 1-704. doi:10.1007/978-1-60327-485-2

Gritsenko, A. A., Weingarten-Gabbay, S., Elias-Kirma, S., Nir, R., de Ridder, D., & Segal, E. (2017). Sequence features of viral and human Internal Ribosome Entry Sites predictive of their activity. *PLoS Comput Biol, 13*(9), e1005734. doi:10.1371/journal.pcbi.1005734

Hafner, M., Landthaler, M., Burger, L., Khorshid, M., Hausser, J., Berninger, P., . . . Tuschl, T. (2010). PAR-CliP--a method to identify transcriptome-wide the binding sites of RNA binding proteins. *J Vis Exp*(41). doi:10.3791/2034

Harrison, P. M., & Arosio, P. (1996). The ferritins: molecular properties, iron storage function and cellular regulation. *Biochimica et Biophysica Acta (BBA) - Bioenergetics, 1275*(3), 161-203. doi:10.1016/0005-2728(96)00022-9

Hinnebusch, A. G. (2006). eIF3: a versatile scaffold for translation initiation complexes. *Trends Biochem Sci, 31*(10), 553-562. doi:10.1016/j.tibs.2006.08.005

Hinnebusch, A. G. (2014). The scanning mechanism of eukaryotic translation initiation. *Annu Rev Biochem, 83*, 779-812. doi:10.1146/annurev-biochem-060713-035802

Hsieh, A. C., Liu, Y., Edlind, M. P., Ingolia, N. T., Janes, M. R., Sher, A., . . . Ruggero, D. (2012). The translational landscape of mTOR signalling steers cancer initiation and metastasis. *Nature, 485*(7396), 55-61. doi:10.1038/nature10912

Huez, I., Creancier, L., Audigier, S., Gensac, M. C., Prats, A. C., & Prats, H. (1998). Two independent internal ribosome entry sites are involved in translation initiation of vascular endothelial growth factor mRNA. *Mol Cell Biol, 18*(11), 6178-6190. doi:10.1128/mcb.18.11.6178

Jackson, R. J., Hellen, C. U., & Pestova, T. V. (2010). The mechanism of eukaryotic translation initiation and principles of its regulation. *Nat Rev Mol Cell Biol, 11*(2), 113-127. doi:10.1038/nrm2838

Jalkanen, A. L., Coleman, S. J., & Wilusz, J. (2014). Determinants and implications of mRNA poly(A) tail size--does this protein make my tail look big? *Semin Cell Dev Biol, 34*, 24-32. doi:10.1016/j.semcdb.2014.05.018

Jang, S. K., Krausslich, H. G., Nicklin, M. J., Duke, G. M., Palmenberg, A. C., & Wimmer, E. (1988). A segment of the 5' nontranslated region of encephalomyocarditis virus RNA directs internal entry of ribosomes during in vitro translation. *J Virol, 62*(8), 2636-2643. Retrieved from https://www.ncbi.nlm.nih.gov/pubmed/2839690

Joshi, B., Cameron, A., & Jagus, R. (2004). Characterization of mammalian eIF4E-family members. *Eur J Biochem, 271*(11), 2189-2203. doi:10.1111/j.1432-1033.2004.04149.x

Joshi, B., Lee, K., Maeder, D. L., & Jagus, R. (2005). Phylogenetic analysis of eIF4E-family members. *BMC Evol Biol, 5*, 48. doi:10.1186/1471-2148-5-48

Kamenska, A., Simpson, C., & Standart, N. (2014). eIF4E-binding proteins: new factors, new locations, new roles. *Biochem Soc Trans, 42*(4), 1238-1245. doi:10.1042/BST20140063

Khan, M. A., Walden, W. E., Theil, E. C., & Goss, D. J. (2017). Thermodynamic and Kinetic Analyses of Iron Response Element (IRE)-mRNA Binding to Iron Regulatory Protein, IRP1. *Sci Rep, 7*(1), 8532. doi:10.1038/s41598-017-09093-5

Kim, S., Kim, D., Cho, S. W., Kim, J., & Kim, J. S. (2014). Highly efficient RNA-guided genome editing in human cells via delivery of purified Cas9 ribonucleoproteins. *Genome Res, 24*(6), 1012-1019. doi:10.1101/gr.171322.113

Kirschman, J. L., Bhosle, S., Vanover, D., Blanchard, E. L., Loomis, K. H., Zurla, C., . . . Santangelo, P. J. (2017). Characterizing exogenous mRNA delivery, trafficking, cytoplasmic release and RNA-protein correlations at the level of single cells. *Nucleic Acids Res, 45*(12), e113. doi:10.1093/nar/gkx290

Knovich, M. A., Storey, J. A., Coffman, L. G., Torti, S. V., & Torti, F. M. (2009). Ferritin for the clinician. *Blood Rev, 23*(3), 95-104. doi:10.1016/j.blre.2008.08.001

Knuckles, P., & Buhler, M. (2018). Adenosine methylation as a molecular imprint defining the fate of RNA. *FEBS Lett, 592*(17), 2845-2859. doi:10.1002/1873-3468.13107

Kohn, M., Lederer, M., Wachter, K., & Huttelmaier, S. (2010). Near-infrared (NIR) dye-labeled RNAs identify binding of ZBP1 to the noncoding Y3-RNA. *RNA, 16*(7), 1420-1428. doi:10.1261/rna.2152710

Kong, Y. W., Cannell, I. G., de Moor, C. H., Hill, K., Garside, P. G., Hamilton, T. L., . . . Bushell, M. (2008). The mechanism of micro-RNA-mediated translation repression is determined by the promoter of the target gene. *Proc Natl Acad Sci U S A, 105*(26), 8866-8871. doi:10.1073/pnas.0800650105

Kozak, M. (1989). The scanning model for translation: an update. *J Cell Biol, 108*(2), 229-241. doi:10.1083/jcb.108.2.229

Kranzusch, P. J., Lee, A. S. Y., Wilson, S. C., Solovykh, M. S., Vance, R. E., Berger, J. M., & Doudna, J. A. (2014). Structure-guided reprogramming of human cGAS dinucleotide linkage specificity. *Cell, 158*(5), 1011-1021. doi:10.1016/j.cell.2014.07.028

Lahr, R. M., Fonseca, B. D., Ciotti, G. E., Al-Ashtal, H. A., Jia, J. J., Niklaus, M. R., . . . Berman, A. J. (2017). La-related protein 1 (LARP1) binds the mRNA cap, blocking eIF4F assembly on TOP mRNAs. *Elife, 6*. doi:10.7554/eLife.24146

Landon, A. L., Muniandy, P. A., Shetty, A. C., Lehrmann, E., Volpon, L., Houng, S., . . . Gartenhaus, R. B. (2014). MNKs act as a regulatory switch for eIF4E1 and eIF4E3 driven mRNA translation in DLBCL. *Nat Commun, 5*, 5413. doi:10.1038/ncomms6413

Lareau, L. F., Hite, D. H., Hogan, G. J., & Brown, P. O. (2014). Distinct stages of the translation elongation cycle revealed by sequencing ribosome-protected mRNA fragments. *Elife, 3*, e01257. doi:10.7554/eLife.01257

Le Quesne, J. P., Spriggs, K. A., Bushell, M., & Willis, A. E. (2010). Dysregulation of protein synthesis and disease. *J Pathol, 220*(2), 140-151. doi:10.1002/path.2627

Lee, A. S., Kranzusch, P. J., & Cate, J. H. (2015). eIF3 targets cell-proliferation messenger RNAs for translational activation or repression. *Nature, 522*(7554), 111-114. doi:10.1038/nature14267

Lee, A. S., Kranzusch, P. J., Doudna, J. A., & Cate, J. H. (2016). eIF3d is an mRNA cap-binding protein that is required for specialized translation initiation. *Nature, 536*(7614), 96-99. doi:10.1038/nature18954

Leppek, K., Das, R., & Barna, M. (2018). Functional 5' UTR mRNA structures in eukaryotic translation regulation and how to find them. *Nat Rev Mol Cell Biol, 19*(3), 158-174. doi:10.1038/nrm.2017.103

Lin, Y., Li, F., Huang, L., Polte, C., Duan, H., Fang, J., . . . Wolf, D. A. (2020). eIF3 Associates with 80S Ribosomes to Promote Translation Elongation, Mitochondrial Homeostasis, and Muscle Health. *Mol Cell*. doi:10.1016/j.molcel.2020.06.003

Linder, M. C. (2013). Mobilization of stored iron in mammals: a review. *Nutrients, 5*(10), 4022-4050. doi:10.3390/nu5104022

Liu, H. D., Li, W., Chen, Z. R., Zhou, M. L., Zhuang, Z., Zhang, D. D., . . . Hang, C. H. (2013). Increased expression of ferritin in cerebral cortex after human traumatic brain injury. *Neurol Sci, 34*(7), 1173-1180. doi:10.1007/s10072-012-1214-7

Lizio, M., Harshbarger, J., Shimoji, H., Severin, J., Kasukawa, T., Sahin, S., . . . consortium, F. (2015). Gateways to the FANTOM5 promoter level mammalian expression atlas. *Genome Biol, 16*, 22. doi:10.1186/s13059-014-0560-6

Lodish H, B. A., Zipursky SL, et al. (2000). Processing of Eukaryotic mRNA. *Molecular Cell Biology., 4th edition*. Retrieved from https://www.ncbi.nlm.nih.gov/books/NBK21563/

Luscieti, S., Tolle, G., Aranda, J., Campos, C. B., Risse, F., Moran, E., . . . Sanchez, M. (2013). Novel mutations in the ferritin-L iron-responsive element that only mildly impair IRP binding cause hereditary hyperferritinaemia cataract syndrome. *Orphanet J Rare Dis, 8*, 30. doi:10.1186/1750-1172-8-30

Ma, J., Haldar, S., Khan, M. A., Sharma, S. D., Merrick, W. C., Theil, E. C., & Goss, D. J. (2012). Fe2+ binds iron responsive element-RNA, selectively changing protein-binding affinities and regulating mRNA repression and activation. *Proc Natl Acad Sci U S A, 109*(22), 8417-8422. doi:10.1073/pnas.1120045109

Macejak, D. G., & Sarnow, P. (1991). Internal initiation of translation mediated by the 5' leader of a cellular mRNA. *Nature, 353*(6339), 90-94. doi:10.1038/353090a0

Mamane, Y., Petroulakis, E., Rong, L., Yoshida, K., Ler, L. W., & Sonenberg, N. (2004). eIF4E--from translation to transformation. *Oncogene, 23*(18), 3172-3179. doi:10.1038/sj.onc.1207549

Martin, J. S., Halvorsen, M., Davis-Neulander, L., Ritz, J., Gopinath, C., Beauregard, A., & Laederach, A. (2012). Structural effects of linkage disequilibrium on the transcriptome. *RNA, 18*(1), 77-87. doi:10.1261/rna.029900.111

Martinez-Salas, E., Francisco-Velilla, R., Fernandez-Chamorro, J., & Embarek, A. M. (2017). Insights into Structural and Mechanistic Features of Viral IRES Elements. *Front Microbiol, 8*, 2629. doi:10.3389/fmicb.2017.02629

McKendrick, L., Morley, S. J., Pain, V. M., Jagus, R., & Joshi, B. (2001). Phosphorylation of eukaryotic initiation factor 4E (eIF4E) at Ser209 is not required for protein synthesis in vitro and in vivo. *Eur J Biochem, 268*(20), 5375-5385. doi:10.1046/j.0014-2956.2001.02478.x

Melanson, G., Timpano, S., & Uniacke, J. (2017). The eIF4E2-Directed Hypoxic Cap-Dependent Translation Machinery Reveals Novel Therapeutic Potential for Cancer Treatment. *Oxid Med Cell Longev, 2017*, 6098107. doi:10.1155/2017/6098107

Meyuhas, O. (2000). Synthesis of the translational apparatus is regulated at the translational level. *Eur J Biochem, 267*(21), 6321-6330. doi:10.1046/j.1432-1327.2000.01719.x

Millonig, G., Muckenthaler, M. U., & Mueller, S. (2010). Hyperferritinaemia-cataract syndrome: worldwide mutations and phenotype of an increasingly diagnosed genetic disorder. *Hum Genomics, 4*(4), 250-262. doi:10.1186/1479-7364-4-4-250

Mokany, E., Tan, Y. L., Bone, S. M., Fuery, C. J., & Todd, A. V. (2013). MNAzyme qPCR with superior multiplexing capacity. *Clin Chem, 59*(2), 419-426. doi:10.1373/clinchem.2012.192930

Morikawa, K., Oseko, F., & Morikawa, S. (1995). A role for ferritin in hematopoiesis and the immune system. *Leuk Lymphoma, 18*(5-6), 429-433. doi:10.3109/10428199509059641

Muckenthaler, M., Gray, N. K., & Hentze, M. W. (1998). IRP-1 Binding to Ferritin mRNA Prevents the Recruitment of the Small Ribosomal Subunit by the Cap-Binding Complex eIF4F. *Molecular Cell, 2*(3), 383-388. doi:10.1016/s1097-2765(00)80282-8

Nicolai, C. J., Wolf, N., Chang, I. C., Kirn, G., Marcus, A., Ndubaku, C. O., . . . Raulet, D. H. (2020). NK cells mediate clearance of CD8(+) T cell-resistant tumors in response to STING agonists. *Sci Immunol, 5*(45). doi:10.1126/sciimmunol.aaz2738

Osborne, M. J., Volpon, L., Kornblatt, J. A., Culjkovic-Kraljacic, B., Baguet, A., & Borden, K. L. (2013). eIF4E3 acts as a tumor suppressor by utilizing an atypical mode of methyl-7-guanosine cap recognition. *Proc Natl Acad Sci U S A, 110*(10), 3877-3882. doi:10.1073/pnas.1216862110

Pakos-Zebrucka, K., Koryga, I., Mnich, K., Ljujic, M., Samali, A., & Gorman, A. M. (2016). The integrated stress response. *EMBO Rep, 17*(10), 1374-1395. doi:10.15252/embr.201642195

Palmer, C., Roberts, R. L., & Bero, C. (1994). Deferoxamine posttreatment reduces ischemic brain injury in neonatal rats. *Stroke, 25*(5), 1039-1045. doi:10.1161/01.str.25.5.1039

Paraskeva, E., Gray, N. K., Schlager, B., Wehr, K., & Hentze, M. W. (1999). Ribosomal pausing and scanning arrest as mechanisms of translational regulation from cap-distal iron-responsive elements. *Mol Cell Biol, 19*(1), 807-816. doi:10.1128/mcb.19.1.807

Pisareva, V. P., & Pisarev, A. V. (2014). eIF5 and eIF5B together stimulate 48S initiation complex formation during ribosomal scanning. *Nucleic Acids Res, 42*(19), 12052-12069. doi:10.1093/nar/gku877

Potez, M., Trappetti, V., Bouchet, A., Fernandez-Palomo, C., Guc, E., Kilarski, W. W., . . . Djonov, V. (2018). Characterization of a B16-F10 melanoma model locally implanted into the ear pinnae of C57BL/6 mice. *PLoS One, 13*(11), e0206693. doi:10.1371/journal.pone.0206693

Pulos-Holmes, M. C., Srole, D. N., Juarez, M. G., Lee, A. S., McSwiggen, D. T., Ingolia, N. T., & Cate, J. H. (2019). Repression of ferritin light chain translation by human eIF3. *Elife, 8*. doi:10.7554/eLife.48193

Ramlee, M. K., Yan, T., Cheung, A. M., Chuah, C. T., & Li, S. (2015). High-throughput genotyping of CRISPR/Cas9-mediated mutants using fluorescent PCR-capillary gel electrophoresis. *Sci Rep, 5*, 15587. doi:10.1038/srep15587

Recalcati, S., Invernizzi, P., Arosio, P., & Cairo, G. (2008). New functions for an iron storage protein: the role of ferritin in immunity and autoimmunity. *J Autoimmun, 30*(1-2), 84-89. doi:10.1016/j.jaut.2007.11.003

Reich, S. H., Sprengeler, P. A., Chiang, G. G., Appleman, J. R., Chen, J., Clarine, J., . . . Webster, K. R. (2018). Structure-based Design of Pyridone-Aminal eFT508 Targeting

Dysregulated Translation by Selective Mitogen-activated Protein Kinase Interacting Kinases 1 and 2 (MNK1/2) Inhibition. *J Med Chem, 61*(8), 3516-3540. doi:10.1021/acs.jmedchem.7b01795

Reyon, D., Tsai, S. Q., Khayter, C., Foden, J. A., Sander, J. D., & Joung, J. K. (2012). FLASH assembly of TALENs for high-throughput genome editing. *Nat Biotechnol, 30*(5), 460-465. doi:10.1038/nbt.2170

Ruibin, W., Zheng, X., Chen, J., Zhang, X., Yang, X., & Lin, Y. (2018). Micro RNA-1298 opposes the effects of chronic oxidative stress on human trabecular meshwork cells via targeting on EIF4E3. *Biomed Pharmacother, 100*, 349-357. doi:10.1016/j.biopha.2018.02.001

Sammarco, M. C., Ditch, S., Banerjee, A., & Grabczyk, E. (2008). Ferritin L and H subunits are differentially regulated on a post-transcriptional level. *J Biol Chem, 283*(8), 4578-4587. doi:10.1074/jbc.M703456200

Santambrogio, P., Levi, S., Arosio, P., Palagi, L., Vecchio, G., Lawson, D. M., . . . Cesareni, G. (1992). Evidence That a Salt Bridge in the Light Chain Contributes to the Physical Stability Difference between Heavy and Light Human Ferritins. *Journal of Biological Chemistry, 267*(20), 14077-14083. doi:1629207

Saxton, R. A., & Sabatini, D. M. (2017). mTOR Signaling in Growth, Metabolism, and Disease. *Cell, 168*(6), 960-976. doi:10.1016/j.cell.2017.02.004

Schneider, B. D., & Leibold, E. A. (2003). Effects of iron regulatory protein regulation on iron homeostasis during hypoxia. *Blood, 102*(9), 3404-3411. doi:10.1182/blood-2003-02-0433

Sheth, U., & Parker, R. (2003). Decapping and decay of messenger RNA occur in cytoplasmic processing bodies. *Science, 300*(5620), 805-808. doi:10.1126/science.1082320

Sonenberg, N., & Hinnebusch, A. G. (2009). Regulation of translation initiation in eukaryotes: mechanisms and biological targets. *Cell, 136*(4), 731-745. doi:10.1016/j.cell.2009.01.042

Sonenberg, N., Morgan, M. A., Merrick, W. C., & Shatkin, A. J. (1978). A polypeptide in eukaryotic initiation factors that crosslinks specifically to the 5'-terminal cap in mRNA. *Proc Natl Acad Sci U S A, 75*(10), 4843-4847. doi:10.1073/pnas.75.10.4843

Stoneley, M., Paulin, F. E., Le Quesne, J. P., Chappell, S. A., & Willis, A. E. (1998). C-Myc 5' untranslated region contains an internal ribosome entry segment. *Oncogene, 16*(3), 423-428. doi:10.1038/sj.onc.1201763

Studier, F. W. (2005). Protein production by auto-induction in high density shaking cultures. *Protein Expr Purif, 41*(1), 207-234. doi:10.1016/j.pep.2005.01.016

Sun, C., Querol-Audi, J., Mortimer, S. A., Arias-Palomo, E., Doudna, J. A., Nogales, E., & Cate, J. H. (2013). Two RNA-binding motifs in eIF3 direct HCV IRES-dependent translation. *Nucleic Acids Res, 41*(15), 7512-7521. doi:10.1093/nar/gkt510

Theil, E. C. (1994). Iron regulatory elements (IREs): a family of mRNA non-coding sequences. *Biochem J, 304 (Pt 1)*, 1-11. doi:10.1042/bj3040001

Thoreen, C. C., Chantranupong, L., Keys, H. R., Wang, T., Gray, N. S., & Sabatini, D. M. (2012). A unifying model for mTORC1-mediated regulation of mRNA translation. *Nature, 485*(7396), 109-113. doi:10.1038/nature11083

Torti, F. M., & Torti, S. V. (2002). Regulation of ferritin genes and protein. *Blood, 99*(10), 3505-3516. doi:10.1182/blood.v99.10.3505

Truitt, M. L., Conn, C. S., Shi, Z., Pang, X., Tokuyasu, T., Coady, A. M., . . . Ruggero, D. (2015). Differential Requirements for eIF4E Dose in Normal Development and Cancer. *Cell, 162*(1), 59-71. doi:10.1016/j.cell.2015.05.049

Ueda, H., Iyo, H., Doi, M., Inoue, M., Ishida, T., Morioka, H., . . . Uesugi, S. (1991). Combination of Trp and Glu residues for recognition of mRNA cap structure Analysis of m7G base recognition site of human cap binding protein (IF-4E) by site-directed mutagenesis. *FEBS Letters, 280*(2), 207-210. doi:10.1016/0014-5793(91)80294-d

Ueda, T., Watanabe-Fukunaga, R., Fukuyama, H., Nagata, S., & Fukunaga, R. (2004). Mnk2 and Mnk1 are essential for constitutive and inducible phosphorylation of eukaryotic initiation factor 4E but not for cell growth or development. *Mol Cell Biol, 24*(15), 6539-6549. doi:10.1128/MCB.24.15.6539-6549.2004

Volpon, L., Osborne, M. J., Culjkovic-Kraljacic, B., & Borden, K. L. (2013). eIF4E3, a new actor in mRNA metabolism and tumor suppression. *Cell Cycle, 12*(8), 1159-1160. doi:10.4161/cc.24566

Voorhees, R. M., & Ramakrishnan, V. (2013). Structural basis of the translational elongation cycle. *Annu Rev Biochem, 82*, 203-236. doi:10.1146/annurev-biochem-113009-092313

Wagner, S., Herrmannova, A., Hronova, V., Gunisova, S., Sen, N. D., Hannan, R. D., . . . Valasek, L. S. (2020). Selective Translation Complex Profiling Reveals Staged Initiation and Co-translational Assembly of Initiation Factor Complexes. *Mol Cell*. doi:10.1016/j.molcel.2020.06.004

Wang, X., Lu, Z., Gomez, A., Hon, G. C., Yue, Y., Han, D., . . . He, C. (2014). N6-methyladenosine-dependent regulation of messenger RNA stability. *Nature, 505*(7481), 117-120. doi:10.1038/nature12730

Wang, X., Zhao, B. S., Roundtree, I. A., Lu, Z., Han, D., Ma, H., . . . He, C. (2015). N(6)-methyladenosine Modulates Messenger RNA Translation Efficiency. *Cell, 161*(6), 1388-1399. doi:10.1016/j.cell.2015.05.014

Wang, Z., Feng, X., Molinolo, A. A., Martin, D., Vitale-Cross, L., Nohata, N., . . . Gutkind, J. S. (2019). 4E-BP1 Is a Tumor Suppressor Protein Reactivated by mTOR Inhibition in Head and Neck Cancer. *Cancer Res, 79*(7), 1438-1450. doi:10.1158/0008-5472.CAN-18-1220

Weingarten-Gabbay, S., Elias-Kirma, S., Nir, R., Gritsenko, A. A., Stern-Ginossar, N., Yakhini, Z., . . . Segal, E. (2016). Comparative genetics. Systematic discovery of cap-independent translation sequences in human and viral genomes. *Science, 351*(6270). doi:10.1126/science.aad4939

Wendel, H. G., Silva, R. L., Malina, A., Mills, J. R., Zhu, H., Ueda, T., . . . Lowe, S. W. (2007). Dissecting eIF4E action in tumorigenesis. *Genes Dev, 21*(24), 3232-3237. doi:10.1101/gad.1604407

Wilkinson, N., & Pantopoulos, K. (2014). The IRP/IRE system in vivo: insights from mouse models. *Front Pharmacol, 5*, 176. doi:10.3389/fphar.2014.00176

Wolf, D. A., Lin, Y., Duan, H., & Cheng, Y. (2020). eIF-Three to Tango: emerging functions of translation initiation factor eIF3 in protein synthesis and disease. *J Mol Cell Biol, 12*(6), 403-409. doi:10.1093/jmcb/mjaa018

Xue, S., Tian, S., Fujii, K., Kladwang, W., Das, R., & Barna, M. (2015). RNA regulons in Hox 5' UTRs confer ribosome specificity to gene regulation. *Nature, 517*(7532), 33-38. doi:10.1038/nature14010

Zhang, B., Babu, K. R., Lim, C. Y., Kwok, Z. H., Li, J., Zhou, S., . . . Tay, Y. (2018). Pan-cancer analysis of RNA binding proteins (RBPs) reveals the involvement of the core pre-mRNA splicing and translation machinery in tumorigenesis. *bioRxiv*. doi:10.1101/341263